Tough Ceramics from Fibrous Monoliths

Contract Number N00014-91-J-1999

Office of Naval Research

ONR Scientific Officer: Steven G. Fishman
01 April 1991- 30 March 1993

Final Technical Report
August 25, 1997

Principal Investigator: John W. Halloran
Department of Materials Science and Engineering
University of Michigan
Ann Arbor, MI 48109-2136

Tough Ceramics from Fibrous Monoliths
Final Technical Report

Abstract

During this 1991-1993 grant, the University of Michigan developed "fibrous monolithic ceramics", a new class of monolithic ceramics with properties comparable to ceramic fiber reinforced ceramic matrix composites [CMC's]. They consist of a 250-micron "cells" of a strong polycrystalline ceramic, such as silicon carbide or silicon nitride, separated by "cell boundaries" from materials, such as boron nitride, which promote crack deflection and delamination. These materials show graceful failure in flexure, with strengths around 350 MPa and work of fracture around 2000 J/m^2. Fibrous monolithic ceramics are made from conventional low-cost ceramic powder, using extrusion methods common in conventional ceramic manufacture. We have demonstrated successful fibrous monoliths with silicon carbide, silicon nitride, and alumina, using weak interfaces of graphite or boron nitride. The boron nitride systems are resistant to oxidation. Their room temperature properties are unaffected by exposure at 1400°C.

ONR Contract Information is summarized below
Contract Title: Tough Ceramics from Fibrous Monoliths
Performing Organization: University of Michigan
Principal Investigator: John W. Halloran
Contract Number: N00014-91-J-1999
R & T Project Number: cer9102---01, cer9102---02
ONR Scientific Officer: Steven G. Fishman
Total Contract Value: $ 335,938
Date Work Started: April 1, 1991_
Contract Signature Date: 10 July, 1991_
Contract End Date: March 30, 1993

A. Scientific Research Goals

Our goal was develop a new type of monolithic ceramic with enhanced toughness and "graceful" fracture behavior, called "fibrous monolithic ceramics", as low cost/high performance structural ceramics. To assure low cost, we emphasized inexpensive materials, such as SiC and alumina, and based our fabrication on powder processing techniques which are compatible with the manufacturing methods now available at existing ceramic industrial facilities.

Our approach was to tailor the structure of the ceramic on a scale of 10-100 microns, to incorporate features which cause crack deflection and promote shear delamination. We did this by compounding the ceramic powder with 40-50 vol% binder and spinning "green fibers". The green fibers were then coated with a second phase to promote deflection and delamination. The coated green fibers were compacted into a formed body, and sintered or hot pressed to yield a dense ceramic with a remnant fibrous texture -- a fibrous monolithic ceramic. The microstructure features dense "cells" created by the fiber relicts, with "cell boundaries" created by the coating phase.

This project was completed at the end of March 1993, but work continued on fibrous monolithic ceramics with a second DARPA-funded program under ONR N00014-93-1-0302, "Advanced Development of Fibrous Monolithic Ceramics", which was renewed and continued through August 1997. The new program (subsequently called the "1993 grant") involved significant improvement of the fibrous monolith process, transfer and scale-up at Advanced Ceramic Research, Inc., who manufactured a fibrous monolith aft combustor plate for testing at Williams International, Inc.

We developed fibrous monoliths based on silicon carbide, silicon nitride, alumina, and zirconia, with crack interaction mechanisms involving local regions of weak interface [SiC cells with graphite cell boundaries, or Si_3N_4 cells with BN cell boundaries, alumina and zirconia with BN cell boundaries], which cause shear delamination. All of these feature graceful fracture, with retained load after fracture begins, and work-of-fracture values of several thousand J/m^2. Silicon carbide and silicon nitride FM's with boron nitride cell boundaries were resistant to oxidation up to 1400°C.

B. Significant results from the Program

We have achieved monolithic ceramics with room temperature properties comparable to ceramic fiber reinforced ceramic matrix composites [CMC's]. These "fibrous monolithic ceramics" are made from conventional low-cost ceramic powder, using methods directly transferable to conventional ceramic manufactures. We have demonstrated successful fibrous monoliths with silicon carbide, silicon nitride, and alumina, using weak interfaces of graphite or boron nitride. The boron nitride systems are resistant to oxidation. Their room temperature properties are unaffected by exposure at 1400°C.

Fabrication Methods

The emphasis early in the program concerned fabrication and exploration of many combinations of cell materials and cell boundary materials. This work was reported in a paper by Baskaran, Nunn, Popovich and Halloran[1]. For the early fabrication work, green fibers were produced by "dry spinning", which involves extrusion of a very viscous solvent-borne suspension, which solidifies by evaporation. This process was described in detail by Baskaran et al.[2] and Nunn et al.[3]. The relation between fiber spinning and suspension rheology was discussed by Subramanian et al.[4] In practice, a relatively fluid suspension was produced by ball milling powders in solution of ethyl methacrylate in methyl ethyl ketone, followed by evaporation of most of the solvent to produce a very viscous 'spinning dope'. The dope was loaded into a dispensing syringe, and extruded into drying column. Dry green fiber was gently collected by hand-spooling. As a substitute and eventual replacement for dry spinning, Popovic' developed a thermoplastic melt spinning process[5]. This later became our only method.

For melt spinning, the ceramic powders are compounded with molten thermoplastic co-polymers ethylene vinyl acetate (EVA) or ethylene ethyl acrylate (EEA) in a heated shear mixer to yield a 50 volume percent mixture. The mixture was thermoplastically compression molded into a cylindrical feedrod and extruded into 250 micron diameter fibers in a fiber extrusion machine, and collected on a spool, as described in Baskaran et al. "Fibrous Monolithic Ceramics: I"

The cell boundary material was applied to the green fibers by a dip-coating process. Simple in concept, dip-coating proved a challenge to control, since the thickness of the coating could not be directly adjusted. A dip-coating suspension had to be developed for each material, which would wet the green fiber and produce a thin and uniform coating, free of bare spots or thick spots. Typically we used isopropanol as a

---

[1] S. Baskaran, S.D. Nunn, D. Popovich, and J.W. Halloran, "Fibrous Monolithic Ceramics: I Fabrication, Microstructure, and Indentation Behavior", J. American Ceramic Soc. 76 [9] 2209-16 (1993)

[2] S. Baskaran, D. Popovic', J. Halloran, G. Subramanian, and S. Bike, "Spinning Fibers from Powder Suspensions", Particulate Science and Technology, **10**, p. 109-119, (1992)

[3] S.D. Nunn, D. Popovic, S. Baskaran, J. W. Halloran, G. Subramanian and S.G. Bike, "Suspension Dry Spinning and Rheological Behavior of Ceramic Powder Loaded Polymer Solutions", J. American Ceramic Soc **76**,[10], p. 2460-2464 (1993)

[4] G. Subramanian, S.G. Bike, S. Baskaran, D. Popovic, and J. W. Halloran, , "The Role of Rheological Characterization of Ceramic Dopes in Predicting Fiber Spinning Performance", in *Flow and Microstructure of Dense Suspensions*, Ed. by L. J. Struble, C. F. Zukowski, and G. C. Maitland, MRS Conference Proceedings. Vol 289, p. 129-134 (1993)

[5] Dragan Popovic', M.S. Thesis, University of Michigan 1993

suspension medium. The compression behavior of the coating/fiber system also had to be appropriate, since the coating must deform with the green fiber in the subsequent warm compaction step. Dip-coating of melt spun was a particular problem, since coatings had to be particularly adherent and flexible for the spooling and handling.

The Masters thesis of PopovicR was, in part, the early development of a thermoplastic co-extrusion process whereby the cell and cell boundary was created simultaneously. This work formed the basis works subsequently developed in the following-on grant, which resulted in a patent[6] on the co-extrusion process. This patent appears in the Appendix. The co-extrusion process was transferred to Advanced Ceramics Research, Inc., who subsequently made many improvements in the follow-on program.

Materials and Properties

During the first year of the program we demonstrated hot pressed SiC/graphite fibrous monoliths with graceful failure by shear delamination. Uniaxially aligned specimens had peak flexural stress [at point of shear failure] of 250 MPa with apparent fracture energy of 1500 J/m^2. This work was reported in detail by Baskaran and Halloran[7], a paper which appears in the Appendix, and in the proceedings of the 1993 Cocoa Beach Conference[8]. This was the prototype of the graceful fibrous monoliths which were subsequently developed. Graphite, of course, could not be used at elevated temperature in air. So we made the obvious substitution of hexagonal boron nitride (h-BN), or 1white graphite× and fabricated SiC/BN fibrous monoliths

The SiC/BN system was originally fabricated by dry-spin/dip-coating by Baskaran[9] displayed higher strength (375 MPa) and much higher work-of fracture at room temperature. It displayed surprisingly good oxidation behavior, retaining similar room temperature strength and graceful failure after 10 hour air exposure at 1500ºC. This is much better oxidation resistance than would be expected for BN, a consequence of the formation of a protective scale of silicate, which

---

[6] U.S. 5, 645,781 July 8, 1997 1Process for Preparing Textured Ceramic Composites× D. PopovicR, J.Halloran, G. Hilmas, G. Brady, S. somers, A. Barda, G. Zywicki

[7] S. Baskaran and J.W. Halloran, 1Fibrous Monolithic Ceramics: II Flexural Strength and Fracture Behavior of the Silicon Carbide/Graphite System×, J. American Ceramic Soc. 76 [9] 2217-24 (1993)

[8] S. Baskaran and J.W. Halloran,"SiC-Based Fibrous Monolithic Ceramics", Ceramic Science and Engineering Proceedings, Vol **14**, No.9-10, pp 813-823 (1993)

[9] S. Baskaran and J.W. Halloran, 1Fibrous Monolithic Ceramics: III, Mechanical Properties and Oxidation Behavior of the Silicon Carbide/Boron Nitride System×, J. American Ceramic Soc. 77 [5] 1249-55 (1994)

covers the BN cell boundaries at the surface of the material. This Baskaran paper is included in the Appendix.

Later we developed higher strength, oxidation-resistant Si_3N_4/BN fibrous monoliths, with graceful failure. The early work was conducted by Popovic', as part of his Masters Thesis. The best properties achieved to date with this material were a flexural strength of 420 MPa and an apparent work of fracture of 3500 J/m^2. Some of the early work was reported in a paper by Popovic' et al.[10], which is also included in the Appendix. Because of the higher strength, the follow-on program emphasized silicon nitride/boron nitride.

Other Materials

The primary focus of this program and the 1993 grant concerned silicon carbide and silicon nitride with low shear strength graphitic cell boundaries. We also, however, explored a number of different systems, with oxide cells, microcracked cell boundaries, and metallic cell boundaries. This section briefly reviews these activities.

Baskaran and Nunn developed ceramic/metal fibrous monoliths, such as alumina with Ni cell boundaries.[11] These had graceful failure, but failed by tensile cracking. With only 7 volume percent Ni, arranged as aligned cell boundaries, graceful failure was achieved by bridging plastic ligaments. The alumina/Ni system was resistant to oxidation to 1400ºC. During the 1993 grant, Hilmas demonstrated a zirconia/Ni FM, using yttria tetragonal zirconia polycrystal, and Abdali conducted a Masters Thesis project on ceramic/metal fibrous monoliths.

Oxide/graphitic analogues were explored by Zywicki, who developed alumina/BN and alumina/graphite fibrous monoliths, with graceful failure. Much of this work was continued in the 1993 program, and is fully described in the Masters thesis of Gregory Zywicki.[12]

Early in the project Nunn and Baskaran investigated systems with cell boundaries having incipient or pre-existing microcracks[Al_2O_3 cells

---

[10] D. Popovic', S. Baskaran, , G. Zywicki, C. Arens, and J.W. Halloran, "Silicon Nitride and Silicon Carbide Fibrous Monolithic Ceramics", p. 173-186 in *Silicon Based Structural Ceramics*, ed. B.W. Sheldon, S.C. Danforth, Ceramic Transactions Vol 42 American Ceramic Soc. Westerville, OH (1994)

[11] S. Baskaran, S.D. Nunn, and J.W. Halloran, 1Fibrous Monolithic Ceramics: IV, Mechanical Properties and Oxidation Behavior of the Alumina/Nickel Systemx, J. American Ceramic Soc. 77 [5] 1256-62 (1994)

[12] Gregory Zywicki, 1Oxide Based Fibrous Monolithic Ceramicsx, MS Thesis, U. Michigan 1996 (research completed 1994)

with Al_2TiO_5 cell boundaries]. These were quite flaw tolerant, but had conventional brittle fracture, so we abandoned the work.

We also demonstrated 12% ceria-zirconia/ alumina-zirconia sintered fibrous monolith. Nomarski interference microscopy showed that the transformation zone in the ceria-zirconia around a microhardness indent was strongly modified by the alumina-zirconia cell boundaries. This suggests that improved toughness is to be expected, although no data has yet been taken. Brittle failure occurs at 250 MPa. This work was not pursued further.

With the collaboration of Prof. David Martin, we demonstrated a tough polymer-ceramic system. These were called "super clamshells", as SiC-polyimide fibrous monolith intended to serve as a high performance version of the bio-inspired design of mineral laminae [with SiC rather than $CaCO_3$] connected by thin polymer layers [with Kapton polyimide instead of protein]. This was prepared by oxidizing away the graphite from a SiC-graphite fibrous monolith, and filling the resulting empty cell boundaries with the precursor of polymellitic dianhydride oxydianiline [PMDA-ODA]. With 2 vol% polyimide, the material showed graceful failure, with a work of fracture above 500 J/m^2, which comparable to dry nacre[13]. After the early exploration, we stopped work on this system, since polymer-ceramic systems were outside the scope of the program. This work was presented at the American Ceramic Society, but not subsequently published.

D. List of Publications/Reports/Presentations

1. Papers Published in Refereed Journals

S. Baskaran, D. Popovic', J. Halloran, G. Subramanian, and S. Bike, "Spinning Fibers from Powder Suspensions", Particulate Science and Technology, **10**, p. 109-119, (1992)

S. Baskaran and J.W. Halloran,"SiC-Based Fibrous Monolithic Ceramics", 17th Annual Conference on Composites and Advanced Ceramic Materials, Cocoa Beach, FL, Jan. 10-15, 1993, Ceramic Science and Engineering Proceedings, Vol 14, No.9-10, pp 813-823 (1993)

[13] A.P. Jackson, J.F.V. Vincent and R.M. Turner, Proc. Roy. Soc. B 234 415 (1988)

S. Baskaran, S. Nunn, D. Popovic', and J.W. Halloran, "Fibrous Monolithic Ceramics, I: Fabrication, Microstructure, and Indentation Behavior", J. American Ceramic Soc **76**,[9], p. 2209-2216 (1993)

S. Baskaran and J.W. Halloran, "Fibrous Monolithic Ceramics, II: Flexural Strength and Fracture Behavior of the SiC/Graphite System", J. American Ceramic Soc **76**,[9], p. 2217-2224 (1993)

S.D. Nunn, D. Popovic, S. Baskaran, J. W. Halloran, G. Subramanian and S.G. Bike, "Suspension Dry Spinning and Rheological Behavior of Ceramic Powder Loaded Polymer Solutions", J. American Ceramic Soc **76**,[10], p. 2460-2464 (1993)

G. Subramanian, S.G. Bike, S. Baskaran, D. Popovic, and J. W. Halloran, , "The Role of Rheological Characterization of Ceramic Dopes in Predicting Fiber Spinning Performance", in Flow and Microstructure of Dense Suspensions, Ed. by L. J. Struble, C. F. Zukowski, and G. C. Maitland, MRS Conference Proceedings. Vol 289, p. 129-134 (1993)

S. Baskaran, D. Popovic', S. Baskaran, , G. Zywicki, C. Arens, and J.W. Halloran, "Silicon Nitride and Silicon Carbide Fibrous Monolithic Ceramics", p. 173-186 in *Silicon Based Structural Ceramics*, ed. B.W. Sheldon, S.C. Danforth, Ceramic Transactions Vol 42 American Ceramic Soc. Westerville, OH (1994) Proceedings of the Silicon Based Structural Ceramics Symposium, American Ceramic Soc. Pacific Rim Meeting, Nov. 7-10, 1993, Honolulu, Hawaii

S. Baskaran and J.W. Halloran, "Fibrous Monolithic Ceramics, III: Mechanical Properties and Oxidation Behavior of the SiC/BN System", submitted to the J. American Ceramic Soc., 77 [5] 1249-55 (1994)

S. Baskaran, S. Nunn, and J.W. Halloran, "Fibrous Monolithic Ceramics: IV, Mechanical Properties and Oxidation Behavior of the Alumina/Ni System", submitted to the J. American Ceramic Soc 77 [5] 1256-62 (1994)

2. Non-Refereed Publications and Published Technical Reports
none

3. Presentations
a. Invited
1992 Pacific Coast Regional Meeting, American Ceramic Society, San Francisco, CA, Nov 3-4, 1992
"Powder Processing for Tough Fibrous Monolithic Ceramics", S. Baskaran, D. Popovic, J. Halloran

American Ceramic Society, Annual Meeting, April18-22, 1993, Cincinnati, Ohio
"Microstructure Design for Fibrous Monolithic Ceramics and Ceramic-Polymer Composites". S. Baskaran, D.C. Martin, and J. Halloran

American Ceramic Society, Annual Meeting, April18-22, 1993, Cincinnati, Ohio
"Properties of Fibrous Monolithic Ceramics". S. Baskaran, D. Popovic, G. Zywicki, and J. Halloran

ONR In-Situ Composites Review/Workshop
June 1-2, 1993, Woods Hole, MA
"Graceful Failure from Monolithic Ceramics with the Fibrous Monolith Structure"

b. Contributed

1992 Pacific Coast Regional Meeting, American Ceramic Society, San Francisco, CA, Nov 3-4, 1992
"Fracture of Fibrous Monolithic Ceramics", S. Baskaran, D. Popovic, J. Halloran

1992 Materials Research Society Fall Meeting, Boston
G. Subramanian, S.G. Bike, S. Baskaran, D. Popovic, and J. W. Halloran, "The Role of Rheological Characterization of Ceramic Dopes in Predicting Fiber Spinning Performance"

American Ceramic Society, 17th Annual Conference on Composites and Advanced Ceramics, Jan. 10-15, 1993 Cocoa Beach, FL
Suresh Baskaran and John Halloran, "SiC -Based Fibrous Monolithic Ceramics"

American Ceramic Soc. Pacific Rim Meeting, Nov. 7-10, 1993, Honolulu, Hawaii, Si-Based Structural Ceramics Symp.
S. Baskaran, D. Popovic', G. Zywicki, C. Arens, and J.W. Halloran, "Silicon Nitride and Silicon Carbide Fibrous Monolithic Ceramics"

4. Books (and sections thereof)
none

E List of Honors/Awards

Name of Person Receiving Awards	Recipient's Institution	Name, Sponsor and Purpose of Award
J. Halloran, S. Baskaran	U. Michigan	Engineering Ceramics Division, American Ceramics Soc. "Second Prize" for Technical Presentation "SiC -Based Fibrous Monolithic Ceramics" 17th Annual Conf. on Composites and Adv. Ceramics, Jan. 10-15, 1993 Cocoa Beach, FL

H. Summary of Publications/Patents/Presentations/Honors/Participants (Number Only)

a.	Number of Papers Submitted to Refereed Journal but not yet published:		0
b.	Number of Papers Published in Refereed Journals:		9
c.	Number of Books or Chapters Submitted but not yet Published:		0
d.	Number of Books or Chapters Published:		0
e.	Number of Printed Technical Reports& Non-Refereed Papers:		0
f.	Number of Patents Filed (in 1994):		1
g.	Number of Patents Granted (in 1997):		1
h.	Number of Invited Presentations at Workshops or Prof. Society Meetings:		4
i.	Number of Contributed Presentations at Workshops or Prof. Society Meetings:		4
j.	Honors/Awards/Prizes for Contract/Grant Employees		1
k.	Number of Graduate Students and Post-Docs Supported at least 25%		3
	Grad Students:	Total	1
		Female	0
		Minority	0
	Post Doc:	Total	2
		Female	0
		Minority	0

Appendix

This Appendix includes reprints or copies of five of the principal publications resulting from this research grant. These are:

S. Baskaran, S.D. Nunn, D. Popovich, and J.W. Halloran, 1Fibrous Monolithic Ceramics: I Fabrication, Microstructure, and Indentation Behavior×, J. American Ceramic Soc. 76 [9] 2209-16 (1993)

S. Baskaran and J.W. Halloran, 1Fibrous Monolithic Ceramics: II Flexural Strength and Fracture Behavior of the Silicon Carbide/Graphite System×, J. American Ceramic Soc. 76 [9] 2217-24 (1993)

S. Baskaran and J.W. Halloran, 1Fibrous Monolithic Ceramics: III, Mechanical Properties and Oxidation Behavior of the Silicon Carbide/Boron Nitride System×, J. American Ceramic Soc. 77 [5] 1249-55 (1994)

S. Baskaran, S.D. Nunn, and J.W. Halloran, 1Fibrous Monolithic Ceramics: IV, Mechanical Properties and Oxidation Behavior of the Alumina/Nickel System×, J. American Ceramic Soc. 77 [5] 1256-62 (1994)

U.S. 5, 645,781 July 8, 1997 1Process for Preparing Textured Ceramic Composites× D. Popovic, J.Halloran, G. Hilmas, G. Brady, S. somers, A. Barda, G. Zywicki

journal

J. Am. Ceram. Soc., 76 [9] 2209–16 (1993)

Fibrous Monolithic Ceramics: I, Fabrication, Microstructure, and Indentation Behavior

Suresh Baskaran,* Stephen D. Nunn,* Dragan Popovic,* and John W. Halloran*

Department of Materials Science and Engineering, University of Michigan, Ann Arbor, Michigan 48109

Monolithic ceramics have been fabricated from coated green fibers to create fibrous microstructures. The *fibrous monoliths* consist of high aspect ratio polycrystalline regions (cells) of a primary phase separated by thin second-phase regions (cell boundaries) designed to improve fracture resistance. The cells are the remnants of the green fiber which consists of ceramic powder and a polymer binder. The coating applied on the green fiber forms the cell boundaries. Fabrication and microstructure are described for fibrous monoliths in the SiC/graphite, silicon nitride/BN, alumina/alumina–zirconia, alumina/aluminum titanate, alumina/nickel and Ce-TZP/alumina–Ce–zirconia systems. The SiC/graphite fibrous monolith displays noncatastrophic failure in flexure, with shear delamination along the weak graphite layers. Indentations in SiC/graphite cause cells to spall, with crack arrest and extrusion of graphite from the cell boundaries. Crack deflection and spalling of cells are also observed in alumina/alumina–zirconia fibrous monoliths. In the Ce-TZP/alumina system, transformed regions around indentations are significantly modified by the alumina-containing cell boundaries.

I. Introduction

MONOLITHIC ceramics which have a fabric of microstructural features designed to interact with crack propagation have improved toughness and show R-curve behavior.[1] Clegg *et al.*[2] produced a laminar fabric of SiC interleaved with graphite films which had flexural stress–strain behavior comparable to fiber-reinforced composites. Duplex structures of Claussen[3] and duplex bimodal ceramics[4,5] are designed with a fabric where the local phase content is varied in a matrix. These result in increasing toughness with crack propagation, or R-curve behavior, and lead to flaw-insensitive ceramics.

The "fibrous monolith" processing approach, introduced by Coblenz,[6] provides a novel and powerful method to fabricate ceramics with controlled fabrics. Fibrous monoliths are sintered (or hot-pressed) monolithic ceramics with a distinct fibrous texture, consisting of *cells* of a primary phase, separated by *cell boundaries* of a tailored secondary phase. This structure is illustrated schematically in Fig. 1. The cells are not fibers, but rather polycrystalline ceramic domains. The cell boundary phases can be, in different designs, weak interfaces, microcrack zones, ductile-phase filaments, or interphases with different physical properties.

We have produced fibrous monoliths from a variety of materials using a simple process for converting ordinary ceramic powder into "green fiber" consisting of the powder and a soft polymer binder. These fibers can be compacted in the green state to create, after sintering, the fabric of polycrystalline cells. The secondary phases for the cell boundaries are introduced as a coating on the green fiber prior to compaction. The process is widely applicable. The cells and cell boundaries can be made from any compatible set of materials available as fine, sinterable powders. The scale of the microstructure is determined by the green fiber diameter (for cell size) and coating thickness (for cell boundaries). A variety of architectures are possible, including compacted felt structures, randomly oriented chopped green fibers, and aligned green fibers. We have prepared fibrous monoliths in the SiC/graphite, Si_3N_4/BN, alumina/alumina–zirconia, alumina/aluminum titanate, Ce-TZP/Ce-TZP–alumina, and alumina/Ni systems.

In the simplest system, the cell boundary is a weak interface and acts as the preferred path for crack propagation. Examples are graphite cell boundaries with silicon carbide or boron nitride cell boundaries in silicon nitride. Fibrous monoliths such as alumina/aluminum titanate or alumina/alumina–zirconia are designed to have microcracked cell boundaries that will affect crack propagation characteristics. Microcracking occurs in fine-grained Al_2TiO_5 because of high thermal expansion anisotropy.[7,8] In particulate composites of Al_2O_3–Al_2TiO_5, high residual stresses due to expansion mismatch result in flaw-tolerant mechanical behavior.[9] In alumina matrices containing unstabilized zirconia, microcracking arises from the transformation of zirconia particles from tetragonal to monoclinic symmetry.[3] An alumina/nickel fibrous monolith has been fabricated as an example of a ductile phase cell boundary. To examine Ce-TZP/alumina laminates[10] in fibrous monolith form, we produced a microstructure with transformable Ce-TZP cells with

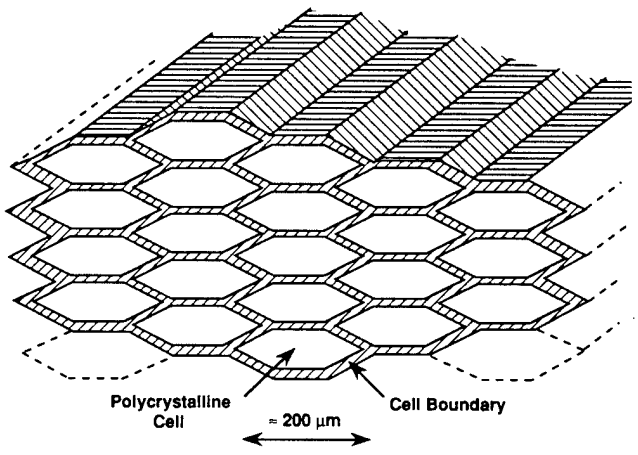

Fig. 1. Schematic illustrating the structure of a fibrous monolith.

B. Lawn—contributing editor

Manuscript No. 195027. Received December 16, 1992; approved May 17, 1993. This article was originally submitted on July 29, 1992 as Manuscript No. 195460.

Supported by the Defense Advanced Research Projects Agency and the Office of Naval Research under Contract No. N0014-91-J-1999.

*Member, American Ceramic Society.

nontransformable alumina + Ce-zirconia cell boundaries. The work of Marshall *et al.*[10] has shown that transformation zone spreading in suitably tailored Ce-TZP/alumina structures can significantly increase the fracture toughness.

This paper is a first report on fibrous monolithic ceramics, emphasizing fabrication, microstructure, and indentation behavior of several different systems, and briefly describing the strength behavior of one system, SiC/graphite. It will be followed by detailed reports on the mechanical properties of particular types of fibrous monoliths.[11]

II. Fabrication Procedure

The fabrication of fibrous monoliths is illustrated in Fig. 2, a process schematic. There are six process steps: (1) spinning the green fiber for the cell, (2) coating the green fiber with the cell boundary material, (3) lay-up of the coated green fibers, (4) consolidation of the soft fibers into a monolithic green body, (5) binder burnout, (6) densification by sintering or hot-pressing.

(1) Fiber Spinning and Coating

Green fibers are made from any fine ceramic powder and appropriate polymer binders. The polymer system depends upon the fabrication method, with thermoplastics used for melt spinning, and solvent-borne resins used for dry spinning. Ease of processing and good binder behavior are the major considerations in polymer selection. The polymer should produce a flexible green fiber which can be easily deformed during consolidation. Green fibers can be made by any of the conventional fiber-forming methods, including suspension dry spinning,[12,13] thermoplastic melt spinning,[14,15] or wet spinning of rayon viscose suspensions.[16] We prepare fibers by dry spinning and melt spinning.

Dry spinning is convenient for small batches. The dry spinning "dope" is prepared rather like a tape casting slip. In the first ball milling step, the ceramic powder is dispersed in a volatile solvent. The polymer solution is added, followed by a second ball milling step to homogenize the slip, producing a dilute slip. Next the slip is concentrated by evaporating the solvent to produce the viscous spinning dope. The dope is extruded into a drying column to produce the fibers.

The dry-spun fibers used in this work had a dry composition of 55–60 vol% ceramic powder + 40–45 vol% ethyl methacrylate (EMA) copolymer (Acryloid B-7 MEK, Rohm and Haas, Philadelphia, PA). The solvent was methyl ethyl ketone (MEK). The ceramic powders in the green fiber that ultimately form the cell phases are listed in Table I. For extrusion, the dope was loaded into a dispensing syringe with a pneumatic piston, and forced through a 330-μm orifice into a drying column at 85–110°C. For our particular extrusion and drying conditions, spinnable dopes had solvent concentrations in the range of 60–70 vol% MEK solvent. The preferred compositions, temperatures, and processing variables are reported elsewhere.[12]

Figure 3(A) shows a typical dry-spun green fiber with an area-equivalent circular diameter of ≈175 μm. Notice the "dog-bone" cross section, an artifact of the high evaporation to diffusion rate ratio during dry spinning in this particular system. A high-magnification view (Fig. 3(B)) shows the edge of a coated fiber. The fiber contains a SiC (+ Y_2O_3, Al_2O_3) ceramic powder and the EMA polymer. We find that unplasticized EMA contents should be at least 20 vol% for lamination of the green fibers into monolithic bodies. Polymer contents of 40–50 vol% are preferred for convenient handling of green fibers.

Melt-spun fibers were prepared using methods similar to those described by Frechette *et al.*[15] Here the ceramic powder is compounded with a thermoplastic, as in the preparation of injection molding mixes. We use a Brabender Plasticorder (C. W. Brabender Instruments, Inc., South Hackensack, NJ) heated to the appropriate temperature, such as 170–180°C for polypropylene (PP) or 180–190°C for ethylene vinyl acetate (EVA) (Elvax 470 Du Pont, Wilmington, DE). The resin is melted, and the ceramic powder gradually added while compounding to produce a homogeneous blend. The spinnable mix is a leathery compound consisting of 50 vol% ceramic powder. Our extruder is a piston-style machine requiring a cylindrical feedrod, so the compounded mix is next formed into a 1-cm-diameter feedrod by compression molding. The feedrod is loaded into the fiber extrusion machine (Bradford University Research, Ltd., Bradford, U.K.) and extruded through a spinnerette. Extrusion conditions depend upon the particular system. For silicon nitride–EVA green fiber with a 250-μm single-hole orifice, for example, we extrude at 215°C and 1–3 MPa. The fiber cools rapidly and is taken up on a cross-wound spool about 1 m below the extruder. Unlike the dry-spun fiber, melt-spun fiber is uniform and round. In this study, only Si_3N_4 green fibers were melt-spun. All other materials were dry-spun.

The cell boundary material is applied by a simple dip coating process in which the green fibers are drawn through a suspension of the coating material. The thickness of the coating is determined by the concentration of the suspension. Figure 3(B) shows a ≈1-μm-thick graphite coating on SiC green fiber. The graphite slurry is simply a commercial aqueous graphite paste (Aquadag, Acheson Colloid, Port Huron, MI), diluted with 2-propanol to a low-viscosity suspension of ≈3 vol% solids. We find that this adheres well to dry-spun fibers with EMA binders. This simple coating is too brittle for melt-spun fibers, which are respooled after coating, so a latex binder (LPR 6632A carboxylated styrene butadiene rubber latex, Goodyear Tire and Rubber Co., Calhoun, GA) is added to the coating slurry to make it adherent and flexible. Boron nitride coatings are applied with a commercial aqueous BN coating slurry (BN Paint, ZYP Coatings, Oak Ridge, TN). The slurry is supplied with 25 wt%

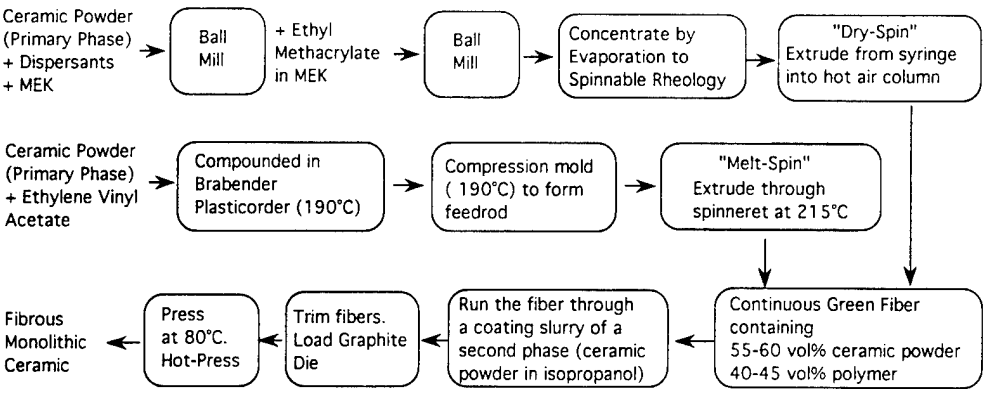

Fig. 2. Flow chart describing fabrication procedure of fibrous monoliths.

Table I. Fibrous Monolith Systems and Fabrication Conditions

Cell material	Cell boundary material	Sintering conditions	Cell ceramic grain size	Cell boundary grain size	Density and open porosity
(1) SiC* + 4 wt% Y_2O_3† + 6 wt% Al_2O_3‡	Graphite	Hot-pressed 1900°C, 1 h, 25 MPa	2–4 μm equiaxed	1–5 μm aligned graphite flakes	3.07 g/cm³, 2.4% open pores in graphite
(2) Si_3N_4§ + 9 wt% Y_2O_3† + 3 wt% Al_2O_3‡	BN	Hot-pressed 1750°C, 1 h, 25 MPA	0.2–0.5 μm equiaxed	2–10 μm aligned BN flakes	3.24 g/cm³, 0% open pores
(3) ZrO_2–12 mol% CeO_2¶	Al_2O_3 + 50 vol% ZrO_2–12 mol% CeO_2	Sintered 1500°C, 2 h	2 μm Ce–ZrO_2	1 μm for Ce–ZrO_2 and Al_2O_3	5.67 g/cm³, 0.4% open pores
(4) Al_2O_3**	Al_2TiO_5	Hot-pressed 1400°C, 0.5 h, 25 MPa	1–2 μm for alumina	2–4 μm Al_2TiO_5	0% open pores
(5) Al_2O_3‡ + 4 vol% ZrO_2–3 mol% Y_2O_3††	Al_2O_3 + 35 vol% unstab. ZrO_2	Hot-pressed 1450°C, 1 h, 25 MPa	0.5–1 μm for alumina	0.5–1 μm alumina and zirconia	4.05 g/cm³, 0% open pores
(6) Al_2O_3‡	Ni	Hot-pressed 1400°C, 1 h, 25 MPa	1–2 μm for alumina		4.13 g/cm³, 0% open pores

*B-10 β-SiC, Hermann C. Starck, Inc., NY. †Johnson Matthey Co., Ward Hill, MA. ‡RC-HP DBM, Malakoff Industries, Malakoff, TX. §E-10, Ube Industries, Tokyo, Japan. ¶TZ-12Ce, 12 mol% CeO_2–ZrO_2, Tosoh USA, Atlanta, GA. **AKP-50, Sumitomo Chemicals, Tokyo, Japan. ††TZ-3Y, Tosoh USA, Atlanta, GA.

solids, with the solids consisting of 87.5 wt% BN and 12.5 wt% alumina.

To produce cell boundaries of aluminum titanate on alumina green fibers, we use a slurry containing the appropriate ratio of reactive submicrometer alumina (RC-HP DBM Malakoff Industries, Malakoff, TX) and titania (J. T. Baker Chemical Co., Phillipsburg, NJ) powders in 2-propanol. The aluminum titanate phase forms via solid-state reaction during sintering. Alumina–zirconia cell boundaries are created by coating alumina green fibers with a similar slurry containing alumina (Malakoff Industries) and unstabilized zirconia powder (SC-101, Magnesium Elektron, Inc., Flemington, NJ). The median particle size of the unstabilized zirconia powder was 0.9 μm. Metallic Ni cell boundaries are obtained by coating alumina green fibers with an aqueous suspension of NiO (N-69, Fisher Scientific Co., Fairlawn, NJ). Reduction to metallic nickel occurs during hot pressing. To produce cell boundaries of Ce-zirconia + alumina on Ce-TZP fibers, we use a slurry containing Ce-zirconia (TZ-12Ce, Tosoh USA, Atlanta, GA) and alumina (Malakoff Industries) powders. All oxide coating slurries contained ≈10 vol% solids.

(2) Forming

The fibrous monoliths are formed by warm-pressing a green fiber preform. We make random compacted felt preforms by simply compressing a tangled mass of fiber. Uniaxial layups are made by arranging the green fibers in a uniaxial pattern prior to compaction. Coated green fibers can also be chopped to <4-mm lengths, simply poured into the die and pressed. Compaction is conducted at temperatures above the glass transition temperature of the ethyl methacrylate copolymer (40°C) where the fibers are soft enough to mold under pressure and laminate into a solid monolith. Typically we load the coated green fiber preform into a cold die, warm the assembled die to 80°C, then compress the preform at 60 MPa in a Carver press. This temperature–pressure condition is sufficient to entirely collapse all the voids between the green fibers.

Uniaxial compaction adds an additional texture to the fibrous monolith, since the soft fibers are mostly deformed along the

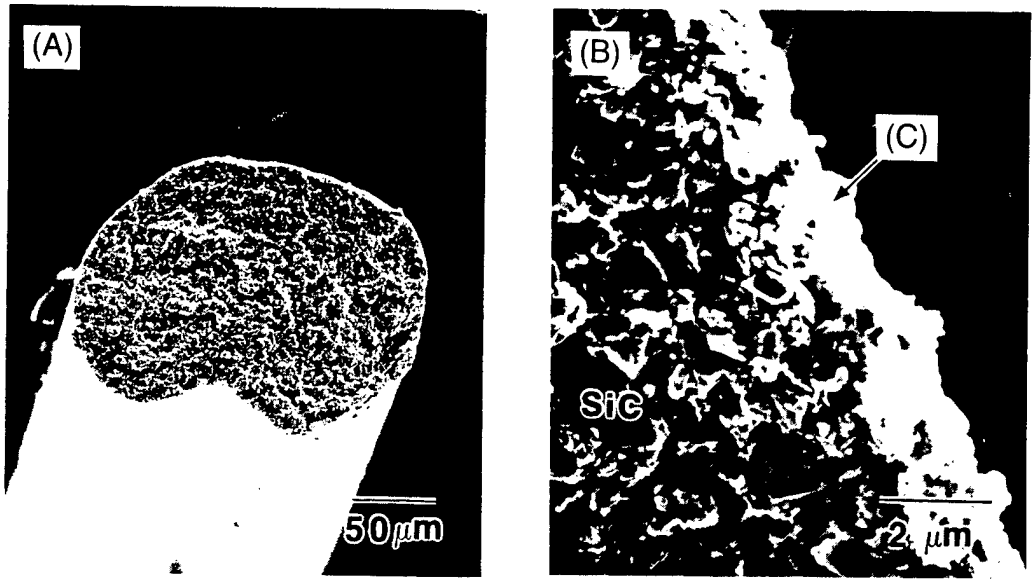

Fig. 3. SEM micrographs of the cross section of a coated SiC green fiber produced by dry spinning: (A) low-magnification view showing fiber cross section; (B) higher-magnification view near the edge. The fiber consists of SiC (+ Y_2O_3,Al_2O_3) powder and ethyl methacrylate. The colloidal graphite (C) coating is indicated by arrow.

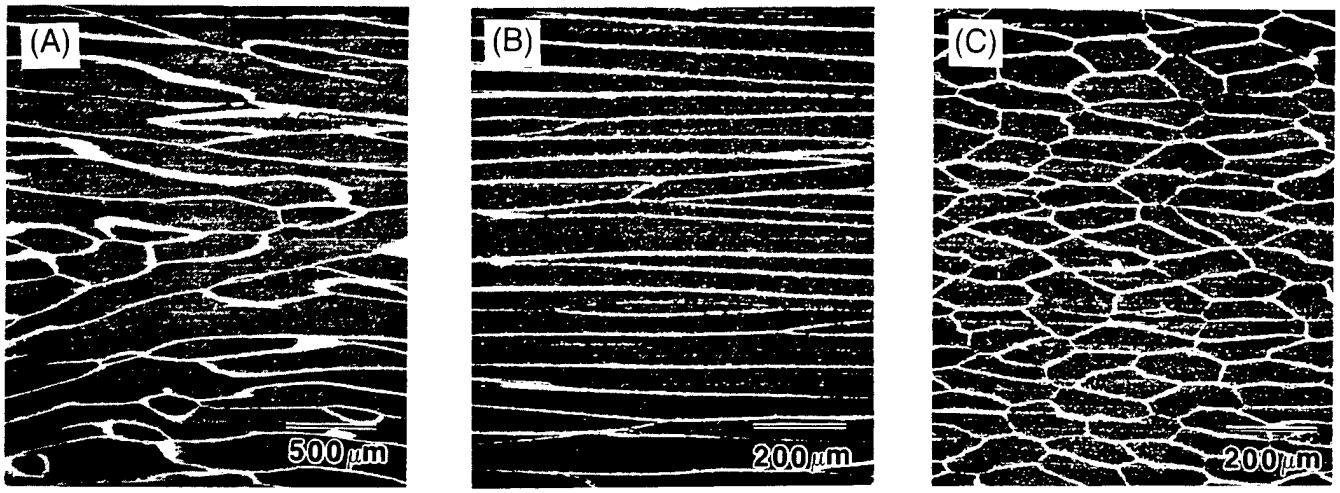

Fig. 4. Ground surfaces of a dense SiC/graphite fibrous monolith prepared with aligned fibers showing polycrystalline SiC cells (gray) and graphite cell boundaries (white): (A) viewed in the hot-pressing direction, (B) viewed normal to the hot-pressing direction, (C) end-on view. Fibers were aligned left–right in (A) and (B).

compression axis. Thus typical green fibers with ≈175-μm equivalent diameters are flattened during warm pressing, and further deformed during uniaxial hot pressing, resulting in cells only ≈60 μm thick and ≈200 μm wide after densification. This imparts distinct transverse versus longitudinal microstructure.

The green fibrous monolith undergoes a conventional binder burnout followed by sintering or hot pressing. For oxides sintered in air, binder burnout is done in air. The heating schedule depends upon the size of the green part. For 7-cm^3 green billets (5.2 cm wide, 2.6 cm long, and 0.5 cm thick), we heat at 60°C/h to 600°C. After binder removal, oxide pellets or billets are isostatically pressed in rubber bags to 310 MPa, and then sintered. The Ce-TZP-based fibrous monolith was fabricated using this procedure. For nonoxide materials which are hot-pressed, such as silicon carbide–graphite, binder removal is accomplished by heating in the graphite die in an actively pumped vacuum. We remove the binder from 7-cm^3 billets by heating at 260°C/h to 800°C, while the part is in the graphite die, before hot pressing. For the alumina/aluminum titanate fibrous monoliths, binder removal and sintering can be done in air, but we chose to hot-press in alumina packing powder for convenience.

(3) Densification and Microstructural Development

Densification is accomplished by sintering or hot pressing at the temperatures appropriate for the particular powder. Table I lists the densification conditions for several systems, along with several microstructural characteristics, such as the grain size of the cell ceramic and the cell boundary material, as estimated from micrographs. Systems 1 and 2, the silicon carbide and silicon nitride materials, are hot-pressed with an yttria–alumina liquid-phase sintering aid. The oxide materials are nominally solid-state densified. The ceria–zirconia fibrous monolith, system 3, was pressureless sintered. All three alumina-based fibrous monoliths were hot-pressed. The aluminas were undoped. Systems 4 and 6 did not have a grain growth inhibitor, while system 5 included 4 vol% of 3Y-TZP as a second-phase grain growth inhibitor.

The volume fraction of the cell boundary phases are not exactly known, since the green coating thicknesses are not precisely controlled. Hence we do not know the theoretical densities of the fibrous monoliths. The densities and open porosity, as determined by the water immersion method, are included in Table I. The cell phases in all materials are essentially fully dense. None of the systems imbibe water, so they have no apparent open porosities. The alumina–Ce–zirconia cell boundary phase in the pressureless sintered system 3 appears to have some porosity (or pullout) in polished sections, but the porosity must be too small to cause measurable water adsorption. In the case of the SiC/graphite, system 1, the cells are fully dense, but we infer a porosity of 30% within the graphite cell boundaries. Since the graphite is present at only 4 wt% overall, this corresponds to about 2.4 vol% porosity. This material does not adsorb water, so the porosity in the graphite phase is inferred indirectly.[11] Fabricated graphites are always porous, so we expect some porosity in the graphite cell boundaries. We assume that the silicon nitride/boron nitride analogue, system 2, has a similar amount of porosity in the BN cell boundaries, although this material also does not adsorb water.

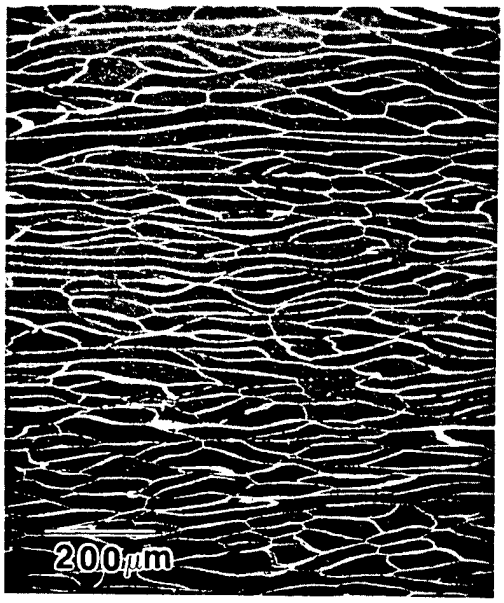

Fig. 5. SEM micrograph of a polished surface of a SiC/graphite fibrous monolith prepared with finely chopped randomly oriented fibers. Viewed normal to the hot-pressing direction.

It should be emphasized that the fibrous monolith structure develops from the heterogeneous cell boundary material. Simple uncoated green fiber, if it is made from equiaxed powder, leaves no trace of the original fibers after consolidation and densification.* We have hot-pressed uncoated SiC green fiber

*However, anisometric particles, flakes, or platelets are aligned during fiber spinning and leave a distinct texture. We are exploring systems such as compacted green fibers of alumina powder + alumina platelets and SiC powder + graphite flakes to produce monolithic ceramics containing locally oriented features.

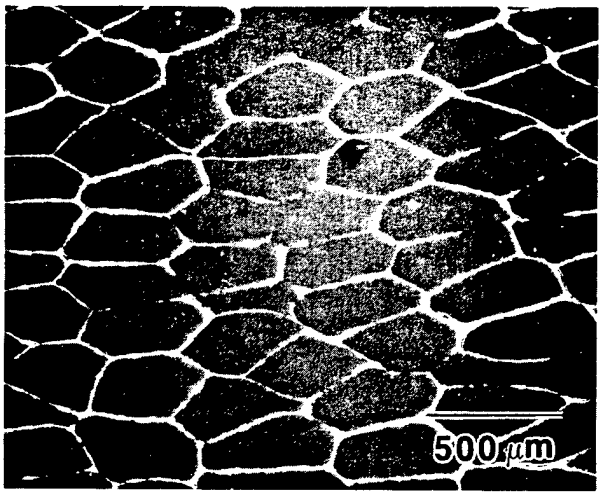

Fig. 6. End-on view of an aligned Si_3N_4/BN fibrous monolith prepared with melt-spun fibers. The BN(+ Al_2O_3) appears bright in the SEM micrograph.

and found no evidence of the fibers in polished sections and fracture surfaces. Similarly, uncoated green fibers of silicon nitride (with yttria + alumina) form monolithic hot-pressed silicon nitride with a microstructure indistinguishable from a body fabricated from ordinary powder.

The cell and cell boundary structure of a fibrous monolith with aligned fibers is illustrated in Fig. 4(A), which is an SEM micrograph of a ground surface of system 1, the SiC–graphite fibrous monolith. The polycrystalline SiC cells and graphite cell boundaries are viewed in the hot-pressing direction. The coated fibers had been placed lengthwise from left to right and then pressed. The SiC fibers are greatly flattened in this direction, creating cells about 200 μm wide. Note that the width of the graphite cell boundaries are exaggerated by this flattening and the preferential polishing of the soft graphite. A view transverse to the hot-pressing direction, Fig. 4(B), shows that the cells are about 65 μm wide in this dimension. The cell lengths vary from a few hundred micrometers to several millimeters. The end-on view of uniaxially aligned SiC/graphite is presented in Fig. 4(C). The cross section of a pellet that was prepared with randomly oriented finely chopped fibers is shown in Fig. 5. The average width of the cells is again about 60 μm but the cell length varies from only 200 to 600 μm. The graphite cell boundary varies from 1 to 10 μm in thickness.

For other fibrous monolith systems, the microstructural dimensions are slightly different. The cell widths depended on how much draw could be obtained during dry spinning, and cell boundary thickness was controlled by coating thickness. The relevant dimensions are mentioned in Section III.

Melt-spun green fibers produce fibrous monoliths with a more uniform network of cells and cell boundaries, a consequence of the constant diameter of melt-spun green fibers. Also, the average cell diameter is larger, a consequence of the larger fiber diameters obtained with our current melt-spinning polymer formulation and spinnerette size. Figure 6 shows an end-on view of a uniaxially aligned silicon nitride/BN fibrous monolith prepared from melt-spun fibers, containing about 10 vol% boron nitride. The cells are ≈165 by ≈360 μm in size.

III. Microstructural Effects on Indentation Behavior

Vickers indentations[*] on the surface give rise to complex crack patterns. The size of the indentations are similar to the cell size, so the fibrous monoliths are quite heterogeneous on the scale of the indentation. Conventional radial/median cracks[17] do not always form, so indentation methods cannot be used to measure fracture toughness. Nonetheless, crack patterns from indentations serve to illustrate how cracks interact with the cells and cell boundaries. Indentation behavior was studied on randomly oriented chopped fiber monoliths for all systems except for the Ce-TZP/alumina and Si_3N_4/BN systems for which aligned-fiber samples were used. All indentation work shown in this study was done on cross-sectional surfaces parallel to the hot-pressing direction.

(1) SiC/Graphite and Si_3N_4/BN

In the weak interface fibrous monoliths, indentation damage is shown in Fig. 7(A), which is an SEM micrograph of a 50-N Vickers indentation. In this orientation, the cells are relatively narrow, but deep. Indentation causes cells to spall. The stress field around indentations causes subsurface lateral cracks;[17] the dislodgement of intact cells can be facilitated by lateral cracks along weak cell boundaries. The higher-magnification micrograph in Fig. 7(B) of the same indentation shows that long radial cracks do not emanate from the indentation corner. Instead, some cells are partially cracked and graphite is extruded from the cell boundaries. At lower loads, where the indentation is smaller than the cell size, radial cracks are confined to a single cell, and tend to arrest at the cell boundary. This is illustrated in Fig. 7(C) for an 8-N indent, where radial cracks running up and down do not propagate past the cell boundaries. On surfaces normal to the hot-pressing direction, the cells are wide but shallow; indentation behavior is similar except there is a greater tendency to spall. Silicon nitride/BN fibrous monoliths behave similarly. Silicon nitride cells spall but BN does not appear to extrude from the cell boundaries.

(2) Alumina /Alumina–Zirconia

A series of specimens was fabricated in an attempt to develop a microcracked cell boundary containing alumina and unstabilized zirconia. The amount of unstabilized zirconia in the cell boundary was either 20, 35, or 50 vol%. These compositions were simply chosen on the basis of Claussen's *pressure zones*[2,18] in duplex structures. The cell width was ≈40 μm (normal to the pressing direction) and the cell length varied from 100 to 300 μm. The cell boundary thickness ranged from ≈3 to ≈20 μm. The sample with a cell boundary containing 50 vol% ZrO_2 cracked on cooling from the hot-pressing temperature. Clearly there was too much residual stress and microcracking to maintain sample integrity. Samples where the cell boundaries contained 20 or 35 vol% ZrO_2 were sound. In system 5, with cell boundaries containing 35 vol% unstabilized zirconia, X-ray diffraction of a polished surface showed that a significant amount of tetragonal zirconia (≈58 vol%; ≈42 vol% was monoclinic[19]) was present. The tetragonal phase reflects contributions from both the 4 vol% 3Y-TZP in the cells and the unstabilized tetragonal zirconia retained in the cell boundaries. When indentations (400-N load) were oriented such that indent diagonals were parallel and perpendicular to the pressing direction, cracks normal to the pressing direction preferred to grow along the "weak" cell boundaries. But cracks parallel to the pressing direction were unaffected by cell boundaries. When indentations were oriented such that the radial crack directions were inclined at 45° to the pressing direction, cells were observed to spall. Cracks from the indentations were not symmetric and showed some tendency to propagate along cell boundaries (see Fig. 8).

(3) Alumina /Aluminum Titanate

The alumina–aluminum titanate fibrous monolith, system 4, had cell widths of 39–40 μm (normal to the pressing direction) and cell lengths of 150–300 μm. Cell boundary thickness was 5–10 μm. X-ray diffraction confirmed that all the titania from the alumina + titania cell boundaries had fully reacted to form Al_2TiO_5. The grain size in the cell boundary was 2–4 μm.

[*] All indentation work was done with a Vickers diamond on a Zwick machine (Zwick of America, Inc., E. Windsor, CT) with 30-s residence time.

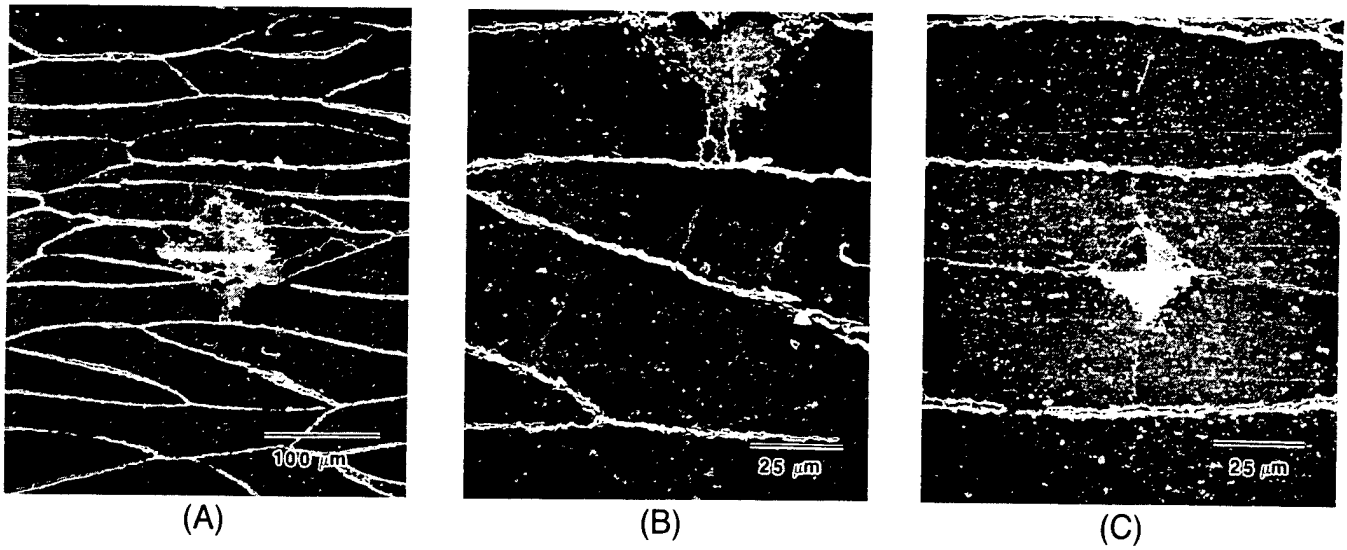

Fig. 7. SEM micrographs of indentation crack patterns in a SiC/graphite fibrous monolith. Indentation load was 50 N in (A) and (B) and 8 N in (C).

Extensive microcracking is known to occur at grain sizes of 3–4 μm in single-phase polycrystalline Al_2TiO_5.[7,8]

Figure 9 shows a typical radial/median indentation crack running through an aluminum titanate cell boundary. No significant crack deflections or spalling were observed at these aluminum titanate cell boundaries with various indentation loads and orientations. We conclude that this multiphase layout with these particular microstructural dimensions does not generate large stress fields to affect indentation cracking in this system.

(4) Ce-TZP/Alumina + Ce-Zirconia

The Ce-TZP/alumina–Ce–zirconia system aligned-fiber monolith consisted of Ce-TZP cells ≈50–100 μm in width (normal to the pressing direction), with alumina–Ce–zirconia cell boundaries ≈10–50 μm in thickness. From density measurements, we infer that the material consists of 75 vol% Ce–zirconia + 25 vol% alumina, but fabricated as a fibrous monolith with pure Ce-TZP cells, and cell boundaries with a composition of 50 vol% Ce–zirconia + 50 vol% alumina. Thus the cells occupy 50 vol% of the material, and the cell boundaries occupy 50%.

An optical micrograph (Nomarski interference) of a 200-N indentation in this system is shown in Fig. 10. The bright regions in the Ce-TZP cells near (especially above) the indentation show the uplift of transformed regions, indicating that transformation zone shapes can be modified by adopting this microstructural design. Compared to the colloidally fabricated Ce-TZP/alumina laminates,[10] there is less uniformity in microstructural dimensions in the fibrous monolith. The shape of the indentation and the asymmetric nature of the transformation zone uplift reflect the nonuniformity in cell/cell boundary dimensions and cell depth beneath the surface. However, there

Fig. 8. Indentation fracture in an alumina/(alumina + zirconia) fibrous monolith. Viewed normal to the hot-pressing direction. Indentation (400-N load) diagonals oriented at 45° to the hot-pressing direction. Arrows indicate cracks from the indentation. The cell boundaries appear bright in the SEM micrograph.

Fig. 9. SEM micrograph showing indentation crack (100-N load) intersecting an aluminum titanate cell boundary in an alumina (A)/aluminum titanate (AT) sample.

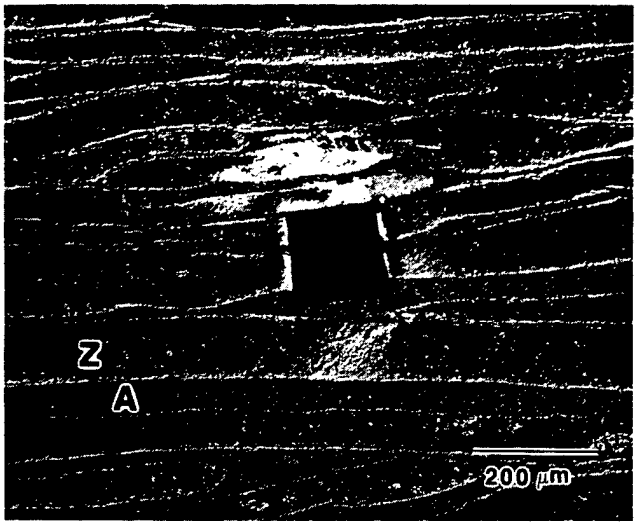

Fig. 10. Optical micrograph (Nomarski interference) of a 200-N indentation in an aligned-fiber Ce-TZP/alumina–Ce–zirconia sample. Viewed normal to the hot-pressing direction. Z = Ce-TZP, A = alumina + Ce-zirconia.

is clearly potential for developing tough Ce-TZP/alumina fibrous monoliths.

(5) Alumina/Nickel

Some preliminary experiments show that it is feasible to produce a fibrous monolith with ductile phase cell boundaries. Figure 11(A) shows the polished surface, viewed in the hot-pressing direction, of an alumina/Ni fibrous monolith, system 6. The cell widths were again about 200 μm viewed in the pressing direction and 40–60 μm normal to the pressing direction. This specimen was a random compacted felt. It was difficult to polish this specimen, and the amount of Ni is greatly exaggerated by polishing artifacts. Density measurements indicate that the actual volume fraction of nickel is only about 3%. This is consistent with the appearance of the fracture surface of a broken pellet (Fig. 11 (B)). In the central part of Fig. 11(B), where the alumina cells are oriented horizontally, the nickel can be seen to consist of thin ribbons between the polycrystalline alumina cells. The ductility of the nickel and its weak adhesion to the alumina are indicated by the peeled-off nickel ribbons. The data of Tuan and Brook[20] for particulate alumina–Ni show a significant toughening increment with Ni additions. Improved toughness and noncatastrophic fracture behavior in alumina–Ni fibrous monoliths will be reported in a subsequent paper. Indentation behavior in this system was not studied.

IV. Flexural Strength of SiC/Graphite

Strengths were measured for the SiC/graphite system with aligned fibers using ≈3 mm × 4 mm × 47 mm specimens tested in four-point bending with a 20-mm inner span and 40-mm outer span at a crosshead speed of 0.05 mm/min. Specimens had been machined and chamfered with a 1000-grit resin-bonded diamond wheel, with the machining direction along the axis of the bar.

The SiC/graphite fibrous monoliths showed unusual and potentially useful fracture behavior. Failure in flexure occurred in a noncatastrophic manner. A typical load–deflection curve for this system is shown in Fig. 12(A). The fibrous monolith behaves like a typical monolithic ceramic until a stress of ≈220 MPa is reached at the tensile surface, beyond which the load drops in a gradual manner. Load drops were accompanied by shear delamination along the graphitic cell boundaries which were parallel to the tensile surface. The bar specimen was removed when the load was less than 30 N, and pulled apart by hand. The fracture surface is shown in Fig. 12(B). The terraced appearance reflects the deflection of the crack path at each successive cell boundary and delamination along the cell boundaries. The apparent work-of-fracture evaluated from the load deflection curve was ≈1450 J/m^2. The work-of-fracture measured for fibrous materials will depend on the loading configuration[21] and specimen dimensions, but the calculated value demonstrates the high *toughness* possible in weak interface fibrous monolithic ceramic systems. The fracture behavior of SiC/graphite fibrous monoliths is presented in detail elsewhere.[11]

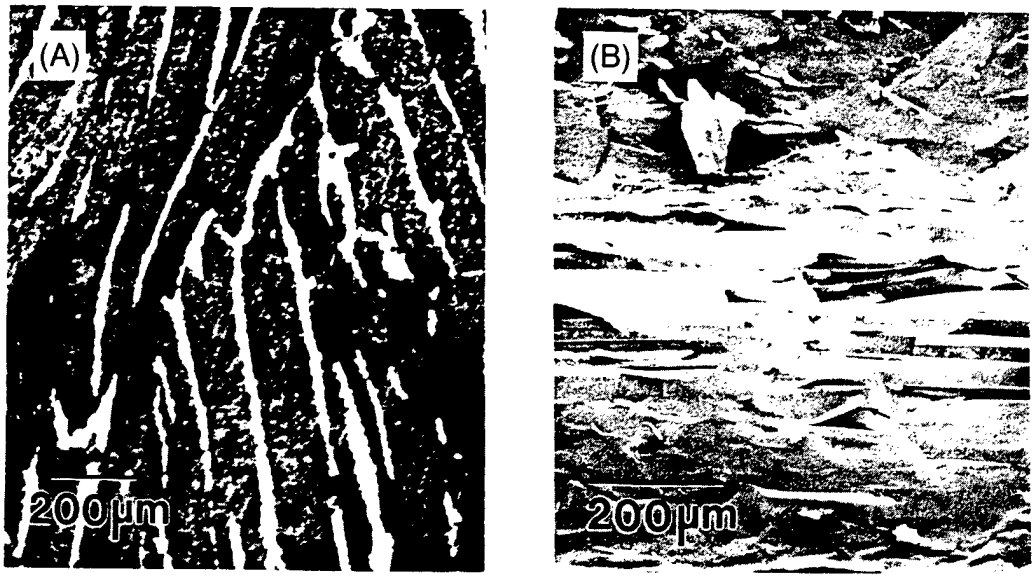

Fig. 11. (A) Optical micrograph of a polished surface of an alumina/Ni fibrous monolith viewed in the hot-pressing direction. (B) SEM micrograph of a fracture surface of an alumina/Ni fibrous monolith. Peeled-off nickel ribbons indicated by arrows.

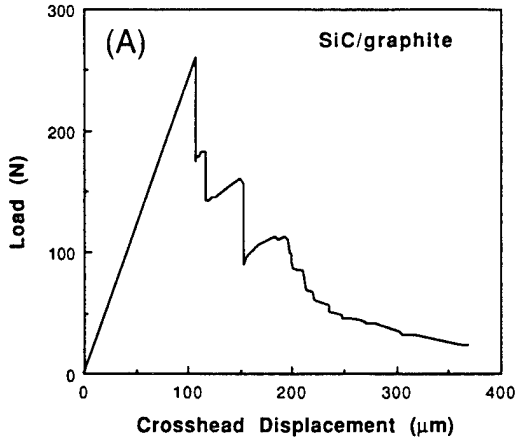

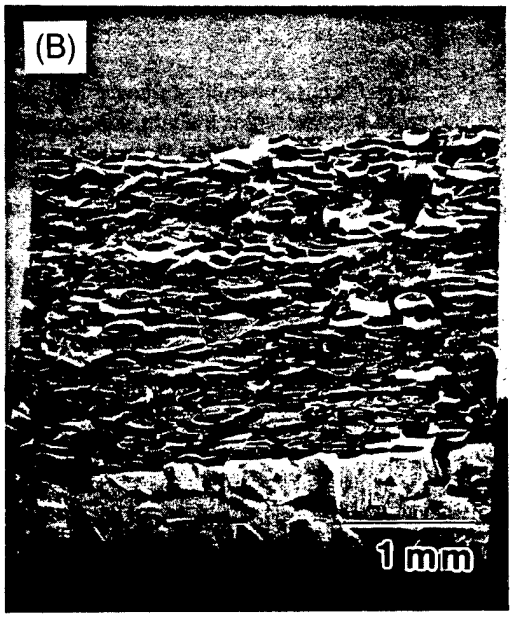

Fig. 12. (A) Load–deflection curve for a SiC/graphite fibrous monolith bend specimen prepared with aligned fibers. (B) Fracture surface of the sample. The compressive side of the bar specimen is visible in the lower part of the SEM micrograph.

V. Conclusion

We have demonstrated the fabrication of dense fibrous monolithic ceramics from coated ceramic green fiber to create microstructures with high aspect ratio polycrystalline cells separated by thin cell boundaries to improve the mechanical properties. A variety of ceramic systems have been fabricated in fibrous monolith form, demonstrating the versatility of this processing route/microstructural design. Indentation fracture in these materials is complex as would be expected in a dual-phase microstructure, with dimensions comparable to the indentation.

Our results indicate that weak-interface fibrous monoliths such as SiC/graphite or Si_3N_4/BN have potential as damage-tolerant materials. In these materials, controlled damage around indentations prevents the formation of long radial cracks. Also, preferential crack propagation along the graphitic cell boundaries, which act as weak interfaces, leads to noncatastrophic failure by shear delamination in SiC/graphite, a behavior similar to ceramic-matrix composites reinforced by high-strength fibers.

Several oxide-based fibrous monoliths are also promising. Indentation of alumina/alumina–zirconia fibrous monoliths results in complex crack patterns and spalling in some orientations. Potential also exists for developing useful Ce-TZP/alumina fibrous monoliths. Transformed regions near indentations are altered by the alumina-containing cell boundaries. Fibrous monoliths were also fabricated in the alumina/aluminum titanate and alumina/nickel systems. Further work is required to establish whether suitably engineered aluminum titanate cell boundaries can be useful. With higher amounts of nickel, the fibrous monolith approach offers a convenient method of fabricating textured ceramics containing ductile, metallic interphases.

Acknowledgments: We thank Timothy Fretter and Lynne Svedberg for their valuable assistance in the laboratory.

References

[1]M. P. Harmer, H. M. Chan, and Gary A. Miller, "Unique Opportunities for Microstructural Engineering with Duplex and Laminar Ceramic Composites," *J. Am. Ceram. Soc.*, **75** [7] 1715–28 (1992).

[2]W. J. Clegg, K. Kendall, N. McN. Alford, T. W. Button, and J. D. Birchall, "A Simple Way to Make Tough Ceramics," *Nature (London)*, **347**, 455–57 (1990).

[3]N. Claussen, "Microstructural Design of Zirconia-Toughened Ceramics (ZTC)"; pp. 325–51 in Advances in Ceramics, Vol. 12, *Science and Technology of Zirconia II*. Edited by N. Claussen, M. Rühle, and A. H. Heuer. American Ceramic Society, Columbus, OH, 1984.

[4]S. J. Bennison, N. P. Padture, J. L. Runyan, and B. R. Lawn, "Flaw-Insensitive Ceramics," *Philos. Mag. Lett.*, **64** [4] 191–95 (1991).

[5]N. P. Padture, S. J. Bennison, and H. M. Chan, "Flaw-Tolerance and Crack Resistance Properties of High Toughness Alumina–Aluminum Titanate Composites with Tailored Microstructures," *J. Am. Ceram. Soc.*, in press.

[6]W. S. Coblenz, "Fibrous Monolithic Ceramic and Method for Production," U.S. Pat. No. 4 772 524, September 20, 1988.

[7]F. J. Parker and R. W. Rice, "Correlation between Grain Size and Thermal Expansion for Aluminum Titanate Materials," *J. Am. Ceram. Soc.*, **72** [12] 2364–66 (1989).

[8]J. J. Cleveland and R. C. Bradt, "Grain Size/Microcracking Relations for Pseudobrookite Oxides," *J. Am. Ceram. Soc.*, **61** [11–12] 478–81 (1978).

[9]J. L. Runyan and S. J. Bennison, "Fabrication of Flaw-Tolerant Alumina–Aluminium Titanate Composites," *J. Eur. Ceram. Soc.*, **7**, 93–99 (1991).

[10]D. B. Marshall, J. J. Ratto, and F. F. Lange, "Enhanced Fracture Toughness in Layered Microcomposites of Ce–ZrO_2 and Al_2O_3," *J. Am. Ceram. Soc.*, **74** [12] 2979–87 (1991).

[11]S. Baskaran and J. W. Halloran, "Fibrous Monolithic Ceramics: II. Flexural Strength and Fracture Behavior of the Silicon Carbide/Graphite System," *J. Am. Ceram. Soc.*, **76** [9] 2217–24 (1993).

[12]S. D. Nunn, D. Popovic, S. Baskaran, J. W. Halloran, G. Subramanian, and S. G. Bike, "Suspension Dry Spinning and Rheological Behavior of Ceramic Green Fibers," *J. Am. Ceram. Soc.*, in review.

[13]L. D. Hart and A. Pearson, "Production of Continuous Ceramic Fibers: Polyethylene Oxide Polymers," U.S. Pat. No. 4 071 594, January 31, 1978.

[14]J. W. Halloran, J. D. Hodge, D. Chandler, L. J. Klemptner, M. J. Neal, M. V. Parish, H. D. Park, V. M. Pathare, G. Bakis, and D. Eagles, "Fabrication and Properties of High Temperature Superconductor Wire by the Green Fiber Method," *J. Am. Ceram. Soc.*, **75** [4] 903–907 (1992).

[15]F. J. Frechette, W. D. G. Boecker, C. H. McMurtry, and M. R. Kasprzyk, "Non-Oxide Sintered Ceramic Fibers," U.S. Pat. No. 4 908 340, March 13, 1990.

[16]R. B. Cass, "Fabrication of Continuous Ceramic Fiber by the Viscous Suspension Spinning Process," *Am. Ceram. Soc. Bull.*, **70** [3] 424, 426, 428–29 (1991).

[17]B. R. Lawn and M. V. Swain, "Microfracture beneath Point Indentations in Brittle Solids," *J. Mater. Sci.*, **10**, 113–22 (1975).

[18]H. E. Lutz and N. Claussen, "Duplex Ceramics: I, Stress Calculations, Fabrication and Microstructure," *J. Eur. Ceram. Soc.*, **7**, 209–18 (1991).

[19]R. C. Garvie and P. S. Nicholson, "Phase Analysis in Zirconia Systems," *J. Am. Ceram. Soc.*, **55** [6] 303–305 (1972).

[20]W. H. Tuan and R. J. Brook, "The Toughening of Alumina with Nickel Inclusions," *J. Eur. Ceram. Soc.*, **6**, 31–37 (1990).

[21]A. G. Evans and D. B. Marshall, "Failure Mechanisms in Ceramic Fiber/Ceramic Matrix Composites," *J. Am. Ceram. Soc.*, **68** [5] 225–31 (1985). □

journal

J. Am. Ceram. Soc., 76 [9] 2217–24 (1993)

Fibrous Monolithic Ceramics: II, Flexural Strength and Fracture Behavior of the Silicon Carbide/Graphite System

Suresh Baskaran* and John W. Halloran*

Department of Materials Science and Engineering, University of Michigan, Ann Arbor, Michigan 48109

The fibrous monolith microstructure consists of high aspect ratio polycrystalline cells of SiC separated by thin cell boundaries containing graphite. The SiC/100% graphite fibrous monolith has noncatastrophic fracture behavior, is damage tolerant, and is notch insensitive. The failure process is characterized by fracture along weak graphite cell boundaries. The room-temperature flexural strength is 300–350 MPa. The estimated shear strength along the graphite cell boundaries is ≈15 MPa. Increasing the strength of the cell boundary by additions of SiC (40–60 vol%) results in a monolithic SiC material showing brittle fracture behavior but retaining damage tolerance. Strength and fracture behavior are also influenced by cell texture and orientation.

I. Introduction

SIGNIFICANT improvements in the mechanical properties of ceramic materials are obtained by microstructural design that promotes interactions of cracks with various microstructural features. Ceramics with duplex compositions have been shown to be flaw tolerant with *R*-curve behavior.[1] Laminar structures have been designed with useful characteristics like high work-of-fracture and graceful failure.[2,3] These microstructural designs and others can be created within a ceramic with additional spatial/dimensional control using the "fibrous monolith" processing approach introduced by Coblenz.[4] Fibrous monoliths are sintered (or hot-pressed) monolithic ceramics with a distinct fibrous texture, consisting of intertwined *cells* of a primary phase, separated by *cell boundaries* of a tailored secondary phase. In a previous paper,[5] the fabrication procedure, microstructure, indentation fracture, and preliminary mechanical properties were described for several fibrous monolithic ceramic systems. The microstructure is derived from a coated green fiber process whereby continuous green fiber containing the primary phase is coated with a slurry of the secondary phase. The coated fibers are pressed and fired, resulting in a monolithic ceramic with a fibrous microstructure.

The SiC/graphite system is an example of a *weak interface fibrous monolith* where the graphitic cell boundary phase acts as the preferred path for crack propagation. Weak interfaces can deflect cracks[6] or delaminate in shear, thereby increasing "toughness" and preventing brittle fracture. The high strain to failure and toughness of brittle ceramic matrices reinforced with high-strength fibers are a consequence of the weak bonding between the fibers and the matrix.[7,8]

In this paper, the fracture behavior of fibrous monoliths in the SiC/graphite system is described. The primary cell phase is polycrystalline SiC. The strength of the interfacial layer is controlled by adjusting the composition of the cell boundary from SiC to graphite. Strength is evaluated in flexure, and damage tolerance assessed by the strength of indented bar specimens. Notched beam tests are used to estimate fracture toughness.

II. Experimental Procedure

Green SiC fibers were prepared by dry spinning of an ethyl methacrylate/methyl ethyl ketone polymer solution loaded with ceramic powder. The starting material was β-SiC powder (B10, Hermann C. Starck, Inc., New York, NY) without sintering aids. Yttria (Johnson Matthey Co., Ward Hill, MA) and alumina (RC-HP DBM Malakoff Industries, Malakoff, TX) were added as sintering aids. The weight ratio of SiC:yttria:alumina was 90:4:6. The volume ratio of ceramic to polymer was 55:45.

The graphite coating slurry was prepared by diluting an aqueous graphite slurry (Aquadag, Acheson Colloid, Port Huron, MI) containing a proprietary binder with 2-propanol to ≈3 vol%. The silicon carbide coating slurry was prepared by milling SiC powder with yttria and alumina in 80 wt% 2-propanol/20 wt% distilled water, and subsequently adding some binder (Carbowax PEG 4000, Fisher Scientific Co., Fairlawn, NJ) to decrease settling and improve the coating properties. The powder solids loading was ≈3 vol%. Coating compositions containing various amounts of SiC to graphite (from 20:80 to 80:20) were prepared by mixtures of the graphite slurry and the milled SiC slurry in the appropriate ratios. The fiber was run through the coating bath immediately upon extrusion and collected on a spool.

The coated fibers were trimmed to ≈51 mm, loaded in a graphite die (26 mm × 52 mm), and pressed at ≈80°C using 5 MPa pressure. This collapsed the fibers and consolidated the material into a green monolithic billet. After binder removal between 200° and 600°C, the billet was hot-pressed at 1900°C in static argon for 1 h at 25 MPa. Most billets were prepared with green fibers aligned in the long direction in the die. A single billet was prepared with finely chopped (lengths <4 mm) randomly oriented fibers with 100% graphite as the fiber coating. In this case, the chopped fibers were simply poured into the die and pressed. The thickness of hot-pressed billets was ≈4.3 mm.

Billets with aligned fibers containing 100% graphite as the cell boundary were machined into bar specimens 4 mm wide and 48 mm long with thickness ranging from 1 to 4 mm. All bars were machined and chamfered with a 1000-grit resin-bonded diamond wheel, with the grinding direction parallel to the length of the specimen. The tensile surface was normal to the hot-pressing direction. Flexural strength was measured using a fully articulated four-point bend fixture with a 20-mm inner span and a 40-mm outer span at a crosshead speed of 0.05 mm/min. The range in specimen thickness provided span-to-depth ratios from 2.5 to 10. The stress values were evaluated from elastic beam equations.

Five bars (3-mm thickness × 4-mm width × ≈48-mm length) were machined from billets corresponding to each cell

R. Ruh—contributing editor

Manuscript No. 195253. Received October 5, 1992; approved May 17, 1993.
Supported by the Defense Advanced Research Projects Agency and the Office of Naval Research under Contract No. N0014-91-J-1999.
*Member, American Ceramic Society.

boundary composition. The tensile surface was again normal to the hot-pressing direction. Three bar specimens corresponding to each cell boundary composition were tested in the as-machined condition. The tension surfaces of the remaining two specimens from each composition were polished, indented with a 100-N load (Vickers indenter, Zwick of America, Inc., E. Windsor, CT), and tested in flexure. An identical procedure was also followed with the billet containing chopped fibers with 100% graphite as the cell boundary.

To determine the effect of texture from uniaxial hot pressing, three bar specimens (≈3 mm × 4 mm × 48 mm) were machined from a SiC/100% graphite billet containing aligned fibers, such that the tensile surface was parallel to the hot-pressing direction, and then tested in flexure.

Five bar specimens ≈4.50 mm × 2.25 mm × 48 mm in dimension were also machined from a SiC/100% graphite billet with aligned fibers. These specimens were notched in the center of the tensile face of the specimen with a 270-μm-thick diamond saw to a notch/height ratio of 0.4 (notch depth of ≈1.8 mm). The notch tip radius was ≈165 μm. The notched beams were tested in four-point flexure using the 20/40 mm fixture at a crosshead speed of 0.05 mm/min.

The side and tensile surfaces of some of the bar specimens used in the flexure and notch beam tests were polished with diamond paste to observe the fracture behavior optically during testing, and by scanning electron microscopy after the test. SEM was also used to characterize the fracture surfaces of the specimens.

III. Results and Discussion

(1) *Microstructure*

The microstructure of SiC/graphite fibrous monoliths with aligned fibers is illustrated in Fig. 1. Flattened SiC cells 60–100 μm thick and 150–200 μm wide are separated by thin cell boundaries. The cross section in Fig. 1(C) shows cells varying in length from about 200 μm to several millimeters in the long direction of the billet. Although long green fibers are placed in the die, the forming procedure can result in finite cell lengths. Green fibers can fracture or bend, and also may not lie perfectly normal to the pressing direction or perfectly parallel to the long die wall. The graphite cell boundaries vary in thickness from 1 to 10 μm, indicating some nonuniformity in fiber coating.

The total graphite content of the SiC/100% graphite fibrous monolith was 4 wt%, as determined by weight loss after 10-h oxidation at 800°C in air. Thermogravimetric analysis showed that weight loss was complete after 1 h at 700°C. After oxidation of the cell boundaries, the sample was essentially loosely bonded SiC cells which could be crushed by hand. The density of the SiC/100% graphite fibrous monolith was 3.07 g/cm^3, as measured by the Archimedes method. There was negligible open porosity. The polycrystalline SiC cells were seen to be pore-free by SEM. We can infer the density of the cells by comparison to the SiC/0% graphite fibrous monolith (i.e., hot-pressed SiC with yttria and alumina), which was 3.20 g/cm^3. By combining this information, we infer that the polycrystalline cells occupied ≈92 vol%, with the cell boundaries occupying ≈8 vol%. The cell boundaries themselves were porous, consisting of ≈70 vol% graphite and ≈30 vol% porosity. The cell phase was β-SiC, as determined by X-ray diffraction.

(2) *Flexural Strength Behavior of SiC/100% Graphite*

The load–deflection curve for a SiC/100% graphite flexure specimen of dimensions 3 mm × 4 mm × 48 mm, machined with the tension side (4 mm wide) normal to the pressing direction, is shown in Fig. 2(A). The apparent tensile stress on the surface increased linearly to a maximum value, followed by a gradual load decrease. The maximum flexural stress on the tension side was 215 MPa. Load drops were accompanied by shear cracking along the midplane of the specimen between the inner and outer loading points. Examination of the specimen after several load drops after deflection of ≈150 μm showed that the shear crack had extended along cell boundaries from the inner loading point to the edge of the specimen. The beam after unloading did not show any curvature or permanent strain. Reloading the specimen showed that the compliance of the specimen had increased. Further crosshead displacement resulted in extensive delaminations, and ultimately cracking below the inner loading point through the thickness of the beam. The side surface of the bent specimen is shown in Fig. 2(B).

The flexural behavior depends upon specimen thickness. For example, the load–deflection curve for a SiC/100% graphite specimen with a thickness of 1.2 mm is shown in Fig. 3. The maximum flexural stress was 322 MPa. Again, a linear increase in stress to the maximum value was followed by a gradual load decrease. Examination of specimens after testing showed that fracture originated at or near the tensile surface between the inner loading points, but was then followed by shear fracture almost parallel to the surface along the graphite cell boundaries. The splintered fracture morphology is illustrated in SEM photomicrographs of the side and tensile surfaces of a specimen after test (Figs. 4(A) and (B)). Fracture cells are visible on the tension side.

The fracture behavior in flexure is consistent with the change in ratio of the shear to tensile stress with decreasing thickness. For elastic beam conditions, the ratio (σ/τ) of tensile stress on the surface to shear stress in the midplane between the inner and outer loading points is equal to $2(L - l)/t$ where L and l are the inner and outer spans of the bend fixture and t is the thickness of the specimen.[9,10] $(L - l)/2$ is the separation distance between the inner and outer loading points. At low span-to-depth ratios ($(L - l)/2t < 5$), failure occurs when the shear stress reaches a critical value, and in this regime, maximum "flexural strength" should increase linearly with the inverse of thickness. The effect of specimen thickness on apparent flexural strength is shown in Fig. 5. The slope of the best-fit line through the data points at low span-to-depth ratios is proportional to the shear strength. The calculated shear strength of the graphite cell boundaries normal to the pressing direction is 15 MPa. This estimate of the shear strength falls within the range of peak shear strength values reported for carbon-rich interfacial layers in tough fiber-reinforced ceramics.[8] At high span-to-depth ratios ($(L - l)/2t \geq 8$), fracture initiates at the tension side, and the maximum flexural stress is not a function of thickness. The average flexural strength is 339 MPa.

The fracture behavior at low span-to-thickness ratios in this fibrous monolithic system is identical to the shear failure observed in ceramic matrices reinforced by high-strength fibers with short beam geometry.[10] But at high span-to-depth ratios, the material fails like wood,[11] with fracture behavior very similar to SiC-fiber-reinforced glass ceramic at high temperatures where higher interfacial shear strength decreases fiber pullout.[12]

(3) *Effect of Cell Boundary Composition*

The low shear strength of the graphite cell boundaries promotes delamination resulting in noncatastrophic failure. The shear strength of the cell boundaries can be increased by adding SiC (with yttria and alumina) to the graphite in the fiber coating. The effect of cell boundary composition on average flexural strength of SiC-based fibrous monoliths is shown in Fig. 6(A). The apparent work-of-fracture calculated from the area under the load–deflection curve and the specimen cross-sectional area is plotted in Fig. 6(B) as a function of cell boundary composition.

The mean flexural strength corresponding to the 100% graphite cell boundary was 216 MPa, with strengths ranging from 210 to 221 MPa. The actual value is not meaningful for this composition since failure for the sample dimensions used in this experiment is dictated only by the shear strength of the cell boundary. However, the value is useful for comparison with the average strength of indented samples which was almost 90% of the unindented strength. Indentation simply results in spalling

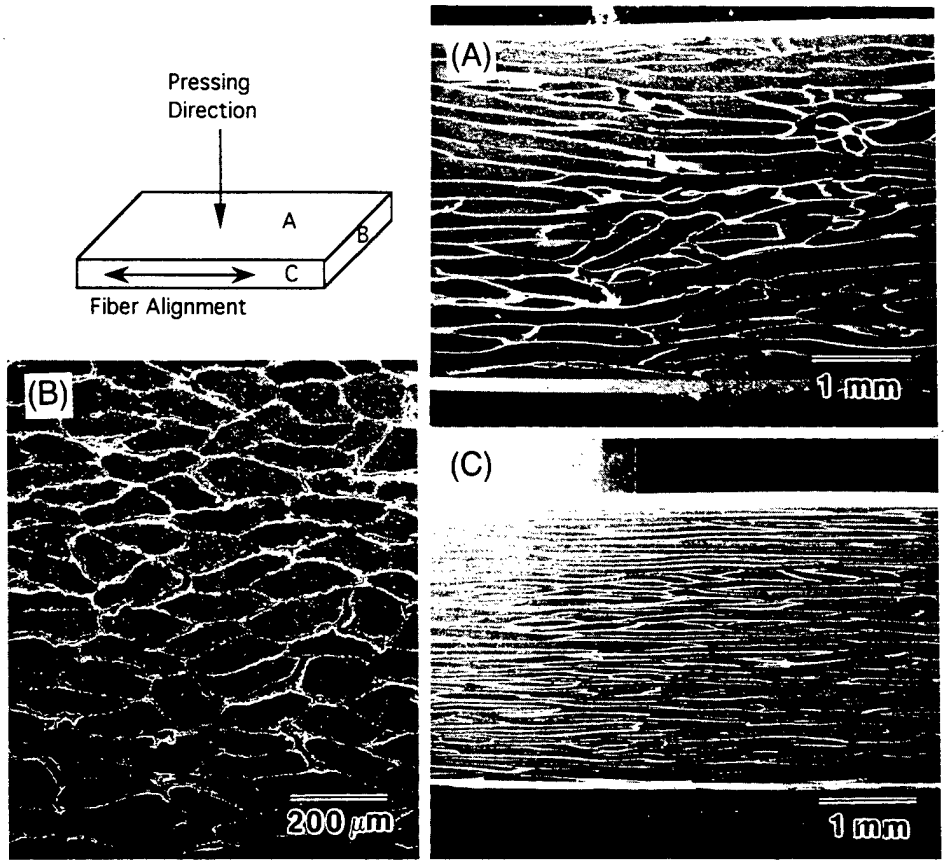

Fig. 1. Microstructure of SiC/graphite fibrous monolith prepared with aligned green fibers. The graphite cell boundaries appear bright in the SEM micrographs.

of cells, and extrusion of graphite from the cell boundaries.[5] Failure does not occur from the indentation, but from shear cracking. As the flexural stress is not indentation sensitive, this cell/cell-boundary combination is considered damage tolerant.

As noted earlier, the samples with 100% graphite at the cell boundaries display graceful failure, and the apparent work-of-fracture is ≈ 1300 J/m^2, which is substantially higher than the work-of-fracture of <100 J/m^2 expected for polycrystalline SiC toughened with additions of yttria and alumina.[13] The calculated work-of-fracture will vary with specimen thickness and loading configuration,[10] but is used here for comparison with other compositions for the same thickness.

A bar specimen with cell boundries of 100% graphite was pulled apart by hand after the test. The fracture surface is shown in Fig. 7(A). The terraced topography in the tensile half of the specimen shows the preferential crack growth along the graphite cell boundaries which appear bright in the SEM micrograph.

Samples with cell boundaries containing 80 vol% graphite/20 vol% SiC behaved in a similar manner, with graceful failure, and slightly higher average strength (234 MPa) and also very little decrease in strength on indentation. Failure again occurred by shear cracking, with the higher flexural strength implying a slight increase in the cell boundary shear strength over that of pure graphite. The apparent work-of-fracture was correspondingly lower at ≈ 1000 J/m^2. The surface of a fractured specimen is also terraced as shown in Fig. 7(B).

When the graphite content in the cell boundary was decreased to 60 vol% (40 vol% SiC), failure occurred in a brittle manner with the load dropping to zero. The average flexural strength of the three samples was ≈ 355 MPa. Two of the three samples with the higher strengths broke in two, but the third specimen with the lowest strength remained intact with some load-bearing ability. The SEM photomicrograph in Fig. 8 of the side surface of this specimen shows the fracture originating on the tension side, with shear fracture occurring beyond the neutral plane. The fracture surface of a broken specimen in Fig. 7(C) shows considerable topography, but noticeably less than samples containing 80% and 100% graphite at the cell boundaries. The indented strength was lower (285 MPa) but was still 80% of the unindented strength, indicating considerable damage tolerance. The work-of-fracture is assumed to be close to that of polycrystalline SiC.

With only 40 vol% graphite in the cell boundary, the bars were brittle but with slightly higher average strength of 383 MPa. The fracture surface of the specimen in Fig. 7(D) is much smoother, with some evidence of stepped fracture at cell boundaries. The indented strength was 80% of the original strength. Cell boundaries with only 40% graphite appear to be effective in limiting indentation damage and making the sample flaw tolerant. It is useful to point out here that although a statistically small sample of two bars was indented for each composition, the two values did not differ by more than 3% for compositions containing greater than 20 vol% graphite.

When the cell boundary composition is 20 vol% graphite/80 vol% SiC, strength is much higher (average $\sigma = 480$ MPa, with strengths ranging from 438 to 532 MPa), and fracture is brittle and relatively featureless near the tensile surface (see Fig. 7(E)). Shear lips at the cell boundaries are evident only from the neutral axis about 1.5 mm from the top edge. The average indented strength is only $\approx 50\%$ of the average unindented strength. The strength loss is significant but still better than polycrystalline SiC.

With 100% SiC (no graphite) at the cell boundary, the material is simply polycrystalline SiC densified with yttria and alumina, with no remnant texture from the green fibers. Average four-point bend strength is 640 MPa (with strengths ranging from 566 to 704 MPa), with brittle fracture and poor flaw tolerance. The indented strength values were 162 and 175 MPa. The

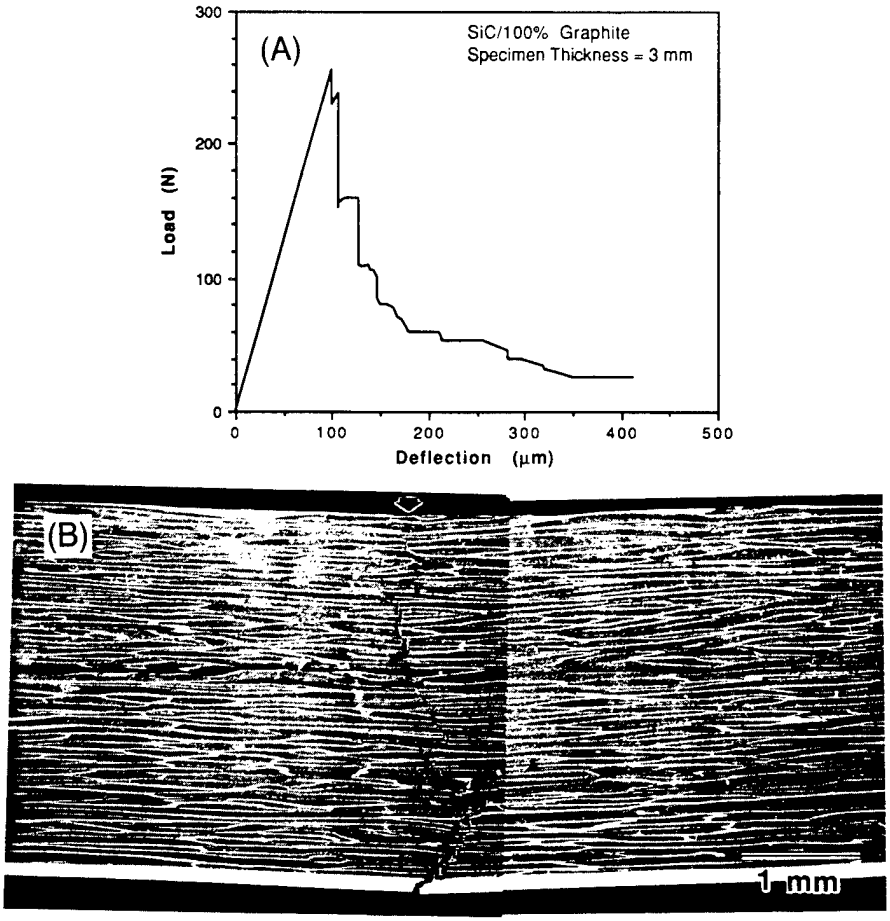

Fig. 2. (A) Load–deflection curve for SiC/graphite flexure specimen of 3-mm thickness. (B) Side surface of bent specimen after test; inner loading point indicated by arrow, outer loading point outside and to the left of field of view.

unindented specimens broke into several pieces on testing, and no fractography was done.

(4) Effect of Anisotropy and Fiber Alignment

It is evident from the micrographs in Fig. 1 that significant texture is present in these billets due to the forming process. The cross section of a billet normal to the fiber direction consists of flattened cells with graphite cell boundaries. The flexural strength behavior presented in Section III(2) has demonstrated that graphite cell boundaries normal to the pressing direction are weak, resulting in shear failure for low (3 to 5) span-to-depth ratios.

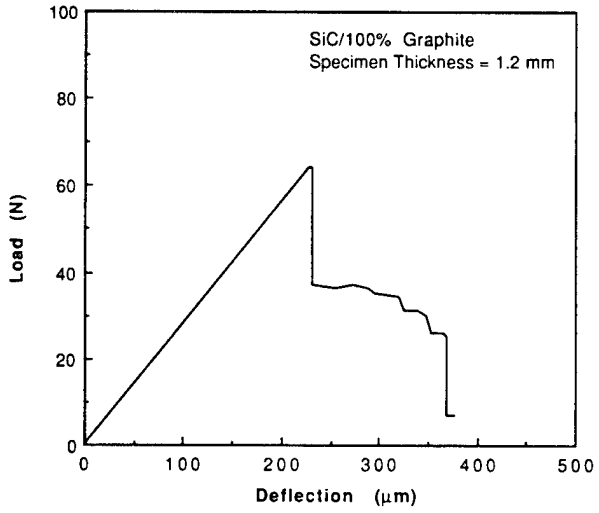

Fig. 3. Load–deflection curve for SiC/graphite flexure specimen with thickness of 1.2 mm.

The fracture behavior is markedly different for bar specimens machined in the *transverse* direction with the tension side parallel to the pressing direction, and tested at a low (3.3) span-to-depth ratio. The average strength of three bars was 303 MPa, with strengths ranging from 283 to 313 MPa. A linear increase to the maximum stress value was followed by a significant load drop. The specimens remained intact with some load-bearing ability. Failure originated at the tensile surface. Good agreement is observed between the measured strength of 303 MPa and the flexural strength of the bars at high span-to-depth ratios shown in Fig. 5.

The specimens machined in the transverse direction do not fail by midplane shear cracking as was expected at low span-to-depth ratios. There are two possible reasons for this fracture behavior. It is possible that hot pressing results in crystallographic orientation of graphite particles in cell boundaries which facilitates shear delamination normal to the pressing direction but not along the planes defined by the cell axis and the pressing direction. But, more likely, the inherent texture and layout of the cell boundaries lead to differences in the propensity for shear fracture between the two orientations. A much greater percentage of cell boundary segments lie normal to rather than parallel with the pressing direction, causing shear cracking only when the specimen neutral plane is normal to the pressing direction.

The strength and fracture behavior of SiC/graphite fibrous monoliths is also influenced by the method of green fiber layup in the die. The data presented so far were obtained with fibers aligned in the long direction of the billet. The microstructure

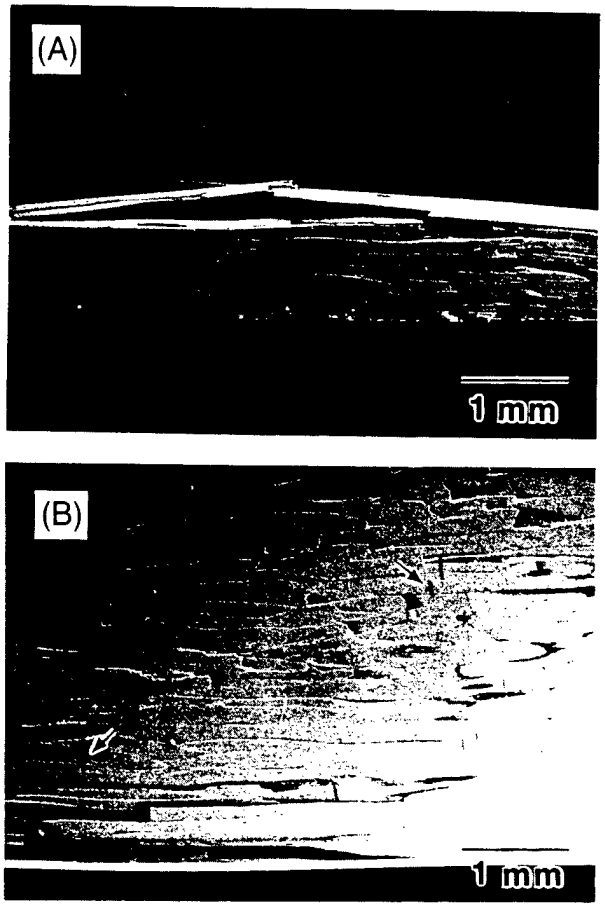

Fig. 4. SEM micrographs of side (A) and tensile (B) surfaces of thin SiC/graphite flexure specimen after test. Fractured cells on the tensile surface are indicated by arrows.

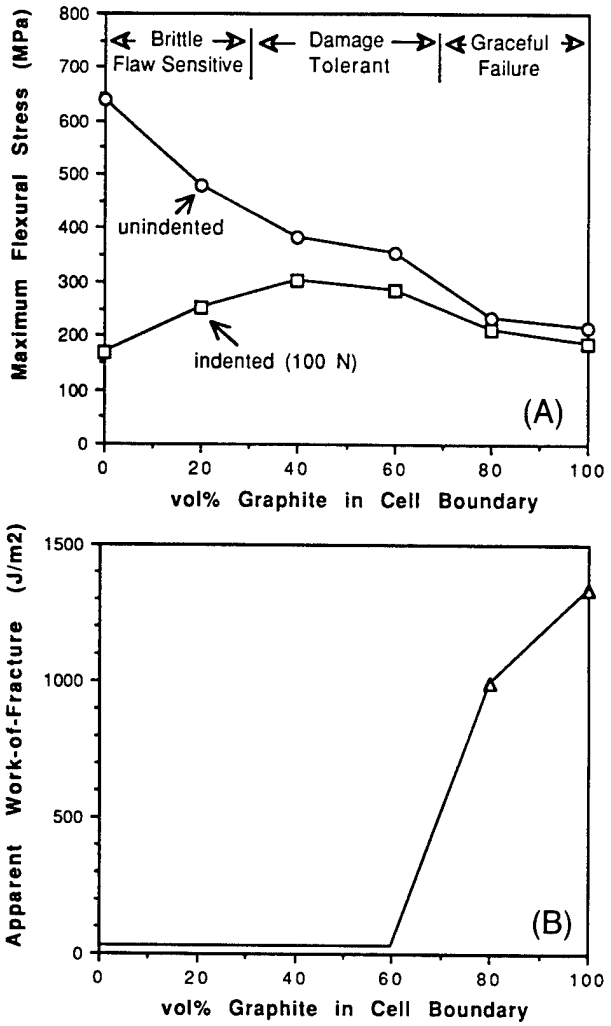

Fig. 6. Effect of cell boundary composition on (A) maximum flexural stress and (B) apparent work of fracture of SiC-based fibrous monoliths.

and fracture behavior are significantly different when the preform is made from randomly oriented green chopped fibers. This die-filling procedure is easier than aligning fibers, as it simply involves pouring the chopped fibers into the die. The side surface of a bar specimen with chopped fibers after testing is shown in Fig. 9(A). Fracture initiates at the tensile surface, followed by crack propagation mostly along the cell boundaries. Average flexural strength for both unindented and indented specimens was 123 MPa. Strengths of unindented samples ranged from 122 to 125 MPa. The randomly oriented cell architecture results in some cells (and, therefore, cell boundaries) being oriented normal to the applied stress. This causes failure initiation at the weak cell boundaries on the tension side as shown in Fig. 9(B), which results in low strengths. The strength simply corresponds to the low off-axis strength expected in a billet with aligned fibers. Cracks do not initiate from indentations[5] and so strength remains the same after indentation.

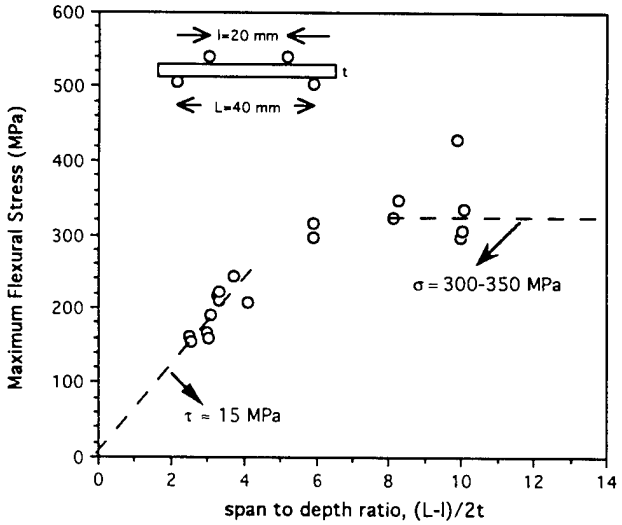

Fig. 5. Apparent flexural strength as a function of span to depth ratio for SiC/graphite.

(5) Notched-Beam Testing of SiC/100% Graphite

The load–deflection behavior of a notched beam of the SiC/100% graphite fibrous monolith tested in four-point flexure is shown in Fig. 10(A). The load increases linearly to ≈52 N followed by a nonlinear increase to the maximum load of 125 N. Observation of the side surface of a notched specimen during the test did not show evidence of cracks at the first sign of nonlinearity. But it is quite possible damage begins to occur along cell boundaries in the interior of the sample. With increasing load, delamination cracks were observed to nucleate and grow axially from the tip of the notch on the surface. The side surface of a notched specimen after the test is shown in Fig. 10(B). Delamination cracking has occurred through the thickness of the specimen ahead of the notch, with stepped fracture through

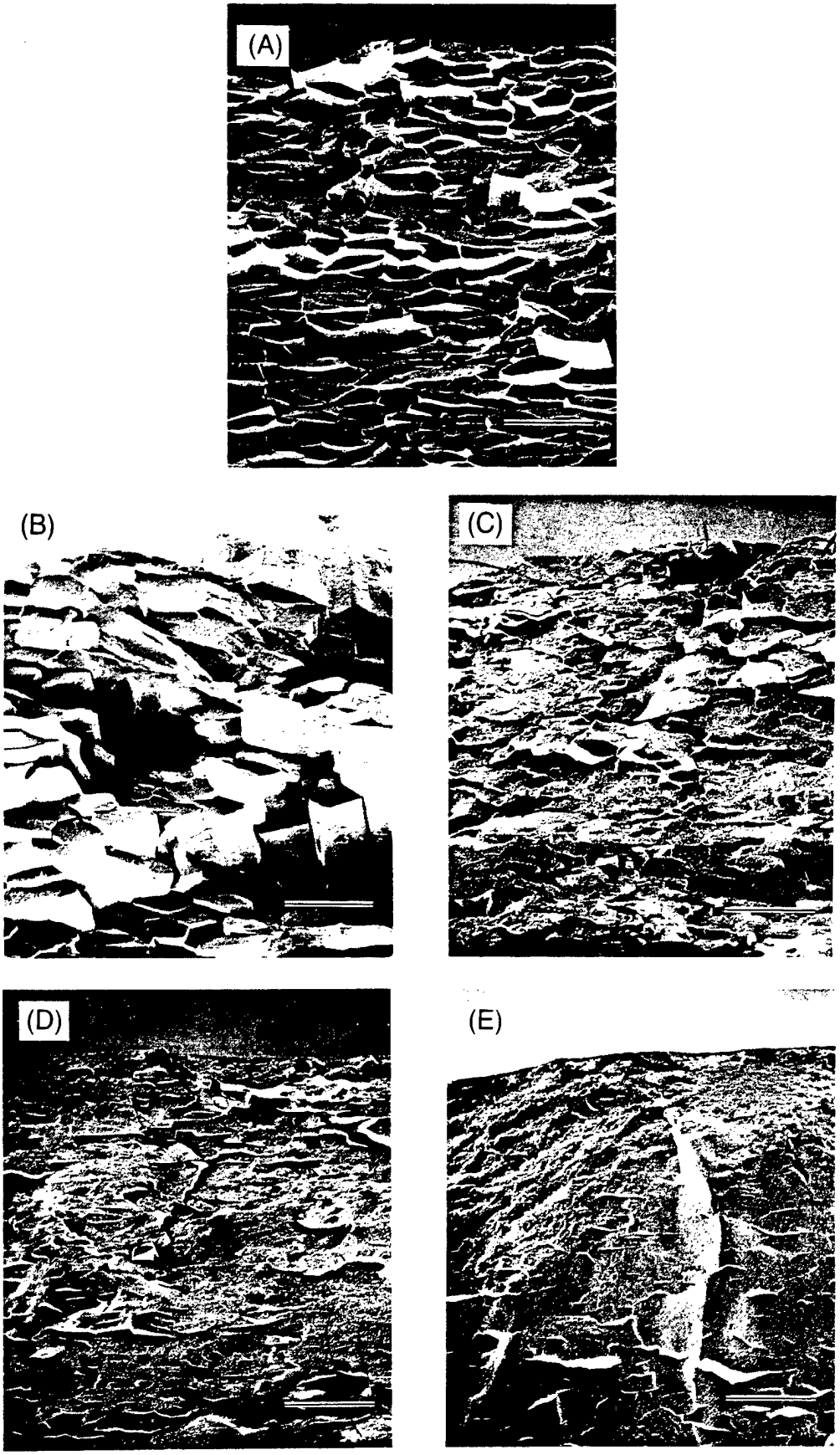

Fig. 7. Fracture surfaces of SiC-based fibrous monoliths with cell boundaries containing (A) 100%, (B) 80%, (C) 60%, (D) 40%, and (E) 20 vol% graphite.

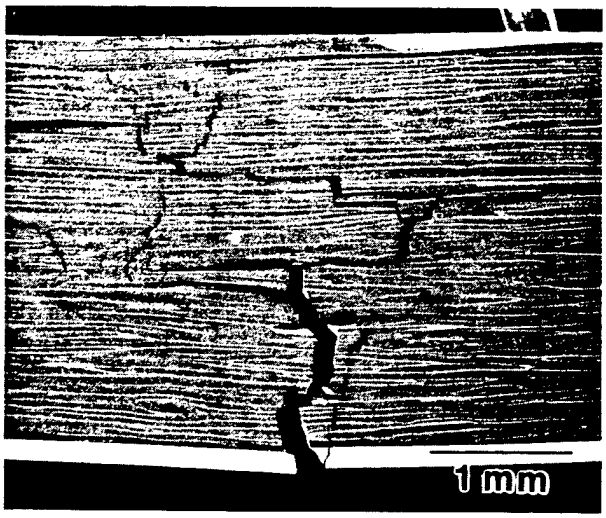

Fig. 8. SEM micrograph of side surface of flexure specimen of SiC/60 vol% graphite. Fracture initiates on the tension side at the bottom.

cells connecting the delamination cracks. Fracture behavior from the notch is similar to the delamination cracking observed in notch-insensitive materials like wood[11] and ceramic composites reinforced with high-strength continuous fibers.[7,10,14] Since extension of a crack in a direction normal to the applied stress does not occur, it is not possible to obtain a Mode I fracture toughness.

IV. Conclusion

High work-of-fracture, flaw tolerance, and "graceful failure" can be obtained in monolithic SiC with the fibrous monolith design. The flexural strength and fracture behavior in the SiC/graphite system depend on a wide range of parameters. Depending on the loading configuration, materials can fail by shear cracking or from the tensile surface. The interfacial strength significantly affects the strength, damage tolerance, and type of failure. Variations in cell boundary composition alter the fracture morphology. Texture and fiber orientation also influence the fracture behavior. Low-strength cell boundaries cause the material to be notch insenstive and prevent extension of cracks normal to the applied stress. This microstructural arrangement shows useful properties which could possibly be improved.

The fibrous monolith microstructure design using weak cell boundaries are in some ways similar to continuous-fiber-reinforced ceramics[7,12] and weak-interface laminates.[2] The microstructural units are polycrystalline cells which are derived from the fiber material, with the cell boundaries derived from

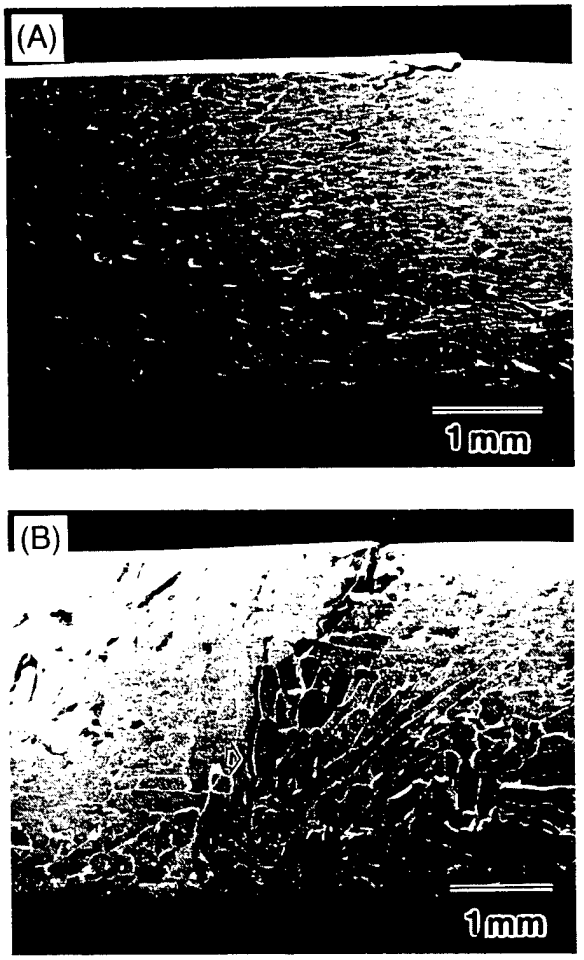

Fig. 9. SEM micrographs showing side (A) and tensile (B) surfaces of flexure specimens of SiC/100% graphite prepared with randomly oriented chopped fibers. Arrow indicates graphite cell boundary normal to applied stress direction on the tensile surface.

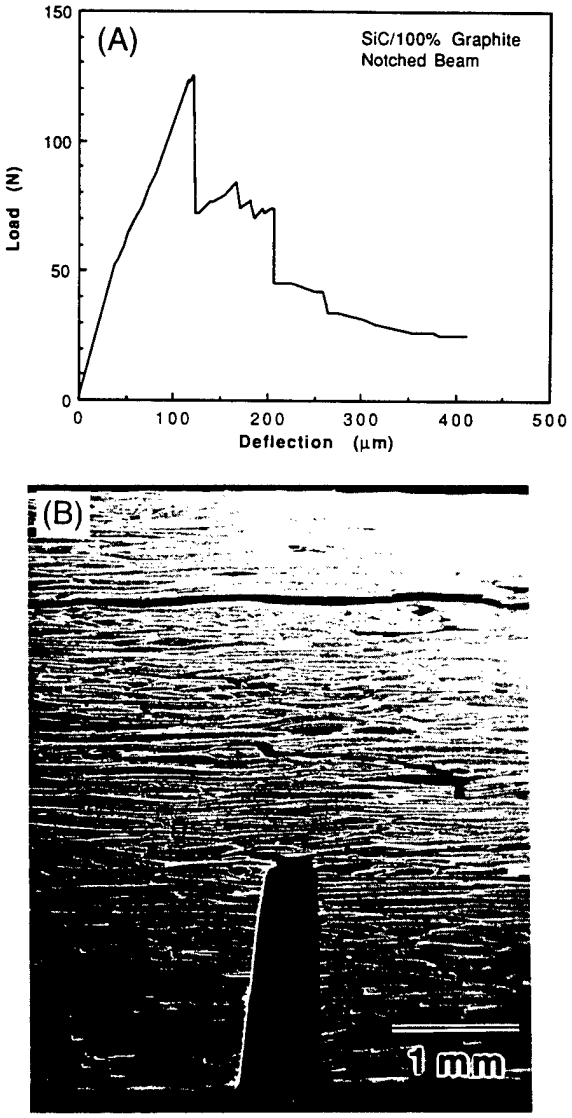

Fig. 10. (A) Load–deflection curve for a notched beam of SiC/100% graphite tested in flexure. (B) Side surface showing delamination cracking in the notched beam.

the fiber coating material. Each cell is not straight and continuous in the axial direction unlike the fibers in ceramic-matrix composites. The cell lengths can be very short when chopped fibers are used. The cells also do not have planar continuity normal to the pressing direction unlike laminates. The cells are however flattened in the pressing direction, resulting in some texture, and orientation effects on the shear properties. The weak-interface fibrous monolith can be best compared with geological rock fabrics consisting of lensoid microlithons with reticulate cleavage.[15]

The mechanical properties show important differences with fiber-reinforced ceramics and laminates. The weak interface fibrous monoliths show linear load–deflection behavior prior to the maximum load. Strain-to-failure at maximum strength is, therefore, low. Strength is lower than the reported value of 630 MPa for SiC/graphite laminates,[2] and the ultimate strengths of fiber-reinforced ceramics.[7,12] But the fibrous monoliths are damage tolerant, notch insensitive, and characterized by noncatastrophic fracture behavior.

For the SiC/100% graphite system, flexural strength is 300–350 MPa, and the shear strength normal to the pressing direction is 15 MPa. Combinations of alternative cell materials (of compatible polycrystalline structural ceramics) and weak cell boundaries (e.g., boron nitride) have the potential for yielding weak-interface fibrous monoliths with higher strength, adequate toughness, and damage tolerance.

Acknowledgment: Experimental assistance in fiber spinning was provided by Tim Fretter.

References

[1]M. P. Harmer, H. M. Chan, and G. A. Miller, "Unique Opportunities for Microstructural Engineering with Duplex and Laminar Ceramic Composites," *J. Am. Ceram. Soc.*, **75** [7] 1715–28 (1992).

[2]W. J. Clegg, K. Kendall, N. McN. Alford, T. W. Button, and J. D. Birchall, "A Simple Way to Make Tough Ceramics," *Nature (London)*, **347,** 455–57 (1990).

[3]C. A. Folsom, F. W. Zok, and F. F. Lange, "Flexural Properties of Brittle Matrix Laminar Composites," *Ceram. Eng. Sci. Proc.*, **13** [7–8] 469–74 (1992).

[4]W. S. Coblenz, "Fibrous Monolithic Ceramic and Method for Production," U.S. Pat. No. 4772524, September 20, 1988.

[5]S. Baskaran, S. D. Nunn, D. Popovic, and J. W. Halloran, "Fibrous Monolithic Ceramics: I, Fabrication, Microstructure, and Indentation Behavior," *J. Am. Ceram. Soc.*, **76** [9] 2209–16 (1993).

[6]J. Cook and J. E. Gordon, "A Mechanism for the Control of Crack Propagation in All-Brittle Systems," *Proc. R. Soc. London*, **A282,** 508–20 (1964).

[7]K. M. Prewo and J. J. Brennan, "High-Strength Silicon Carbide Fiber-Reinforced Glass-Matrix Composites," *J. Mater. Sci.*, **15,** 463–68 (1980).

[8]R. J. Kerans, R. S. Hay, N. J. Pagano, and T. A. Parthasarathy, "The Role of the Fiber–Matrix Interface in Ceramic Composites," *Am. Ceram. Soc. Bull.*, **68** [2] 429–42 (1989).

[9]R. J. Roark, *Formulas for Stress and Strain*, 4th ed.; Ch. 8. McGraw-Hill, New York, 1965.

[10]D. B. Marshall and A. G. Evans, "Failure Mechanisms in Ceramic-Fiber/Ceramic-Matrix Composites," *J. Am. Ceram. Soc.*, **68** [5] 225–31 (1985).

[11]M. F. Ashby, K. E. Easterling, R. Harrysson, and S. K. Maiti, "The Fracture and Toughness of Woods," *Proc. R. Soc. London, A*, **398,** 261–80 (1985).

[12]K. M. Prewo, "Tension and Flexural Strength of Silicon Carbide Fiber-Reinfoced Glass Ceramics," *J. Mater. Sci.*, **21,** 3590–600 (1986).

[13]K. Y. Chia and C. K. Lau, "High Toughness Silicon Carbide," *Ceram. Eng. Sci. Proc.*, **12** [9–10] 1845–61 (1991).

[14]O. Sbaizero, P. G. Charalambides, and A. G. Evans, "Delamination Cracking in a Laminated Ceramic-Matrix Composite," *J. Am. Ceram. Soc.*, **73** [7] 1936–40 (1990).

[15]G. J. Borradaile, M. B. Bayly, and C. M. Powell, *Atlas of Deformational and Metamorphic Rock Fabrics*; p. 2. Springer-Verlag, New York, 1982. □

journal

J. Am. Ceram. Soc., 77 [5] 1249–55 (1994)

Fibrous Monolithic Ceramics: III, Mechanical Properties and Oxidation Behavior of the Silicon Carbide/Boron Nitride System

Suresh Baskaran*,† and John W. Halloran*

Department of Materials Science and Engineering, University of Michigan, Ann Arbor, Michigan 48109-2136

Fibrous monolithic ceramics were fabricated in the SiC/BN system. The microstructure consists of high-aspect-ratio polycrystalline cells of SiC separated by cell boundaries of BN. The fibrous monolith with aligned cells fails noncatastrophically in flexure, with delamination cracking along the BN cell boundaries. Indentations cause controlled damage on the surface, but no strength-degrading flaws. The flexural strength is in the range 300–375 MPa, and the estimated shear strength is ≈14 MPa. The SiC/BN fibrous monoliths also show excellent resistance to high-temperature oxidation in air. Noncatastrophic fracture behavior is observed at room temperature after heat treatments between 1200° and 1500°C. The SiC cells on the surface are oxidized to form a protective silicate scale, which prevents deterioration of the BN cell boundaries.

I. Introduction

THE incorporation of high-strength ceramic fibers in ceramic matrices has led to a new generation of advanced composites with high toughness and graceful failure characteristics.[1,2] Fiber-reinforced ceramic matrix composites are candidate materials for many lightweight, high-temperature structural applications such as gas turbine engine components. However, these materials have found only limited use because of their high cost. Composites use expensive fibers, and must be fabricated using costly processing methods such as coatings by chemical vapor deposition and, in some cases, matrix formation by chemical vapor infiltration. A monolithic ceramic material fabricated with inexpensive powders and showing noncatastrophic fracture behavior would prove to be more useful. Clegg *et al.*[3] demonstrated this concept with tough SiC/graphite tape-cast laminates in which the graphite interlayers delaminated during flexural failure. Similarly, SiC-based ceramics fabricated from powders by the "fibrous monolith" approach[4] have shown useful mechanical properties.[5,6] These new materials have commercial potential because of their damage-tolerant mechanical behavior combined with low cost.

The "fibrous monolith" microstructure consists of high-aspect-ratio polycrystalline cells of a primary phase separated by thin cell boundaries of a second phase.[5] There are no reinforcing fibers. The cells are polycrystalline regions (e.g., SiC) that are remnants of "green" powder-loaded polymer fibers. A coating applied on the green fiber forms the cell boundary, which can be any thermodynamically compatible second phase designed to enhance the fracture resistance of the material. When the cell boundary is graphite, there is preferred crack propagation along the cell boundaries. The fibrous monolith fails noncatastrophically in flexure and is flaw-tolerant and notch-insensitive.[6]

SiC/graphite fibrous monoliths have limited applications because of oxidation of the graphite cell boundaries at high temperatures in air. Thermogravimetric analysis of SiC/graphite fibrous monoliths has shown that weight loss due to oxidation of cell boundaries begins at ≈250°C and is complete after 1 h at 700°C.[7] An alternative weak cell boundary material with better oxidation resistance is hexagonal (α) boron nitride, which is similar in structure to graphite. High-performance fiber-reinforced composites have been fabricated with CVD coatings of BN on fibers.[8–10] The weak BN interfacial layers between fibers and matrix result in debonding and fiber pullout, giving rise to useful fracture behavior. In this paper, processing and mechanical properties of SiC/BN fibrous monoliths are described. Fracture behavior is compared with SiC monolith and SiC/graphite fibrous monolith.[6,11] The effect of oxidation is evaluated by microstructural analysis and room-temperature flexural tests after high-temperature treatments in air.

II. Experimental Procedure

Suspensions of SiC powder (B-10, β-SiC powder, H. C. Starck, New York) in an ethyl methacrylate (EMA)/methyl ethyl ketone (MEK) solution (B7/MEK Acryloid, 30 wt% solution, Rohm and Haas, Philadelphia, PA) were ball-milled, and then concentrated by evaporation of the MEK. The concentrated "dopes" were extruded to form soft "green fibers" by dry-spinning into a hot-air column maintained at 100°C. Yttria (Johnson Matthey, Ward Hill, MA) and alumina (RC-HP DBM, Malakoff Industries, Malakoff, TX) were used as sintering aids. The weight ratio of $SiC:Y_2O_3:Al_2O_3$ was 90:4:6. The volume ratio of ceramic powder to ethyl methacrylate polymer in the dry fiber was 55:45. Green fibers typically had a "dog-bone" cross section,[5] with an area-equivalent circular diameter of ≈150–200 μm.

The green fibers were run through a coating slurry of $BN(+Al_2O_3)$[‡] immediately after extrusion. Boron nitride was present as 1–10-μm-wide platelets in suspension. The coated fibers were loaded in a 52 mm × 26 mm graphite die using one of two fiber architectures: either aligned fibers using ≈51-mm lengths or finely chopped, randomly oriented fiber segments. To simply evaluate the fracture behavior, both die filling techniques were tested. To study the effect of oxidation treatments, only aligned fiber billets were used. The chopped fiber die-filling method was evaluated because it was relatively easy.

The green fibers were pressed at ≈80°C, using 5-MPa pressure. This softens the polymer and consolidates the fibers into a dense monolithic billet with 45 vol% polymer. After removal of the polymer binder between 200°C and 600°C in an actively pumped vacuum, the billet was hot-pressed at 1900°C in argon

K. Jakus—contributing editor

Manuscript No. 194350. Received July 23, 1993; approved January 31, 1994.
Supported by the Advanced Research Projects Agency and the Office of Naval Research under Contract No. N0014-91-J-1999.

*Member, American Ceramic Society.
†Now with Battelle Pacific Northwest Laboratory, Richland, WA.

‡ZYP paint, (25 weight parts BN, 5 parts hydrated alumina, 70 parts water), ZYP Inc., Oak Ridge, TN. Actual ceramic solids was 87.5 wt% BN, 12.5 wt% Al_2O_3.

for 1 h, using 25-MPa ram pressure. Hot-pressed billets were 4.0–4.5 mm in thickness.

Most hot-pressed billets were machined into bar specimens 3 mm thick, 4 mm wide, and 48 mm long. Three bar specimens from an aligned fiber billet were machined down to 1-mm thickness. The 3-mm-thick samples provided a span-to-depth ratio of 3.33, which caused samples to fail by midplane shear cracking.[6,12] The 1-mm-thick samples were used to evaluate the true flexural strength of the material at high (≈9) span-to-depth ratio. All bars were machined and chamfered with a 1000-grit resin-bonded diamond wheel, with the grinding direction parallel to the length of the specimen. The tension side was normal to the pressing direction. In some cases, the side surfaces of samples were polished prior to testing. Flexural strength was measured using a fully articulated four-point bend fixture with a 20-mm inner span and a 40-mm outer span at a crosshead speed of 0.05 mm/min. Stress values were calculated from elastic beam equations.

The density of the bars was measured by the Archimedes method. Young's modulus was measured on bar specimens by the flexural resonance method[13,14] (Grindo-Sonic, J. W. Lemmens, St. Louis, MO). In this technique, the bar is set in resonance, and the frequency is measured with a contact probe. Damage and cracking from Vickers indentations were studied using a Zwick (E. Windsor, CT) indenter. An indentation load of 5 kg (≈50 N) was used with 30-s residence time.

Machined bar specimens of 3-mm thickness were heat-treated in air at high temperatures. Bars were held for 10 h between 1200° and 1500°C. Some bars were also held at 1400°C for 10, 50, and 250 h. Heating and cooling rates were 15°C/min between ≈500°C and the heat-treatment temperature. Heat-treated bars were tested in flexure. The 3-mm-thick specimens were used to study the effect of oxidation on the material's shear characteristics which are responsible for the non-catastrophic fracture behavior.

After testing, all heat-treated bars were inspected, using optical and scanning electron microscopy. Bars invariably shear cracked on only one-half of the specimen. Cross sections ≈5 mm from the undamaged end were polished and then studied by optical microscopy. Elemental analysis was done on polished sections with an electron microprobe, using X-ray wavelength dispersive spectrometry and appropriate standards.

III. Results and Discussion

(1) Microstructure, Elastic Modulus, and Indentation Behavior

The microstructure of SiC/BN fibrous monoliths with aligned fibers is shown in Fig. 1. Flattened SiC cells 50–100 μm thick and 150–200 μm wide are separated by cell boundaries a few micrometers to ≈25 μm in thickness. The cell sections visible in the micrographs of Figs. 1(A) and (C) vary in length from about 200 μm to several millimeters in the long direction of the billet. Although long green fibers are placed in the die, the forming procedure can result in finite cell lengths. Green fibers can fracture or bend and also may not lie perfectly normal to the pressing direction or perfectly parallel to the long die wall. Only short cell segments are visible in the micrographs, but individual cells could actually have continuity and extend for longer distances (approximately a few centimeters) up to a maximum of 5.2 cm.

The microstructure of a chopped fiber monolith is shown in Fig. 2. Here the cell cross sections on surfaces parallel to the pressing direction are quite small. Cell lengths vary from 200 to 600 μm. Viewed in the pressing direction, the sample consists of randomly oriented cells several hundred micrometers long and about 200 μm wide.

The volume fraction of the cell boundary was determined to be ≈23 vol% from point counts on optical micrographs of cell cross sections. The analyzed area encompassed about 300 cells. The 23 vol% cell boundary in SiC/BN is considerably more than the 8 vol% cell boundary in SiC/graphite.[6] This reflects the differences in coating thickness from the commercial BN slurry used in this study and the diluted Aquadag (Acheson Colloid, Port Huron, MI) graphite slurry used to fabricate SiC/graphite.[6]

The SiC cell microstructure is shown in Fig. 3. The backscattered electron image from the electron microprobe shows elongated grains of SiC with the yttria–alumina intergranular phase in bright contrast. The cell phase determined by X-ray diffraction was predominantly β-SiC, with 10–20 vol% hexagonal SiC polytypes.

The density of the SiC/BN fibrous monolith was 2.99 g/cm^3. The samples did not imbibe water. The density of the cells is inferred by comparison to the SiC monolith (i.e., hot-pressed SiC with yttria and alumina), which was 3.20 g/cm^3. By combining this information, the cell boundaries are estimated to be ≈96 vol% BN(+ Al_2O_3) and ≈4 vol% porosity.

For aligned fibrous monoliths, Young's modulus measured on two bar specimens was 341–342 GPa. Single-phase polycrystalline SiC densified with small additions of B and C has modulus ranging from 410 to 440 GPa.[15] The lower modulus compared to SiC reflects the contributions from ≈8 vol% yttria–alumina within cells and the high volume fraction of the lower-modulus BN cell boundary phase. The modulus of hot-pressed single-phase hexagonal BN is in the range 35–72 GPa,[16] and there is ≈23 vol% of this cell boundary. Literature values of Young's modulus values for SiC/BN particulate composites with 20 vol% BN are in the range 260–320 GPa.[17] The elastic modulus of SiC/graphite fibrous monolith measured by the same technique was slightly higher at 355–360 GPa, presumably due to lower (≈8 vol%) cell boundary content.[11] Combined with the low density, the modulus of the aligned fiber SiC/BN makes this material useful in applications requiring high specific modulus.

For the chopped-fiber layout, the modulus was significantly lower (275 GPa). The lower modulus can arise from both cell geometry considerations and BN texture within the cell boundaries. With the chopped-fiber layout, many cells lie at orientations almost perpendicular to the bar axis. A higher volume fraction of the BN cell boundaries lies in series with the SiC in the axial direction of the bar, resulting in lower stiffness. Furthermore, the coating process and the compaction could result in some alignment of cell boundary platelets along cell axes. In the randomly oriented cell geometry, where cells can lie normal to the bar axis, a significant fraction of BN platelets at the cell boundaries could be oriented with their weak c-axis direction along the bar axis. This could also result in lower elastic modulus.

From scanning electron microscopy of polished cross sections, it was difficult to determine whether platelets had preferred orientation. But X-ray diffraction of an aligned fiber monolith showed evidence of texture in the BN cell boundaries. The integrated intensity ratios of $(002)_{BN}$ to $(001)_{b\text{-}SiC}$ were 1:1.2, 1:4.2 and 1:15 from the sample cross sections shown in Figs. 1(A), (C), and (B), respectively. Other BN peaks were too weak to give useful information. The integrated intensity ratios indicate that BN platelets were mostly aligned with their c-axes in the hot-pressing direction. The preferred orientation of the lubricious BN platelets due to hot-pressing should result in low shear strength on planes normal to the pressing direction. From the moderate intensity of the $(002)_{BN}$ from the side of the specimen (cross section in Fig. 1(C)), there also appears to be some alignment of the BN platelets with their c-axes normal to the pressing direction and the cell axes. This alignment must result from slurry application on the green fibers.

Surface damage from a Vickers indentation is shown in Fig. 4. The section of a chopped fiber pellet parallel to the pressing direction was indented. Indentation causes cells to spall or crack, with the soft BN being extruded out from the cell boundaries. Unlike classically brittle materials, long radial cracks do not form upon indentation. So, just as in SiC/graphite,[6] strength would be unaffected by point contact damage.

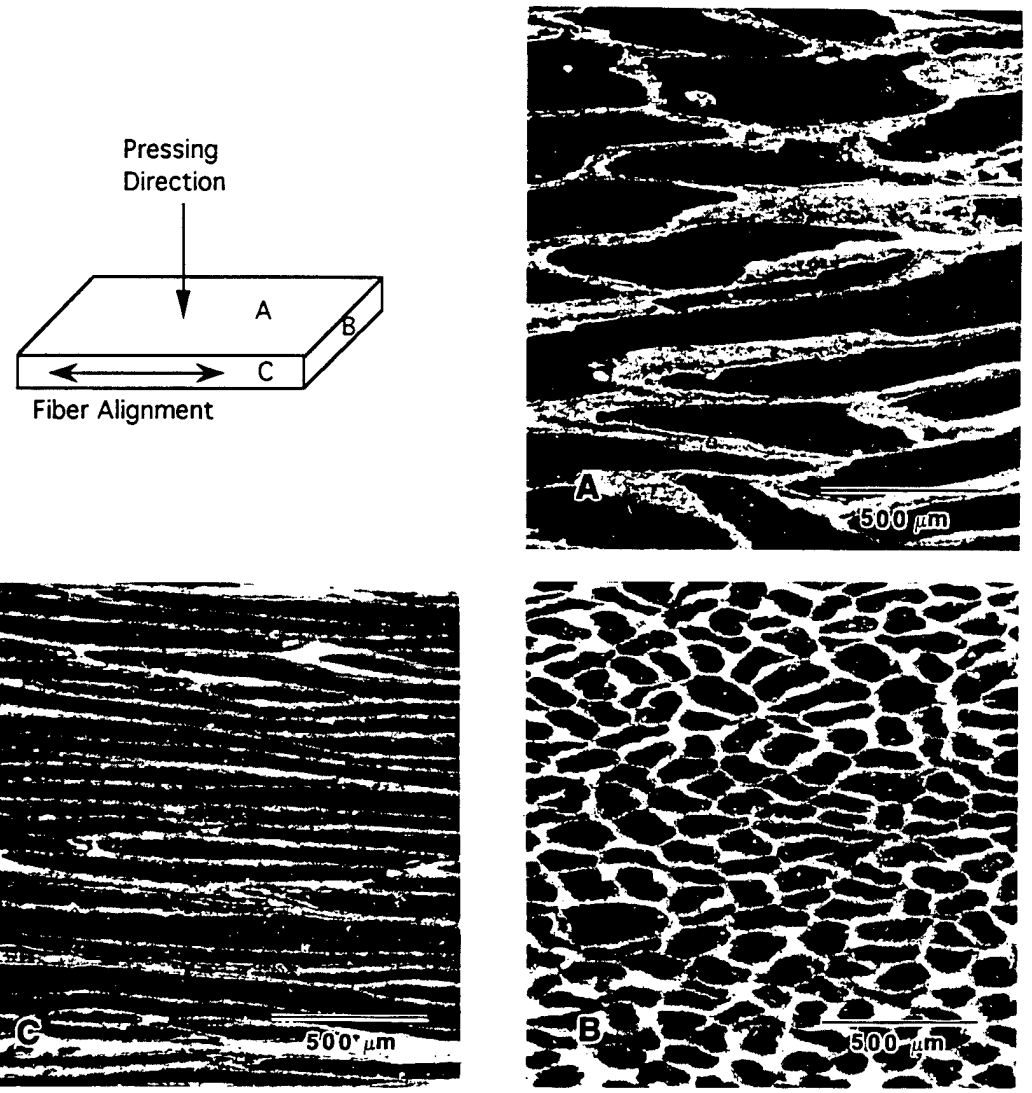

Fig. 1. Optical micrographs of a SiC/BN fibrous monolith prepared with aligned green fibers showing polycrystalline SiC cells (dark) and BN cell boundaries (light).

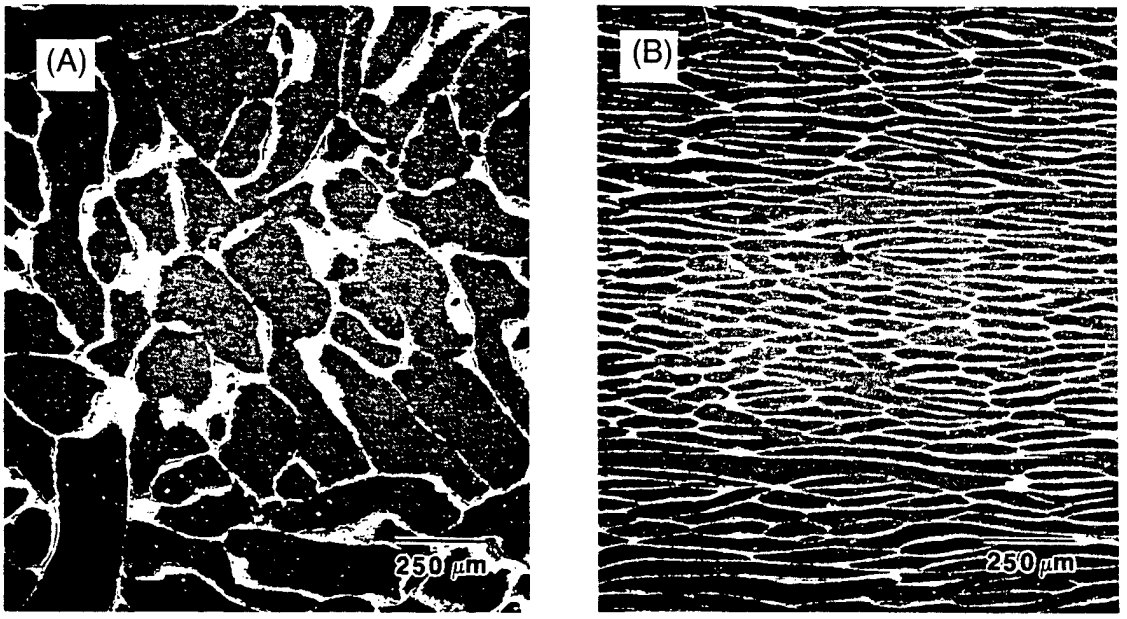

Fig. 2. SEM micrographs of polished surfaces of a SiC/BN fibrous monolith prepared with finely chopped, randomly oriented fibers (A) viewed in the hot-pressing direction and (B) viewed normal to the hot-pressing direction.

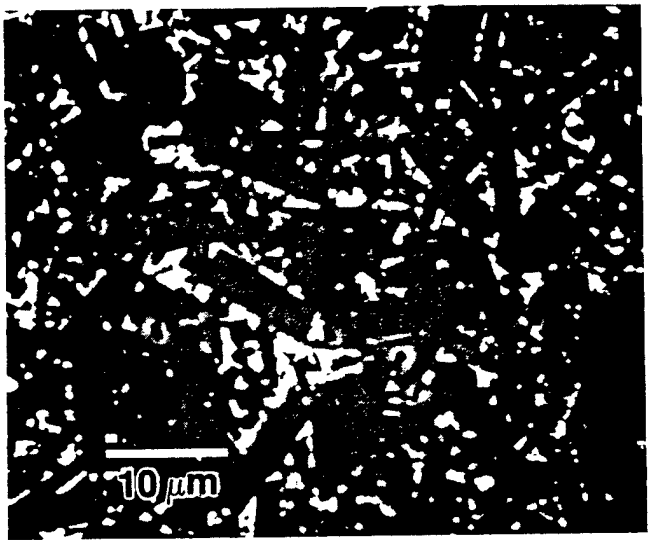

Fig. 3. Backscattered electron image of a SiC cell showing elongated grains of SiC (gray), and the yttria–alumina intergranular phase (white).

Fig. 4. SEM micrograph showing indentation fracture in a SiC/BN fibrous monolith (load = 50 N). Indented surface was parallel to the hot-pressing direction. Note extrusion of cell boundary material and absence of long radial cracks.

(2) *Flexural Strength and Fracture Behavior*

Load–deflection curves for two sample geometries of aligned-fiber SiC/BN are compared with data for a SiC monolith[11] in Fig. 5. The applied stress value is meaningful until the first load drop in each of the samples. The SiC monolith shows high strength but brittle fracture behavior. The fibrous monoliths for both span-to-depth ratios display noncatastrophic fracture behavior, with significant load-retaining capability after fracture commences. The lower modulus of the fibrous monolith is apparent from the lower slope of the 3-mm-thick SiC/BN specimen compared to SiC.

The strength values and modes of fracture were very similar to the SiC/graphite.[6] For thin specimens, fracture initiated from the tension side, and the sample then proceeded to delaminate like wood. The flexural strength values measured at this high

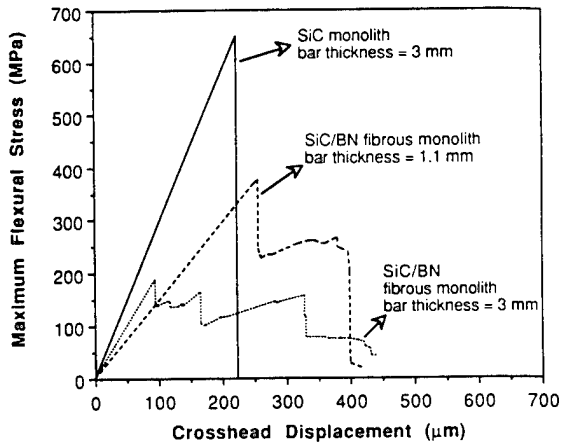

Fig. 5. Flexural strength behavior of aligned-fiber SiC/BN compared to monolithic SiC. Load–deflection traces for the fibrous monolith at two different span-to-depth ratios are shown.

span-to-depth ratio were in the range 300–375 MPa. For thick specimens, the samples shear-cracked starting at the midplane of the bar specimens between an inner and an outer loading point, where applied shear stresses are highest. The apparent strength of 186 MPa is not meaningful, since failure begins when the applied $\tau_{midplane}$ reaches the shear strength of the material. The interlaminar shear strength estimated from the thick specimens using elastic beam equations[6,12] was 14.1 MPa. The side surface after the test for a 3-mm-thick specimen is shown in Fig. 6. Extensive delamination cracking occurs along the length of the bar specimen. An apparent work-of-fracture measured from the area under the load–displacement curve and the specimen cross-sectional area was 2430 J/m^2.

The load–deflection behavior for a chopped-fiber bar specimen in flexure is presented in Fig. 7(A). The strength is 128 MPa, almost identical to the strength of SiC/graphite with similar cell architecture.[6] The side surface of the specimen after testing is shown in Fig. 7(B). Fracture initiates at the weak cell boundaries normal to the applied stress on the tension side. The shear characteristics of the material cause the crack to deflect towards the bar axis and propagate along the weak cell boundaries. The specimen does not fall apart after the test, but has almost no load-bearing capability.

From the cell architectures studied, it appears that, with suitable fiber lay-up methods, SiC/BN fibrous monoliths can be fabricated with sufficient strength and tough fracture behavior. Earlier work with SiC/graphite[11] has shown that the off-axis strength in aligned fibrous monoliths is low (≈70 MPa), but

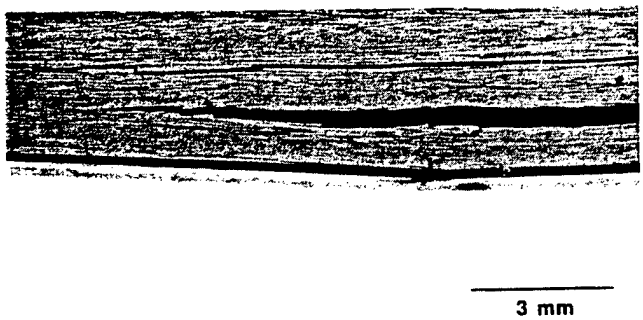

Fig. 6. Side surface of SiC/BN bend specimen after test showing delamination cracking (optical micrograph).

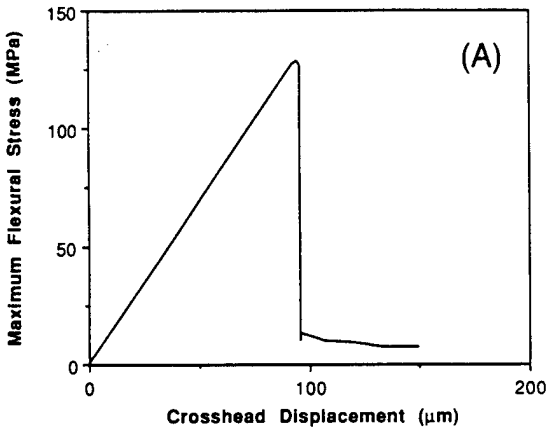

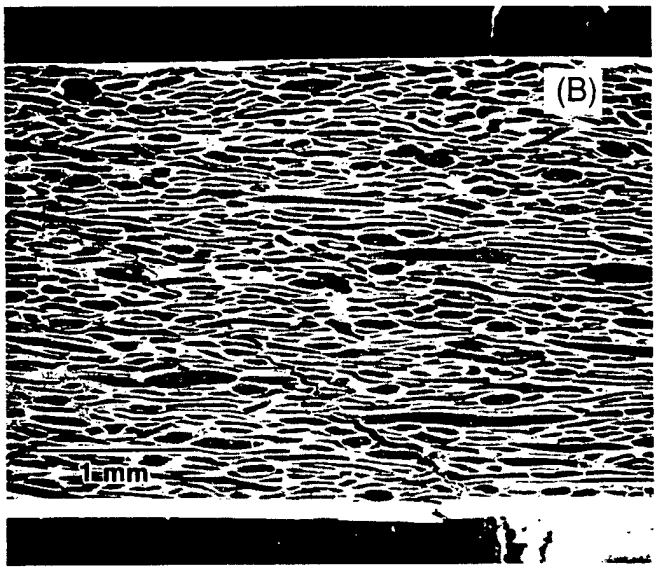

Fig. 7. (A) Flexural strength behavior of chopped-fiber SiC/BN. (B) SEM micrograph of the side surface of the specimen after test.

a 0°/90° cross-ply structure has strength ≈150 MPa. Other microstructural arrangements such as woven fabrics of SiC/BN may have a combination of tensile and shear strengths that meets design requirements of some structural components.

(3) Effect of Oxidation

The room-temperature strength behavior of oxidized bars after 10-h heat treatments at 1200° to 1500°C in air is shown in Fig. 8. Noncatastrophic fracture behavior is observed even in samples heat-treated to 1500°C. All samples were glazed after heat treatment. The bar specimens' thickness and width had increased about 3%–4%. The high temperature (1400° and 1500°C) heat treatments resulted in substantial bubble formation, with gas entrapment and foaminess in the scale. In the sample held at 1500°C, the scale had foamed up a few millimeters, presumably because of lower viscosity of the scale at the high temperature. For this specimen, the foam was scraped off before testing. In Fig. 8, the apparent strengths are again not meaningful and do not reflect the true flexural strength of the materials. For all samples, failure initiated by midplane shear cracking, followed by extensive damage primarily below the inner loading point. The oxidation treatment had apparently not affected the shear properties (i.e., not affected the bulk of the BN cell boundaries) significantly. Then the bar specimen shear cracked between an inner and outer loading point, which chipped off part of the scale, as shown in Fig. 9.

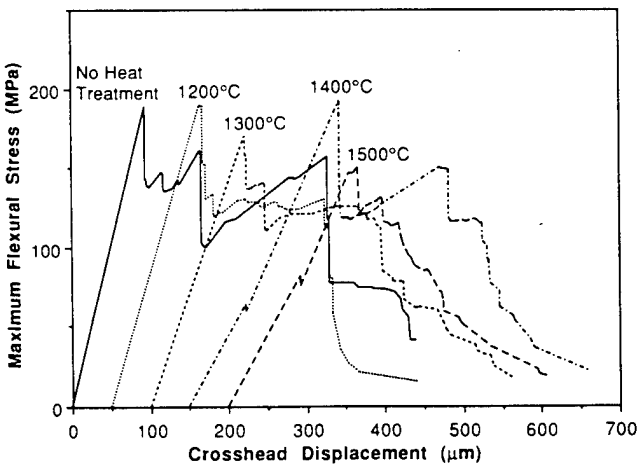

Fig. 8. Room-temperature strength behavior of aligned-fiber SiC/BN after 10-h heat treatments in air at high temperatures.

The room-temperature load deflection behavior of bar specimens heat-treated at 1400° for 10, 50, and 250 h is shown in Fig. 10. Here again, all samples failed by shear delamination along the cell boundaries. Noncatastrophic fracture behavior was recorded even after 250 h (>10 days) at 1400°C. The bar that had undergone the long 250-h heat treatment was covered with a foamy, translucent scale. The side surface of this bar in Fig. 11 shows delamination cracking and damage in the section below the inner loading point. The fibrous structure is visible in regions where the scale has come off.

Table I lists the room-temperature flexure properties for all the SiC/BN samples after heat treatment. Interlaminar shear strengths calculated from the maximum flexural stress are generally low after all the heat treatments. The long 1400°C hold results in some increase in the shear strength to 18 MPa. Apparent work-of-fracture values are also high for all the specimens.

The polished section of a bar specimen after 1400°C/250 h is compared with an untreated sample in Fig. 12. The optical micrographs show the chamfered corners of the bar section. The scale on the heat-treated sample is 25–50 μm thick on average, and >100 μm thick in some areas. There was no measurable

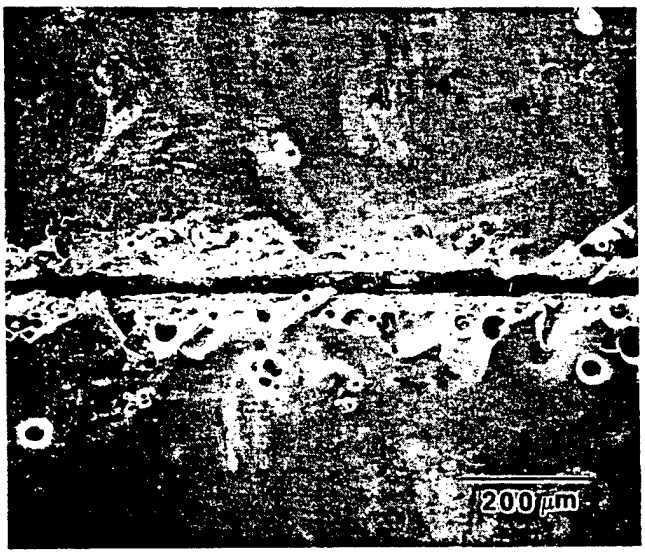

Fig. 9. SEM micrograph showing side surface of heat-treated (1400°C/10 h) SiC/BN specimen after bend test.

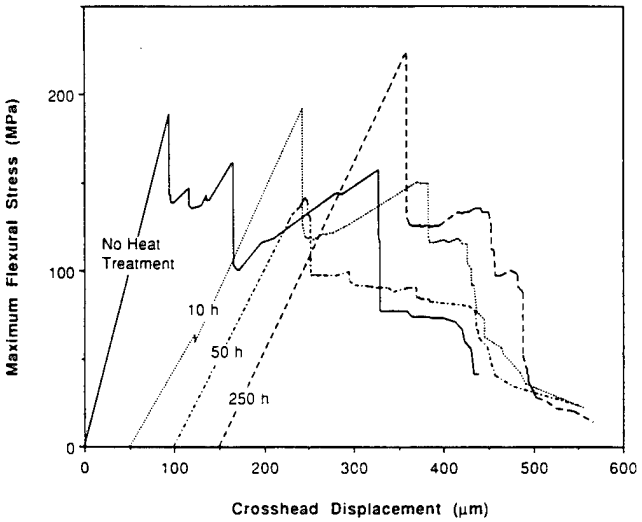

Fig. 10. Room-temperature strength behavior of aligned-fiber SiC/BN heat-treated at 1400°C in air for various times.

Table I. Room-Temperature Properties of Aligned-Fiber SiC/BN from Flexure Tests

Heat treatment	σ_{max} (MPa)	$\tau_{i\,max}$ (MPa)	Apparent work-of-fracture (J/m²)
None	186	14.1	2430
1200°C (10 h)	189	14.7	1770
1300°C (10 h)	171	13.5	2130
1400°C (10 h)	192	15.6	2210
1500°C (10 h)	146	11.6	1480
1400°C (50 h)	141	11.3	1800
1400°C (250 h)	223	18.0	2230

change in the cell and cell boundary dimensions. There was also no evidence of degradation or reactions in the cell boundaries or cells in the interior of the sample. This is consistent with retention of low-shear-strength BN cell boundaries and noncatastrophic fracture behavior even after 10 d at 1400°C.

A backscattered electron image of a polished section of heat-treated SiC/BN is shown in Fig. 13. The micrograph shows the scale appearing in bright contrast. The scale contains faceted inclusions. The SiC cell in the interior, as in Fig. 3, shows bright Y- and Al-containing intergranular phases. Elemental microanalysis was done on the different phases in many areas of this sample, as well as on unoxidized samples. The bright scale contained yttrium, aluminum, silicon, and oxygen. The inclusion was a crystalline form of silica, most likely cristobalite.[18] There was no evidence of an oxidation product of BN extending into the BN-rich cell boundary. It was not possible to determine whether boron was present in the scale, since our spectrometer could not detect boron in this sample. A wavelength spectrometer scan of the emissions from the scale did not show the characteristic peak for nitrogen, which indicated that there was no dissolved N in the glass. The compositions of the cell phase were the same in the unoxidized and heat-treated samples. Some pieces of monolithic SiC (with the same yttria–alumina additions) were also heat-treated for comparison. Similar oxide scale formation was observed in these samples, with identical elemental compositions.

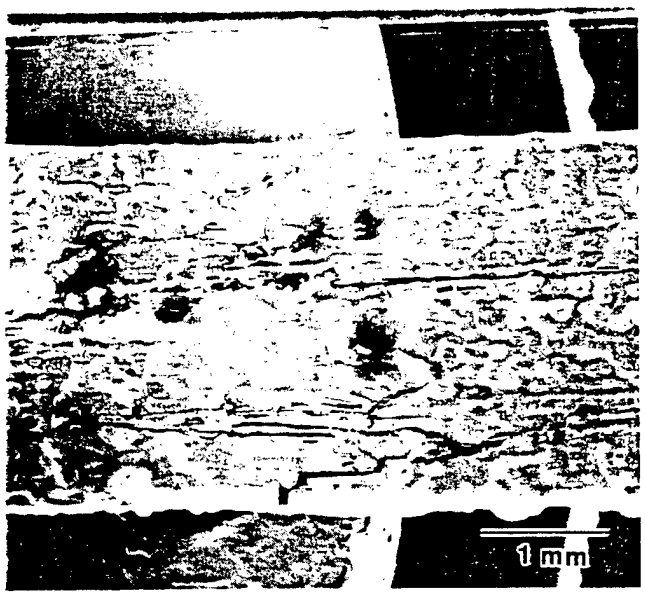

Fig. 11. SEM micrograph showing side surface of heat-treated (1400°C/250 h) SiC/BN specimen after bend test.

From the microstructural observations and elemental analysis, it is evident that the SiC cells on the surface are oxidized to form a protective layer of Y–Al-containing silicate scale with SiO_2 inclusions. BN appears to be unoxidized beneath this scale even after long-term exposure at 1400°C. The stability of BN in this environment can be explained in terms of the equilibrium partial pressures of oxygen expected at SiC/SiO_2 and BN/B_2O_3 interfaces at 1400°C. The oxidation of SiC is assumed to be controlled both by diffusion and interface reaction, as suggested by Luthra.[18] The most probable reaction for the oxidation of SiC cells is

$$SiC + \tfrac{3}{2}O_2 \rightarrow SiO_2 + CO$$

From free energies of formation,[19] ΔG for the above reaction can be calculated. With this information, and assuming 1 bar ($\approx$1 atm) pressure of CO at the interface, the equilibrium P_{O_2} at the SiC/SiO_2 interface has been estimated to be $\approx 7 \times 10^{-17}$ atm.

The oxygen partial pressure required for BN oxidation can also be calculated from the free-energy change of the reaction

$$2BN + \tfrac{3}{2}O_2 \rightarrow B_2O_3 + N_2$$

The nitrogen partial pressure beneath the scale can be assumed to be 1 bar. The equilibrium P_{O_2} at a hypothetical BN/B_2O_3 interface is then calculated to be 1.5×10^{-14}. This value of oxygen partial pressure is $\approx$150 times the equilibrium P_{O_2} at SiC/SiO_2 interfaces. The calculated value for the P_{O_2} at the SiC/SiO_2 interface is not expected to be significantly different when the oxidation product is a Y–Al–Si–O scale containing SiO_2 inclusions. The low equilibrium P_{O_2} associated with SiC oxidation establishes the oxygen partial pressure beneath the scale; this pressure is then too low for BN oxidation at 1200°–1500°C. The material retains low interlaminar shear strength BN cell boundaries after heat treatment, resulting in graceful failure behavior at room temperature. Further work on oxidation and high-temperature flexure properties is under way and will be reported in subsequent papers.

IV. Conclusion

SiC-based fibrous monoliths with weak cell boundaries of BN show potentially useful mechanical properties at room temperature. Noncatastrophic fracture behavior with significant load-bearing capability is observed in SiC/BN with aligned green fibers. As in SiC/graphite, delamination cracking of the BN cell boundaries occurs during failure. Young's modulus of SiC/BN with aligned fibers is $\approx$340 GPa. Flexural strength is in the range 300–375 MPa, and interlaminar shear strength on planes normal to the pressing direction is $\approx$14 MPa. The low shear strength should render the material notch-insensitive under flexural loading conditions. Delamination cracks initiated

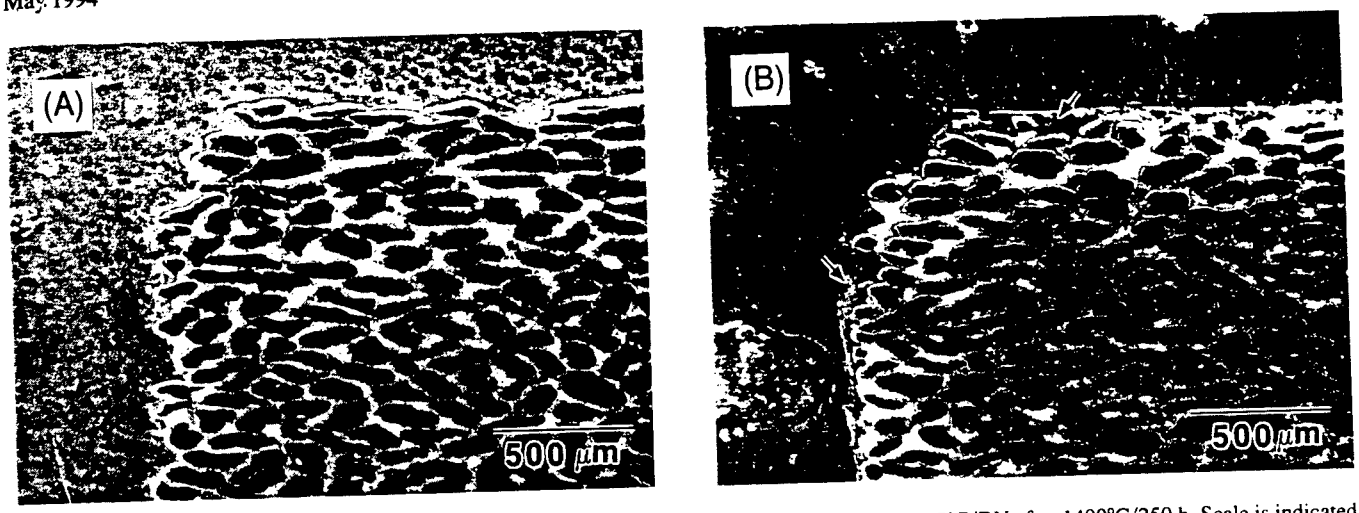

Fig. 12. Optical micrographs comparing polished cross sections of (A) unoxidized SiC/BN and (B) SiC/BN after 1400°C/250 h. Scale is indicated by arrows.

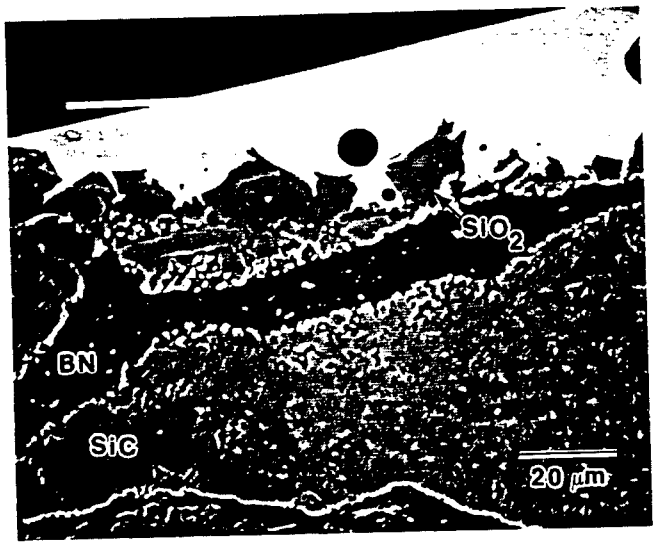

Fig. 13. Backscattered electron image of a polished section of SiC/BN heat-treated to 1400°C/250 h. The edge of the sample is shown with the various phases labeled.

from notch tips will cause the load to rise even after cracking has begun.[6]

The SiC/BN system also shows potential for use in oxidizing environments at high temperatures. The low-shear-strength BN cell boundaries are retained even after heat treatment at 1400°C for 10 days in air. The oxidation of SiC cells on the surface forms a protective silicate layer preventing the oxidation of subsurface BN cell boundaries. Shear cracking and noncatastrophic failure is observed in room-temperature flexure tests after heat treatments in air between 1200° and 1500°C. Further studies on these materials will include evaluation of high-temperature mechanical properties, and microstructural refinement of the cell and cell boundary phases to optimize properties.

Acknowledgments: Lynne Svedberg and Tim Fretter provided assistance in fiber spinning. Carl Henderson performed the microprobe analysis. The authors also acknowledge useful discussions with Cynthia Arens.

References

[1]K. M. Prewo and J. J. Brennan, "High Strength Silicon Carbide Fiber-Reinforced Glass–Matrix Composites," *J. Mater. Sci.*, **15**, 463–68 (1980).
[2]K. M. Prewo, "Fiber-Reinforced Ceramics: New Opportunities for Composite Applications," *Am. Ceram. Soc. Bull.*, **68** [2] 395–400 (1989).
[3]W. J. Clegg, K. Kendall, N. McN. Alford, T. W. Button, and J. D. Birchall, "A Simple Way to Make Tough Ceramics," *Nature*, **347**, 455–57 (1990).
[4]W. S. Coblenz, "Fibrous Monolithic Ceramic and Method for Production," U.S. Pat. No. 4 772 524, September 20, 1988.
[5]S. Baskaran, S. D. Nunn, D. Popovic, and J. W. Halloran, "Fibrous Monolithic Ceramics: I, Fabrication, Microstructure, and Indentation Behavior," *J. Am. Ceram. Soc.*, **76** [9] 2209–16 (1993).
[6]S. Baskaran and J. W. Halloran, "Fibrous Monolithic Ceramics: II, Flexural Strength and Fracture Behavior of the Silicon Carbide/Graphite System," *J. Am. Ceram. Soc.*, **76** [9] 2217–24 (1993).
[7]C. Arens, "Oxidation of Fibrous Monolithic Ceramics"; M.S. thesis in progress, University of Michigan, Ann Arbor, MI, unpublished work.
[8]R. N. Singh and M. K. Brun, "Effect of Boron Nitride Coating on Fiber–Matrix Interactions," *Ceram. Eng. Sci. Proc.*, **8** [7–8] 636–43 (1987).
[9]R. N. Singh and A. R. Gaddipati, "Mechanical Properties of a Uniaxially Reinforced Mullite–Silicon Carbide Composite," *J. Am. Ceram. Soc.*, **71** [2] C-100–C-103 (1988).
[10]J. J. Brennan, "Glass and Glass-Ceramic Matrix Composites"; presented at the 95th Annual Meeting of the American Ceramic Society, Cincinnati, OH, April 1993 (Paper No. SII-81-93).
[11]S. Baskaran and J. W. Halloran, "SiC-based Fibrous Monolithic Ceramics," *Ceram. Eng. Sci. Proc.*, in press.
[12]D. B. Marshall and A. G. Evans, "Failure Mechanisms in Ceramic-Fiber/Ceramic-Matrix Composites," *J. Am. Ceram. Soc.*, **68** [5] 225–31 (1985).
[13]E. Schreiber, O. L. Anderson, and N. Soga, *Elastic Constants and Their Measurement*; Ch. 4, McGraw-Hill, New York, 1973.
[14]S. Spinner and W. E. Tefft, "A Method for Determining Mechanical Resonance Frequencies and for Calculating Elastic Moduli from these Frequencies," *Proc. Am. Soc. Test. Mater.*, **61**, 1229 (1961).
[15]S. J. Schneider (Ed.), Engineering Materials Handbook, Vol. 4, *Ceramics and Glass*, Sect. II, Properties of Carbides. ASM International, Metals Park, OH, 1991.
[16]A. Lipp, K. A. Schwetz, and K. Harold, "Hexagonal Boron Nitride: Fabrication, Properties and Applications," *J. Eur. Ceram. Soc.*, **5**, 3–9 (1989).
[17]R. Ruh, A. Zangvil, and R. R. Wills, "Phase and Property Studies of SiC/BN Composites," *Adv. Ceram. Mater.*, **3** [4] 411–15 (1988).
[18]K. L. Luthra, "Some New Perspectives on Oxidation of Silicon Carbide and Silicon Nitride," *J. Am. Ceram. Soc.*, **74** [5] 1095–103 (1991).
[19]D. R. Stull and H. Prophet (Eds.), *JANAF Thermochemical Tables*, 2nd ed. National Bureau of Standards, Washington, DC, 1971. □

journal

J. Am. Ceram. Soc., 77 [5] 1256–62 (1994)

Fibrous Monolithic Ceramics: IV, Mechanical Properties and Oxidation Behavior of the Alumina/Nickel System

Suresh Baskaran,*,† Stephen D. Nunn,*,‡ and John W. Halloran*

Department of Materials Science and Engineering, University of Michigan, Ann Arbor, Michigan 48109-2136

Fibrous monolithic ceramics were fabricated in the alumina/nickel system. The microstructure consists of high-aspect-ratio polycrystalline cells of alumina separated by thin cell boundaries of nickel. The nickel content in the material is 3 to 8 vol%. The fibrous monolith with uniaxially aligned cells fails noncatastrophically in flexure. Bridging ligaments of nickel, crack deflection along cell boundaries, and crack branching in the axial direction are observed in flexure bars and notched beams. Strength values range from 246 to 375 MPa. Indentations cause controlled damage on the surface but do not introduce strength-degrading flaws. The alumina/nickel fibrous monoliths also show potential for use at high temperatures in oxidizing environments. Noncatastrophic fracture behavior is observed at room temperature after 10 h at 1200°C in air. The Ni cell boundary network is oxidized to a depth of 50 to 100 μm by this heat treatment. The NiO oxidation product in the cell boundaries reacts partly with alumina from the cells to form $NiAl_2O_4$, which would provide better protection.

I. Introduction

IN METAL-TOUGHENED ceramics, ductile ligaments bridge crack surfaces, and the plastic work associated with stretching these ligaments during fracture results in enhanced toughness.[1-9] The reinforcing metal phase can exist as discrete inclusions[1,2] or can have connectivity in all three directions.[3,4,6] In both cases, the metal reinforcements increase the resistance to propagation of cracks (increase fracture toughness) but still result in brittle, catastrophic failure in strength tests. When the metal phase is present as thick (>100-μm) layers with planar continuity as in the alumina/Ni laminates of Chen and Mecholsky,[9] the composite shows noncatastrophic fracture behavior. The thick sheets of Ni bridge the crack surfaces in flexure tests and keep the specimens intact.

The "fibrous monolith" approach[10,11] is a new process for creating ceramic microstructures with metallic/ceramic interphases. The fibrous monolith microstructure consists of high-aspect-ratio polycrystalline *cells* of a primary phase separated by thin *cell boundaries* of a second phase. There are no reinforcing fibers. The cells are flattened polycrystalline regions (e.g., alumina) that are remnants of powder-loaded polymer "green" fibers. A coating applied on the green fiber forms the cell boundary (e.g., nickel), which can be any thermodynamically compatible second phase designed to enhance the fracture resistance of the material. When the cell boundary has low shear strength (graphite or BN), the material fails noncatastrophically in flexure.[11-13] The fibrous monolith is flaw-tolerant and notch-insensitive.

The fabrication of fibrous monoliths in the alumina/Ni system has been described earlier.[11] Two features of this ceramic–metal microstructure are unique. The Ni cell boundary phase is thin and occupies only about 3 to 8 vol% of the material. This is quite small compared to alumina/Ni laminates,[9] which contained about 30 to 45 vol%. The Ni cell boundary phase also isolates each of the long alumina cells and has connectivity in all three directions. The objective in this study was to determine the effect of this microstructural layout on the fracture behavior of the alumina/nickel system. Mechanical properties of an alumina/Ni fibrous monolith with aligned cells were evaluated. The experiments addressed the following questions: (1) How does the material fracture in a "standard" flexure test? (2) What is the effect of a stress intensifier such as a notch in a flexure specimen? (3) Is the strength significantly reduced by point contact damage? (4) Since tough ceramics with high specific modulus are candidate materials for replacing Ni-base superalloys in gas turbine engine applications, do alumina/Ni fibrous monoliths have potential for use at high temperature?

II. Experimental Procedure

Suspensions of alumina powder (RC-HP DBM, Malakoff Industries, Malakoff, TX) in an ethyl methacrylate (EMA)/methyl ethyl ketone (MEK) solution (B7/MEK Acryloid, 30 wt% solution, Rohm and Haas, Philadelphia, PA) were ball-milled. A phosphate ester (P5-21A, Witco, New York) was used as the dispersant. The milled suspensions were then concentrated by evaporation of the MEK to a pastelike consistency. The concentrated "dopes" were extruded to form soft "green fibers" by dry-spinning into a hot-air column maintained at 100°C. Yttria-stabilized zirconia (TZ-3Y, Tosoh USA, Bridgewater, NJ) was used as a grain growth inhibitor for the alumina. The volume ratio of Al_2O_3 to ZrO_2 was 96:4 (weight ratio of 94:6). The volume ratio of ceramic powder to ethyl methacrylate polymer in the dry fiber was 60:40. Green fibers typically had a "dog-bone" cross section,[11] with an area-equivalent circular diameter of 100–150 μm. More details on dope preparation and spinning are given elsewhere.[11]

The green fibers were run through a coating slurry of NiO (N-69, Fisher Scientific, Fairlawn, NJ) immediately after extrusion. The suspension medium for the coating slurry was a mixture of iso(propyl alcohol) and deionized water. Menhaden fish oil (Z-3, Kellox Div., Textron, Buffalo, NY) was used as a dispersant, with poly(vinyl alcohol) (KH175, Nippon Gohsei, Tokyo, Japan) as the binder and poly(ethylene glycol) (Carbowax PEG 4000, Fisher) as plasticizer. (Coating thickness was adjusted by controlling slurry composition and properties to provide a final nickel content of ~8 vol% in the material. A single billet was made with a thinner coating, adjusted for about 3 vol% final nickel content.) The coated fibers with the thick NiO coating (corresponding to 8 vol% Ni) were trimmed to 51-mm lengths and loaded in a 52 mm × 26 mm graphite die with the

N. S. Jacobson—contributing editor

Manuscript No. 194283. Received August 23, 1993; approved January 31, 1994.
Supported by the Advanced Research Projects Agency and the Office of Naval Research under Contract No. N00014-91-J-1999.
*Member, American Ceramic Society.
†Now with Battelle Pacific Northwest Laboratory, Richland, WA.
‡Now with Oak Ridge National Laboratory, Oak Ridge, TN.

fibers aligned parallel to the long die wall. The fibers with the thinner coating were trimmed to 41-mm lengths and loaded in a 32 × 42 mm die. The different sizes reflect availability of dies in different stages of this study.

The green fibers were pressed at 80°C using 5-MPa pressure. This softens the polymer and consolidates the fibers into a dense monolithic billet with 40 vol% polymer. After removal of the polymer binder between 200° and 600°C in an actively pumped vacuum, the billets were hot-pressed at 1400°C in nitrogen for 1 h using 25-MPa ram pressure. During hot-pressing, NiO is reduced to Ni cell boundaries in the material. Hot-pressed billets varied from 3.5 to 5.5 mm in thickness.

Billets with 8 vol% nickel were machined either into bar specimens 3 to 4.5 mm thick, 4 mm wide, and 48 mm long, or into tall beams 4.5 mm high, 2.3 mm wide, and 48 mm long. All specimens were machined with a 1000-grit resin-bonded diamond wheel, with the grinding direction parallel to the length of the specimen. The bars for flexure tests were also chamfered. The tension side was normal to the pressing direction. In some cases, the side surfaces of samples were polished prior to testing. Flexural strength was measured on two bars, using a fully articulated four-point bend fixture with a 20-mm inner span and a 40-mm outer span at a crosshead speed of 0.05 mm/min. A single bar specimen was polished, indented with a Vickers diamond (Zwick Indenter, Zwick of America, E. Windsor, CT) using a 10-kg load, and tested to failure. Stress values were calculated from elastic beam equations.

The tall beams were notched to a depth of about 1.8 mm using a 250-μm-wide diamond wafering blade. Notch depth/specimen height was about 0.4. Actual notch radii were 140 μm. The notched beams were tested in the same 20/40-mm four-point fixture used for the bend bars. The equation of Brown and Srawley[14] was used to estimate fracture toughness from the maximum load.

The smaller billet with 3 vol% nickel was machined into bars 2 mm × 2 mm × 42 mm in size, and into tall beams 2 mm wide, 3 mm high, and 42 mm long. The tall beams were notched with the 250-μm-wide diamond blade to a depth of 1.15 mm. The bars were tested in a four-point bend fixture with a 15-mm inner span and a 30-mm outer span.

Density of bars was measured by the Archimedes method. Young's modulus was measured on bar specimens with 8 vol% nickel by the flexural resonance method,[15,16] using Grindo-Sonic (J. W. Lemmens, St. Louis, MO) equipment. Damage and cracking from Vickers indentations (Zwick) were studied on the side surface of a bar with 8 vol% nickel. An indentation load of 10 kg (about 100 N) was used with 30-s residence time.

Machined bar and notched beam specimens containing 8 vol% nickel were also heat-treated in air at 1200°C for 10 h. Heating and cooling rates were 15°C/min between 500°C and the heat-treatment temperature. The heat-treated specimens were tested in flexure at room temperature.

Fractured specimens were inspected using optical and scanning electron microscopy. Some specimens were inspected with an optical microscope during the flexure test. Cross sections after test were polished and then studied by optical microscopy.

III. Results and Discussion

(1) *Microstructure, Elastic Modulus, and Indentation Behavior*

The microstructure of alumina/Ni fibrous monoliths with aligned fibers is shown in Fig. 1. The alumina cells are flattened by the forming process, with thickness (Fig. 1(C)) ranging from 60 to 100 μm, and width (Fig. 1(A)) from 100 to 160 μm. Only short cell lengths up to a few millimeters are visible in the micrographs, but individual cells could actually have continuity and extend for long distances up to a maximum of 5.2 cm. The Ni cell boundary thickness varies from 1 to 15 μm.

The density of the alumina(+zirconia)/nickel fibrous monolith with the thicker cell boundary was 4.45 g/cm³. X-ray diffraction of the outside surface of the billet showed that the only phases present were alumina, nickel, and tetragonal zirconia. The alumina cells were seen to be pore-free by scanning electron microscopy. About 0.5 vol% porosity in the material was present at the cell boundaries (see Fig. 1(B)). From the theoretical density of alumina(+4 vol% zirconia) and nickel metal, the volume fraction of nickel is estimated to be about 0.08. The alumina/nickel billet with less nickel had a density of 4.13 g/cm³, which is equivalent to alumina with about 3 vol% nickel.

From optical microscopy of billet cross sections containing 8 vol% nickel, the color of the cells was found to vary from blue in the central section (about 2.5-mm thickness), to gray in the outer layers (1-mm thickness), which were near the graphite die walls during hot-pressing. The starting NiO powder was a moderately dark green, and $NiAl_2O_4$ is known to be blue in color. X-ray diffraction indicated that the central section was predominantly alumina and nickel, with a small (<5%) amount of $NiAl_2O_4$ and trace NiO. It appears that the blue coloration is due to trace amounts of $NiAl_2O_4$ formed from reaction of the alumina with some NiO that was not reduced in the central section of the billet.[§] An exact determination of the spatial distribution of the $NiAl_2O_4$ phase awaits detailed inspection of the Ni/alumina interface by transmission electron microscopy.

The Young's modulus values of three bar specimens of the alumina/8 vol% Ni fibrous monolith were 335, 343, and 347 GPa. Young's modulus of dense polycrystalline alumina (density = 3.95–3.99 g/cm³) is in the range 380–400 GPa. Nickel metal with density of 8.9 g/cm³ has a modulus of 205 GPa.[17] The low density and high modulus of the alumina/nickel fibrous monolith make this material attractive for applications requiring high specific stiffness, especially in comparison with nickel alloys.

Surface damage from a Vickers indentation on the 8 vol% Ni-fibrous monolith is shown in Fig. 2. Indents in the load range 10–100 N are comparable in size to the cell width, so crack patterns typical of homogeneous brittle materials do not form. The nickel cell boundaries prevent the formation of long cracks. Interfacial cracks that form along the cell boundaries are seen to propagate into the cells at about 45° to the cell boundaries some distance from the indent. The radial cracks in the direction normal to the cell axes are generally confined to one cell width. Deformation and uplift of the Ni cell boundaries at the top and bottom indent corners are also observed. Since cells are only 50–150 μm deep, the lateral cracks from indentation also cause some parts of cells to spall.

(2) *Flexural Strength Behavior*

The strength behavior of the alumina/8 vol% Ni fibrous monolith is shown in Fig. 3. Maximum stress on the tension side is plotted as a function of crosshead displacement for a 3-mm-thick bar specimen. The applied stress value is meaningful only up to the first load drop, beyond which elastic beam equations are not valid. Peak stress is 268 MPa, and the material displays noncatastrophic fracture behavior, retaining about 40% of the maximum load after the first fracture event. Failure initiates on the tension side between the inner loading points, with the crack propagating past the neutral axis. The side surface of the specimen on the tension side of the neutral axis is shown in Fig. 4. Both crack deflection/branching along the cell boundaries and deformation of Ni that had bridged across the fracture surfaces during the test are evident. Beyond the neutral axis near the compression side, significant crack branching occurs in the axial direction. This, combined with some bridging ligaments of Ni, provides load-bearing capability in the cracked specimen.

The amount of nickel at the cell boundary affects the fracture behavior. Two bars from the billet containing 3 vol% nickel were tested. Both samples failed in a brittle fashion, breaking in two. The strength values were 287 and 375 MPa. These results

[§]Preliminary experiments using NiO plus small amounts of graphite as the fiber coating indicate that complete reduction to Ni in thick sections can be achieved.

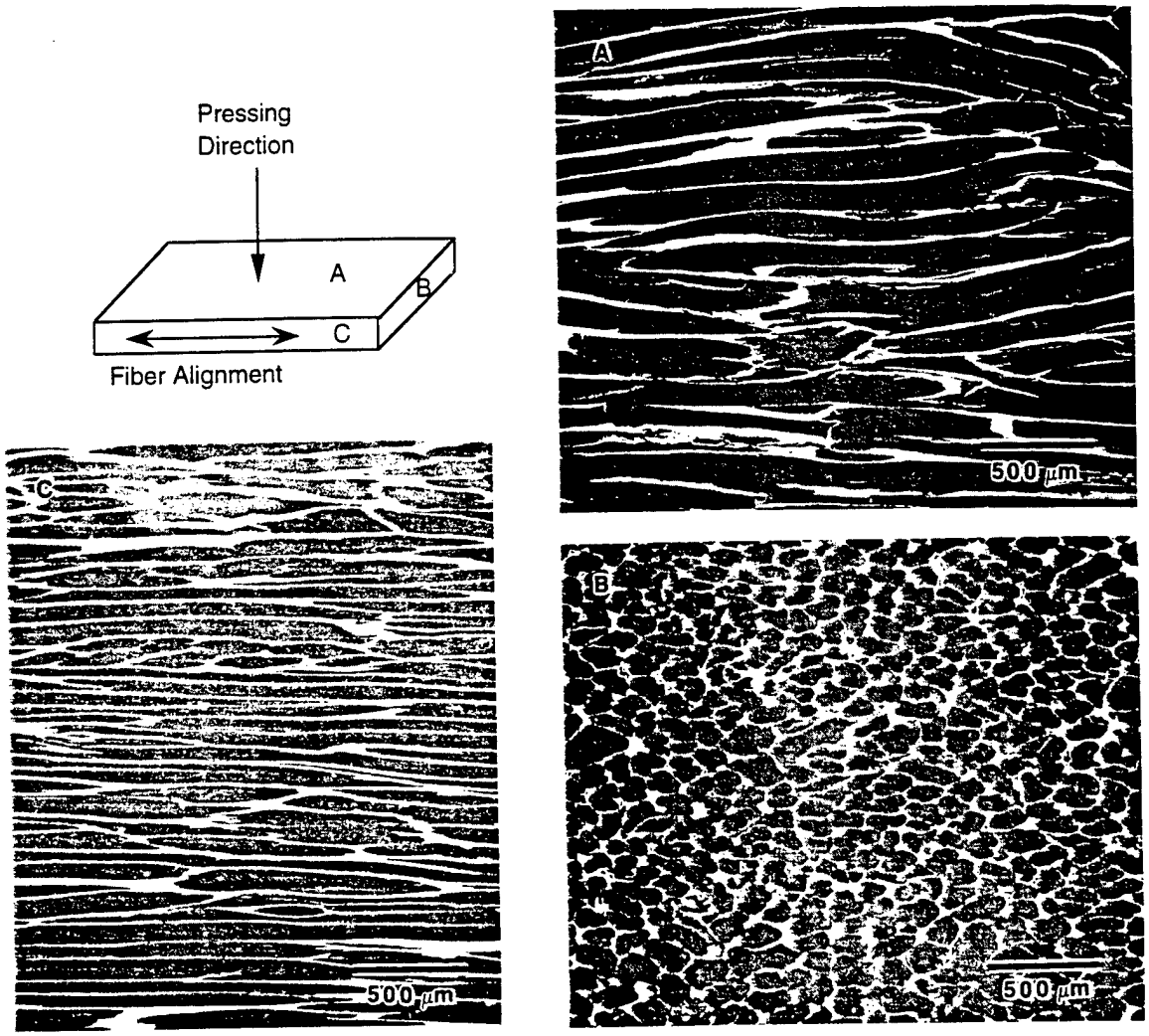

Fig. 1. Microstructure of alumina/nickel fibrous monolith prepared with aligned green fibers. The nickel cell boundaries appear bright in the SEM micrographs.

indicate that a minimum amount of nickel is required at the cell boundaries to prevent brittle fracture in flexure bars.

A concern in uniaxial structures of dissimilar materials is the possibility of interfacial cracking preceding other fracture events. In thick bend specimens, the applied shear stresses between the inner and outer loading points are high and can cause delamination cracking when interlaminar shear strengths are low.[12,13] For a thick (4.5-mm) bar of the alumina/8 vol% Ni, strength was 246 MPa and the sample failed in a noncatastrophic manner. Fracture initiated from the tension side, and not by midplane shear delamination. For an applied tensile stress of 246 MPa, the maximum applied shear stress is 28 MPa for this specimen/fixture configuration.[12] The absence of shear cracking in this thick sample indicated that the Ni/alumina interfaces had reasonably high shear strengths and that failure by delamination was not a critical issue.

The load–deflection behavior for a single-edge-notched beam (SENB) if alumina/8 vol% Ni is shown in Fig. 5. Fracture is noncatastrophic. The load continues to rise after fracture has begun, followed by a gradual decrease in load. The SEM micrograph in Fig. 6(A) shows a primary crack has propagated straight ahead from the tip of the notch. The primary crack was observed at the first sign of nonlinearity in the load–deflection curve. With further crosshead displacement, a secondary crack, which ran almost parallel to the primary crack, was initiated at the tip of the notch. As is evident from Fig. 6(A), there is some tendency for crack deflection along the cell boundaries, and also thick ligaments of Ni bridging the crack surfaces. In Fig. 6(B), the fractured surface of a section of a notched beam pulled apart after the test shows ductile ridges of Ni, as well as plastic rupture of a long nickel section by void growth, both typical of metal fracture.[5,6,9]

The K_{I_c} calculated from the maximum load was 5.8 MPa·$m^{1/2}$. This K_{I_c} value is slightly higher than typical values for alumina, but the toughness from notched beams is also affected by experimental parameters such as notching techniques and notch width.[18,19] The important observation here is that fracture is not catastrophic from a stress concentration in a flexure specimen of the fibrous monolith.

The load–deflection behavior for a SENB specimen of the alumina/3 vol% Ni fibrous monolith is shown in Fig. 7. Here, the first fracture event immediately results in a load decrease. Once the crack has initiated, the thinner nickel cell boundary network results in less load-bearing capability. But the sample with only 3 vol% Ni continues to sustain load with further crosshead displacement and does not break in two. The mode I fracture toughness calculated from the peak load was 6.2 MPa·$m^{1/2}$.

A noteworthy feature in the flexural response of the alumina/nickel fibrous monolith is that noncatastrophic fracture behavior is observed in spite of infrequent occurrence of plastically stretched ligaments of nickel. The ligaments are generally thin (1 to 15 μm), and only the thicker metal elements appear to bridge crack surfaces (Fig. 6(A)). The thickness effect is consistent with other investigations[5,9] on metal-toughened ceramics which have shown that the toughening contribution (i.e., work of stretching) from the metal increases with ligament size. The Ni cell boundaries are thin, but the nickel is present in the form

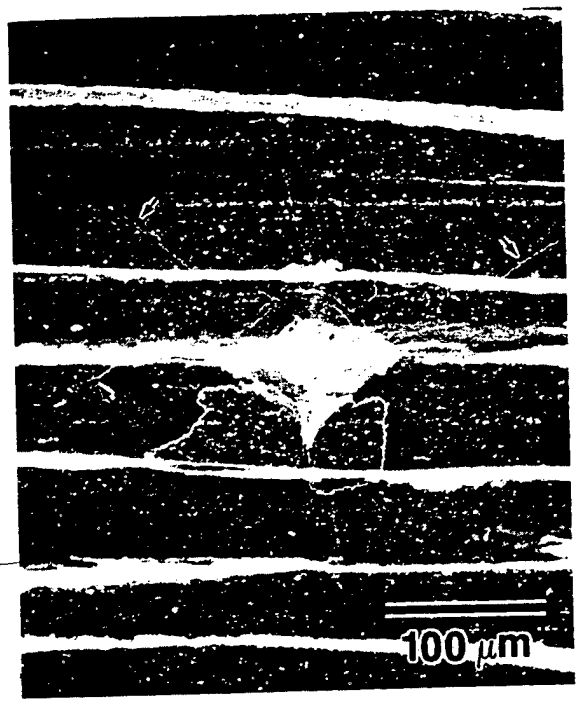

Fig. 2. SEM micrograph showing indentation fracture in an alumina/nickel fibrous monolith (load = 100 N). Indented surface was parallel to the hot-pressing direction. Arrows indicate cracks propagating into cells from the cell boundaries.

Fig. 4. SEM micrograph showing side surface of alumina/8 vol% nickel bend specimen after test. Arrows indicate cracking along cell boundaries and nickel ligaments that had bridged the crack surfaces.

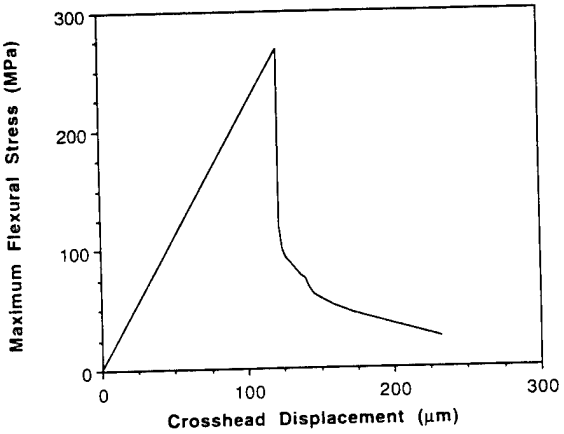

Fig. 3. Flexural strength behavior of aligned-fiber alumina/8 vol% nickel. Thickness of flexure specimen was 3 mm.

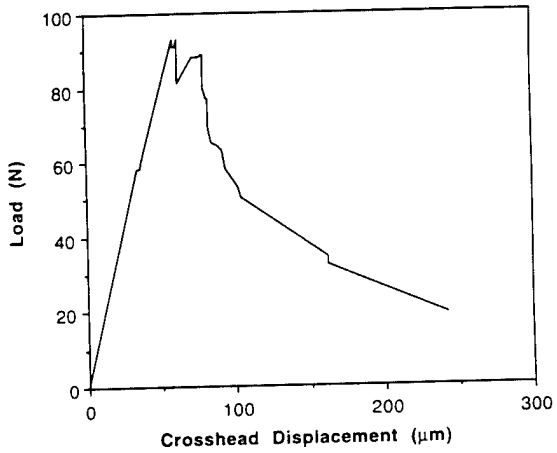

Fig. 5. Load–deflection behavior for a notched beam of the alumina/8 vol% nickel fibrous monolith in flexure.

of interconnected thin-walled tubes which are filled with dense, polycrystalline alumina. It is this contiguous network form of nickel, at only 8 vol% of the composite structure, that imparts toughness to the material and prevents brittle fracture in strength specimens. In SENB specimens, as little as 3 vol% nickel in the form of a cell boundary network is enough to prevent brittle fracture.

The effect of indentation on strength behavior of alumina/8 vol% Ni is shown in Fig. 8(A). Fracture is not catastrophic, and strength is essentially unchanged (251 MPa). Indentation does not result in strength-degrading flaws (Section III(1), Fig. 2). The SEM micrograph of the tension side of this specimen shown in Fig. 8(B) confirms that failure does not initiate from the indent.

(3) Effect of Oxidation

The effect of heat treatment at 1200°C on the room-temperature flexural strength behavior of the alumina/8 vol% nickel fibrous monolith is compared with an untreated sample in Fig. 9. Fracture is noncatastrophic, and the apparent strength is 216 MPa. The effect of heat treatment on the load–deflection behavior of a notched beam is shown in Fig. 10. The specimen does not fail in a brittle manner. Significant load-bearing ability is recorded after a crack has propagated from the notch. For the heat-treated notched beam, the K_{Ic} calculated from the load, notch depth, and specimen dimensions is 5.9 MPa·m$^{1/2}$, which is almost the same as for the untreated material.

The side surface of the flexure bar after the test is shown in Fig. 11. The optical micrograph in Fig. 11(A) shows the surface of the bar has turned bluish-green on heat treatment. The bar remains intact after significant bending during the test. The SEM micrograph in Fig. 11(B) illustrates the fracture path. The primary crack has deflected along a cell boundary in the mid-section of the bar, leading to additional crack branching both on the left and right of the main crack.

X-ray diffraction of the side surface of the heat-treated bar indicates that the major phase is alumina, with NiO, $NiAl_2O_4$, Ni, and tetragonal ZrO_2 as the minor phases. Optical microscope examination of a polished section of a specimen oxidized

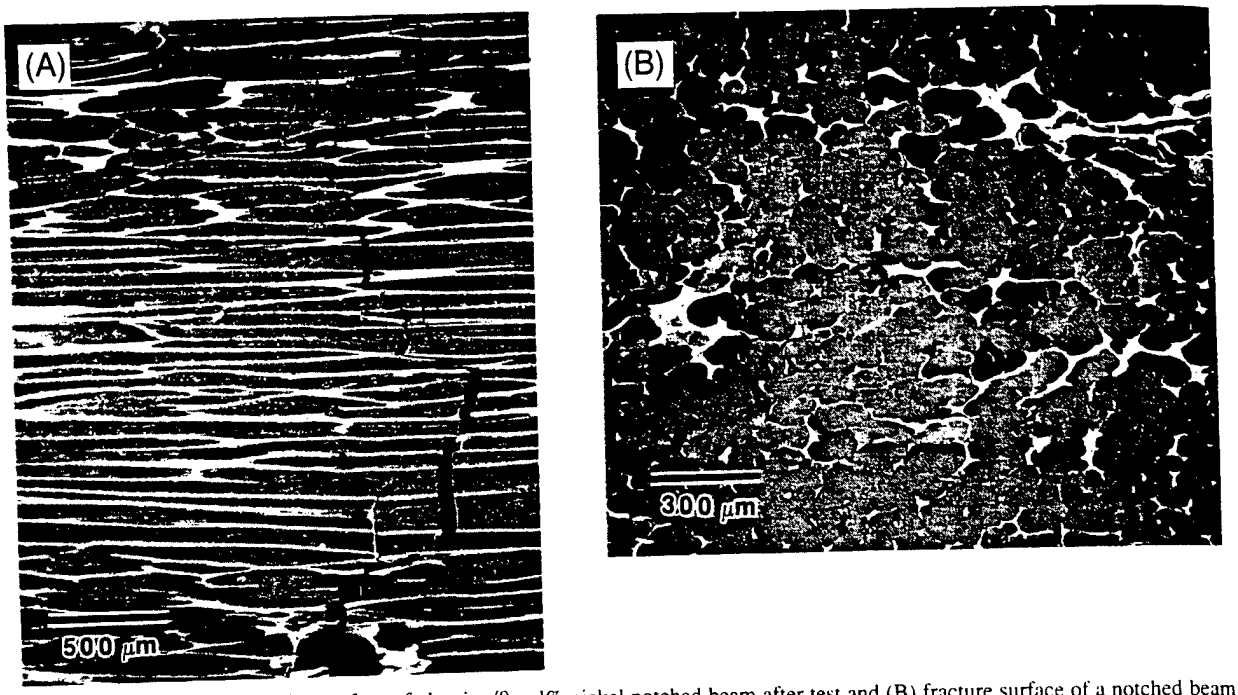

Fig. 6. SEM micrographs showing (A) side surface of alumina/8 vol% nickel notched beam after test and (B) fracture surface of a notched beam pulled apart after the test.

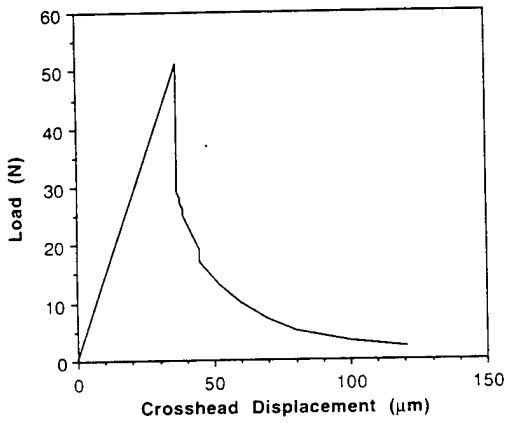

Fig. 7. Load–deflection behavior for a notched beam of the alumina/3 vol% nickel fibrous monolith in flexure.

10 h at 1200°C shows that the cell boundaries on the surface have turned bluish-green. The color extends to a depth of 50 to 100 μm, or about a half-cell deep. The green NiO color predominates in the deeper portion of the colored region, with blue $NiAl_2O_4$ present nearer the surface. This suggests that the nickel aluminate forms by reaction of the NiO with the alumina in the adjacent cells. Since the bulk of the alumina/Ni material is unaffected by the 1200°C(10-h) heat treatment, the fracture behavior is unchanged.

The depth of the oxidized cell boundary network correlates well with a NiO scale thickness of 60 μm expected after a similar heat treatment on pure nickel, assuming a parabolic rate constant of 10^{-9} $g^2/(cm^4 \cdot s)$ for Ni oxidation.[20,21] The first oxidation product, semiconducting NiO, would be relatively unprotective. However, reaction with the alumina cells would seal the cell boundaries with nickel aluminate, which has a lower electrical conductivity. This should result in better oxidation resistance. In nickel-base supperalloys, the formation of aluminum-containing oxides is very desirable for oxidation resistance.[21]

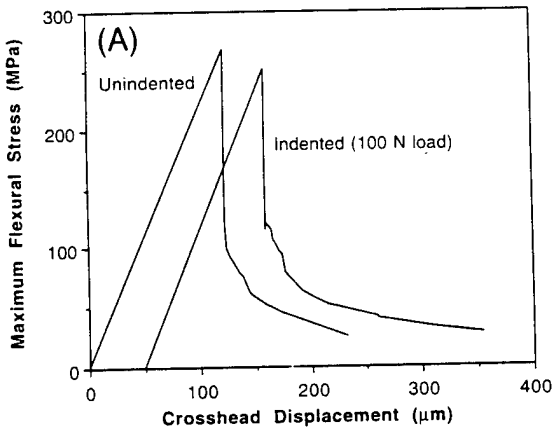

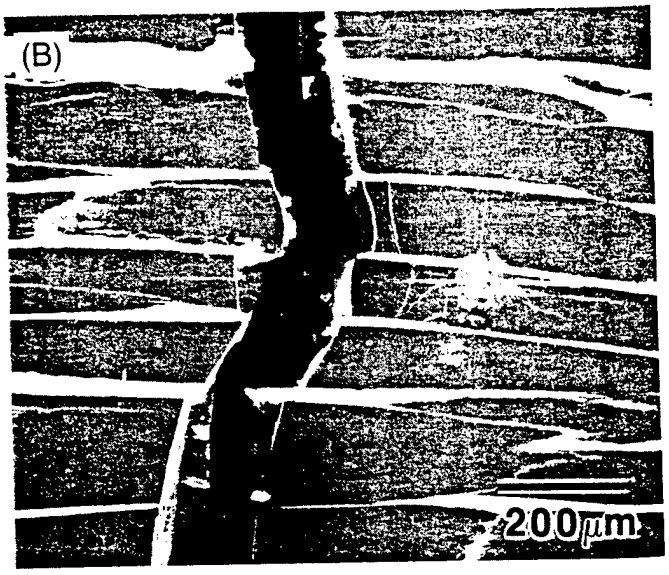

Fig. 8. (A) Flexural strength behavior of aligned-fiber alumina/nickel showing effect of indentation. (B) SEM micrograph of the tension side of the indented bar specimen. Failure does not initiate at indent.

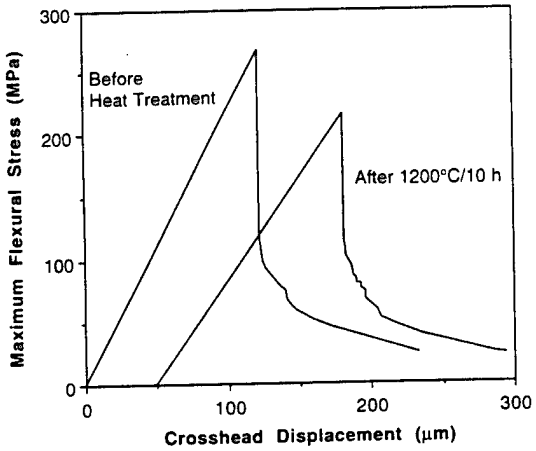

Fig. 9. Room-temperature flexural strength behavior of alumina/8 vol% nickel fibrous monolith showing effect of 10-h heat treatment at 1200°C.

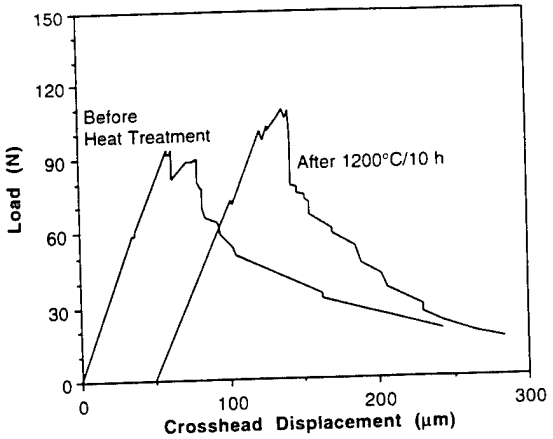

Fig. 10. Room-temperature load–deflection behavior of alumina/8 vol% nickel notched beam showing effect of 10-h heat tretment at 1200°C.

The oxidation resistance of the fibrous monolith can possibly be improved by using well-established methods for protecting nickel alloys.[21,22] For example, using a Ni–Cr alloy with 5–20 wt% Cr, or simply using alumina-formers such as MCrAlY (M = Ni,Co) overlay materials as the cell boundary phase, may significantly improve the resistance of the fibrous monolith to high-temperature degradation.

(4) Concluding Remarks

Nickel is the first example of a ductile phase incorporated into a fibrous monolith structure as the cell boundary by reduction of the oxide during firing. Other metals (e.g., Fe) could also be introduced as the cell boundary phase by this method, provided the thermodynamics favor reduction of the corresponding metal oxides in carbon-rich or reducing environments. Alternatively, a slurry of a fine metal powder may be used to coat the green ceramic fiber.

The alumina/nickel fibrous monolith also has potential because of its low cost. The alumina powder is inexpensive, and the most expensive NiO powder is used only in small quantities. In this study, hot-pressing was used for convenience, but the material can be densified by sintering. Alumina/nickel particulate composites[2] and laminates[9] have been densified by pressureless sintering. Other alumina-based fibrous monoliths have also been sintered to full density.[11] Sintered alumina/nickel fibrous monolith could be a cost-effective high-temperature engineering material.

IV. Conclusions

Fibrous monolithic ceramics can be fabricated with polycrystalline alumina cells with thin ribbons of nickel as cell boundaries. Uniaxially aligned alumina/Ni fibrous monoths with 8 vol% Ni have flexural strengths in the range of 246–375 MPa. Fracture is noncatastrophic, with retained loads up to 40% of the peak load. Fracture occurs by tensile cracking. Bridging ligaments of Ni, crack deflection along alumina/Ni cell boundaries, and crack branching in the axial directions can be observed. Strength is not significantly degraded by 100-N Vickers indentations. Uniaxially aligned alumina/Ni fibrous monothis with 3 vol% Ni have brittle fracture in flexure. The 3 vol% Ni and 8 vol% Ni specimens display noncatastrophic fracture in the single-edge-notched beam test. Failure begins at a load corresponding to a K_{Ic} = 5.9 MPa·m$^{1/2}$, but load continues to rise after fracture initiates. The room-temperature flexural behavior is not significantly changed by 10-h oxidation in air at 1200°C, suggesting useful oxidation resistance. The NiO cell boundary oxidation product reacts with alumina to form nickel aluminate spinel.

Acknowledgment: Lynne Svedberg provided valuable assistance in fiber spinning.

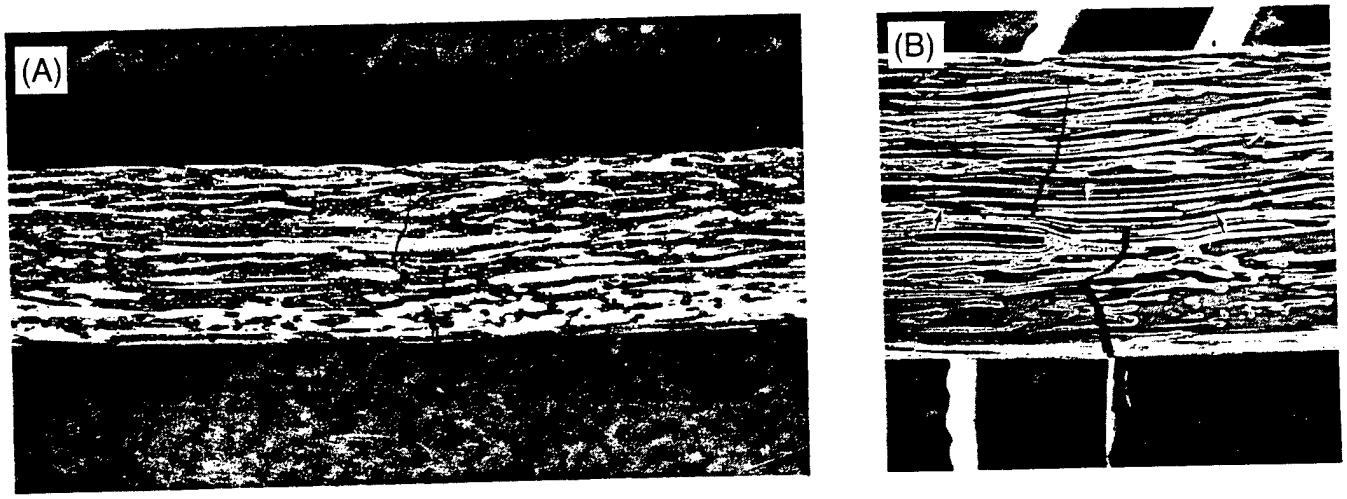

Fig. 11. (A) Optical micrograph showing side surface of heat-treated bar after test. (B) Higher magnification SEM micrograph of the crack profile on the side surface. Arrows indicate cracks branching off the main crack. Magnification in micrographs can be estimated from the 3-mm thickness of the test specimen.

References

[1]V. V. Krstic, P. S. Nicholson, and R. G. Hoagland, "Toughening of Glasses by Metallic Particles," *J. Am. Ceram. Soc.*, **64** [9] 499–504 (1981).

[2]W. H. Tuan and R. J. Brook, "The Toughening of Alumina with Nickel Inclusions," *J. Eur. Ceram. Soc.*, **6**, 31–37 (1990).

[3]M. S. Newkirk, A. W. Urquhart, H. R. Zwicker, and E. Breval, "Formation of Lanxide™ Ceramic Composite Materials," *J. Mater. Res.*, **1** [1] 81–89 (1986).

[4]M. K. Aghajanian, N. H. McMillan, C. R. Kennedy, S. J. Luszcz, and R. Roy, "Properties and Microstructure of Lanxide™ Al_2O_3–Al Ceramic Composite Materials," *J. Mater. Sci.*, **24**, 658–70 (1989).

[5]M. K. Ashby, F. J. Blunt, and M. Bannister, "Flow Characteristics of Highly Constrained Metal Wires," *Acta Metall.*, **37** [7] 1847–57 (1989).

[6]B. D. Flinn, M. Ruhle, and A. G. Evans, "Toughening in Composites of Al_2O_3 Reinforced with Al," *Acta Metall.*, **37** [11] 3001–3006 (1989).

[7]B. D. Flinn, C. S. Lo, F. W. Zok, and A. G. Evans, "Fracture Resistance Characteristics of a Metal-Toughened Ceramic," *J. Am. Ceram. Soc.*, **76** [2] 369–75 (1993).

[8]M. Yasrebi, G. H. Kim, K. E. Gunnison, D. L. Milius, M. Sarikaya, and I. A. Aksay, "Biomimetic Processing of Ceramics and Ceramic–Metal Composites," *Mater. Res. Soc. Symp. Proc.*, **180**, 625–35 (1990).

[9]Z. Chen and J. J. Mecholsky, Jr., "Toughening by Metallic Lamina in Nickel/Alumina Composites," *J. Am. Ceram. Soc.*, **76** [5] 1258–64 (1993).

[10]W. S. Coblenz, "Fibrous Monolithic Ceramic and Method for Production," U.S. Pat. No. 4 772 524, September 20, 1988.

[11]S. Baskaran, S. D. Nunn, D. Popovic, and J. W. Halloran, "Fibrous Monolithic Ceramics: I, Fabrication, Microstructure, and Indentation Behavior," *J. Am. Ceram. Soc.*, **76** [9] 2209–16 (1993).

[12]S. Baskaran and J. W. Halloran, "Fibrous Monolithic Ceramics: II, Flexural Strength and Fracture Behavior of the Silicon Carbide Graphite System," *J. Am. Ceram. Soc.*, **76** [9] 2217–24 (1993).

[13]S. Baskaran and J. W. Halloran, "Fibrous Monolithic Ceramics: III, Mechanical Properties and Oxidation Behavior of the Silicon Carbide/Boron Nitride System," *J. Am. Ceram. Soc.*, **77** [5] 1249–55 1994.

[14]W. F. Brown, Jr., and J. E. Srawley, "Plane Strain Crack Toughness Testing of High Strength Metallic Materials," STP 410, 13–14, American Society for Testing and Materials, Philadelphia, PA, 1966.

[15]E. Schreiber, O. L. Anderson, and N. Soga, *Elastic Constants and Their Measurement*; Ch. 4, McGraw-Hill, New York, 1973.

[16]S. Spinner and W. E. Tefft, "A Method for Determining Mechanical Resonance Frequencies and for Calculating Elastic Moduli from these Frequencies," *Proc. Am. Soc. Test. Mater.*, **61**, 1229 (1961).

[17]R. C. Weast (Ed.), *CRC Handbook of Chemistry and Physics*, 64th ed. CRC Press, Boca Raton, FL, 1983–84.

[18]K. Y. Chia, S. G. Seshadri, and M. Srinivasan, "Notching Techniques Used in SENB Fracture Toughness," *Ceram. Eng. Sci. Proc.*, **7** [7–8] 795–801 (1986).

[19]J. Wang, W. M. Rainforth, I. Wadsworth, and R. Stevens, "The Effects of Notch Width on the SENB Toughness for Oxide Ceramics," *J. Eur. Ceram. Soc.*, **10** [1] 21–31 (1992).

[20]P. Kofstad; p. 256 in *Nonstoichiometry, Diffusion and Electrical Conductivity in Binary Metal Oxides*, Wiley, New York, 1972.

[21]J. L. Smialek and G. M. Meier, "High-Temperature Oxidation"; pp. 293–326 in *Superalloys II, High Temperature Materials for Aerospace and Industrial Power*, Wiley, New York, 1987.

[22]J. H. Wood and E. Goldman, "Protective Coatings"; see Ref. 21, pp. 359–84.

US005645781A

United States Patent [19]

Popovic' et al.

[11] Patent Number: 5,645,781

[45] Date of Patent: Jul. 8, 1997

[54] **PROCESS FOR PREPARING TEXTURED CERAMIC COMPOSITES**

[75] Inventors: **Dragan Popovic'**, Tucson, Ariz.; **John W. Halloran**, Ann Arbor, Mich.; **Gregory E. Hilmas**, Saline, Mich.; **Guy Allen Brady**, Ann Arbor, Mich.; **Scott Somers**, East Lansing, Mich.; **Andrew Barda**, Battle Creek, Mich.; **Gregory Zywicki**, Warren, Mich.

[73] Assignee: **The Regents of the University of Michigan**, Ann Arbor, Mich.

[21] Appl. No.: **309,853**

[22] Filed: **Sep. 21, 1994**

[51] **Int. Cl.**[6] **B29C 47/06**; B29C 63/00; B28B 5/00

[52] **U.S. Cl.** **264/639**; 264/172.15; 264/250

[58] **Field of Search** 264/60, 115, 172.15, 264/250

[56] **References Cited**

U.S. PATENT DOCUMENTS

2,699,415	1/1955	Nachtman	154/91
3,098,723	7/1963	Micks	29/183.5
3,793,041	2/1974	Sowman	106/67
3,795,524	3/1974	Sowman	106/65
3,811,920	5/1974	Galasso	117/69
3,953,636	4/1976	Kirchner	428/155
3,996,145	12/1976	Hepburn	252/62
4,521,360	6/1985	Fiorentino	264/108
4,605,594	8/1986	Owens et al.	428/373
4,640,848	2/1987	Cerdan-Diaz et al.	427/426
4,642,271	2/1987	Rice	428/698
4,772,524	9/1988	Coblenz	428/699
4,908,340	3/1990	Frechette et al.	501/95
4,990,490	2/1991	Pathare et al.	505/1
5,041,248	8/1991	Renlund et al.	264/44
5,053,092	10/1991	Lachman	156/89

FOREIGN PATENT DOCUMENTS

1397955	6/1975	United Kingdom

Primary Examiner—Christopher A. Fiorilla
Attorney, Agent, or Firm—Leydig, Voit & Mayer, Ltd.

[57] **ABSTRACT**

A method for the preparation of a fibrous monolithic ceramic which exhibits non-brittle fracture characteristics from green monofilament ceramic fibers having a controlled texture. This method includes the steps of: (a) forming a first ceramic-laden composition includes a thermoplastic polymer and at least about 40 vol. % of a ceramic particulate into a substantially cylindrical core, (b) applying a layer of a second ceramic-laden composition includes a thermoplastic polymer and at least about 40 vol. % of a ceramic particulate which differs from the particulate contained in the first composition onto the core to form a substantially cylindrical feed rod having an average initial diameter, (c) extruding the feed rod to form a green ceramic monofilament fiber which has an average diameter that is less than the average diameter of the feed rod, and (e) arranging the green ceramic monofilament fibers into a desired configuration to provide a green fibrous monolith, wherein, during the extrusion step, each ceramic-laden composition has a viscosity which is approximately equivalent to that of each other ceramic-laden composition, and, if the ceramics present in the extruded ceramic monofilament fiber are sintered, a plane of weakness defined by the interface of the core and the layer is provided, the interface being relatively weaker than the core. The green fibrous monolith may be sintered to provide a fibrous monolith.

14 Claims, 12 Drawing Sheets

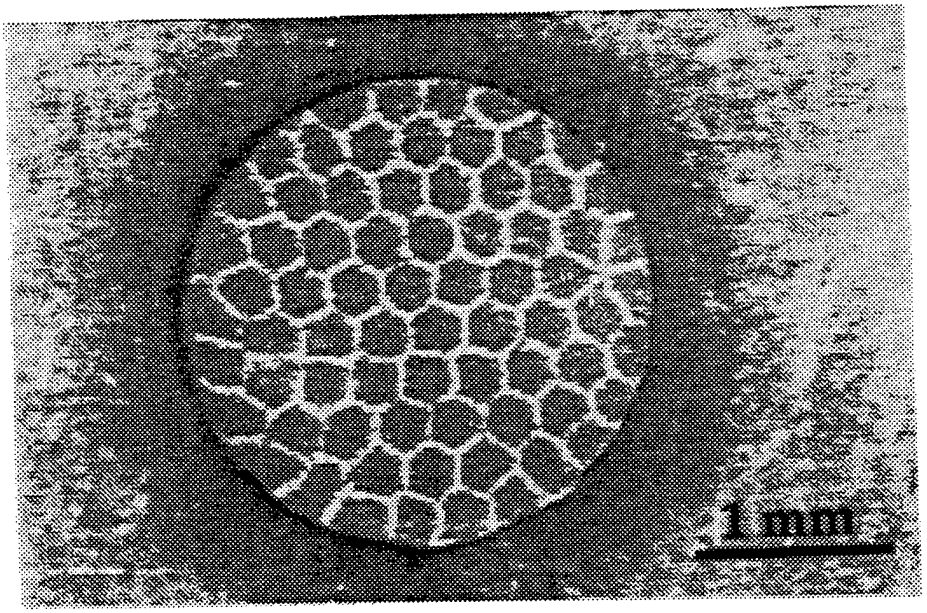

nance fees
rs and six
after upon
he mainte-
applicable
ate the fee
the end of

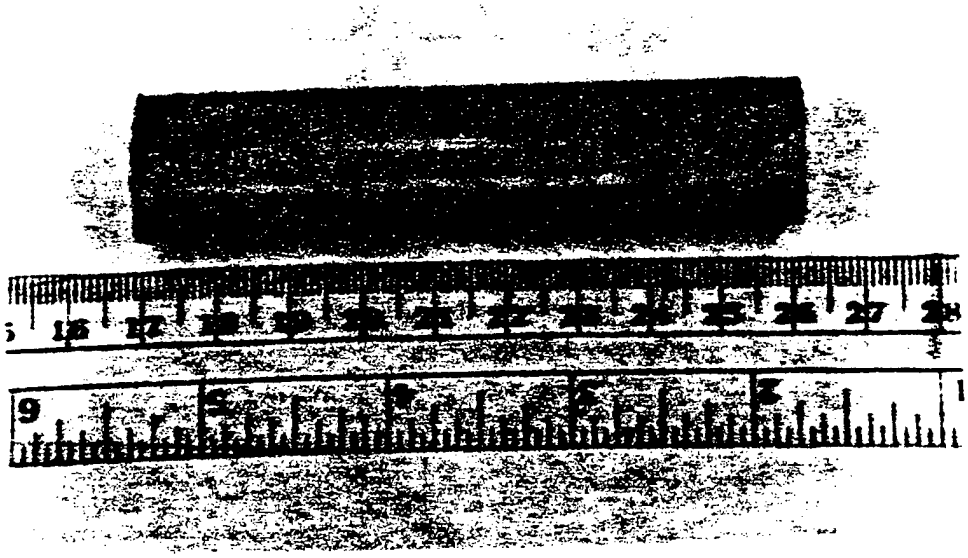

FIG. 1

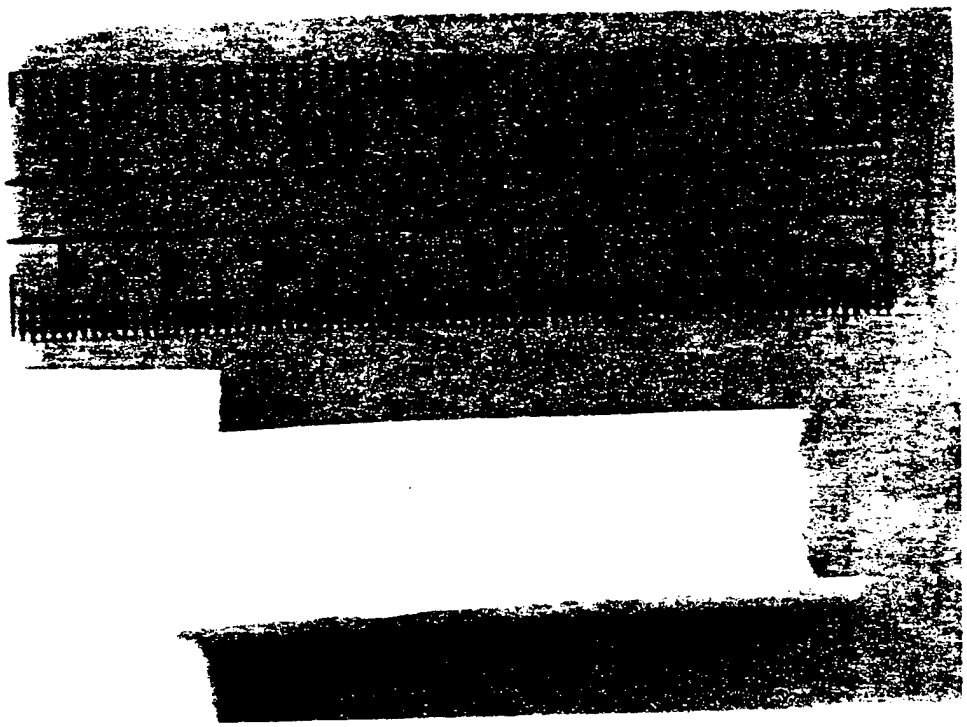

FIG. 2

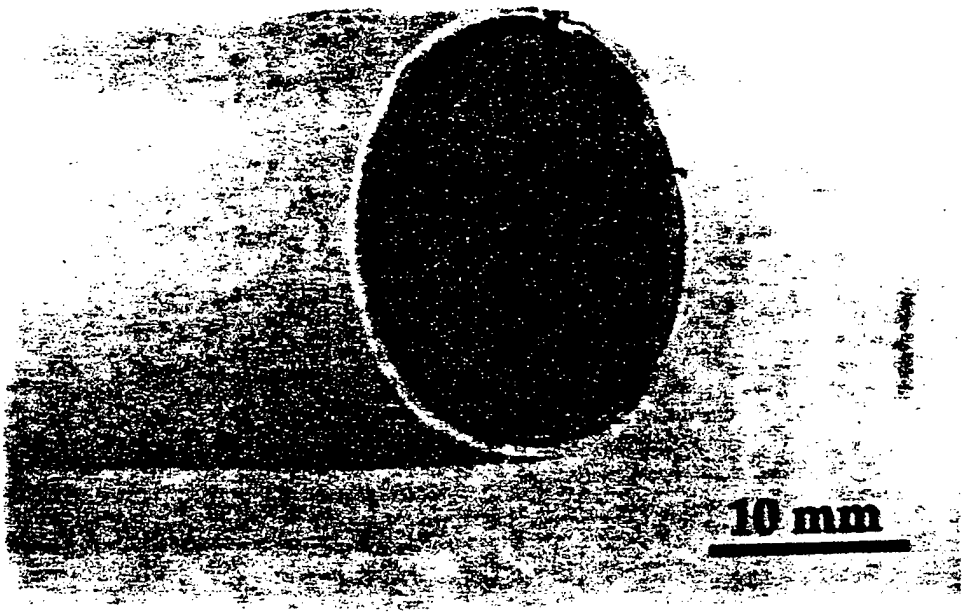

FIG. 3

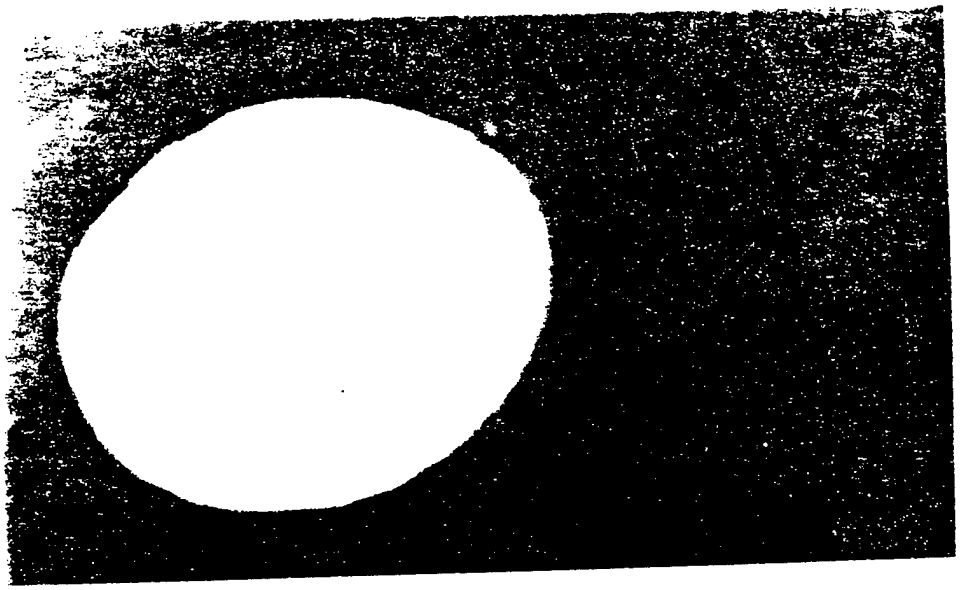

FIG. 4

FIG. 5

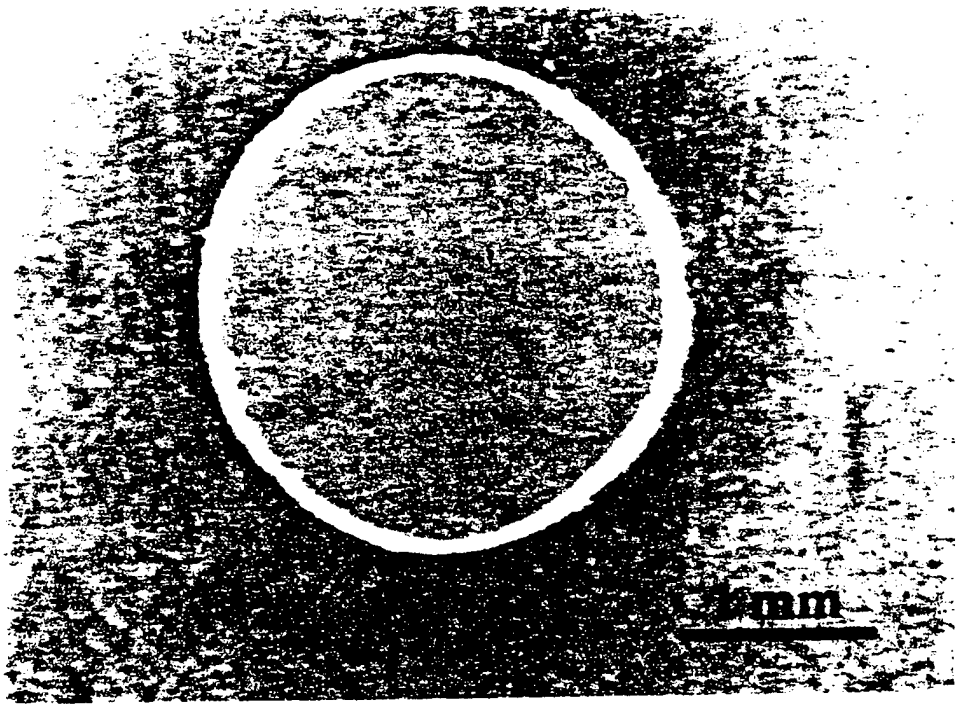

FIG. 6

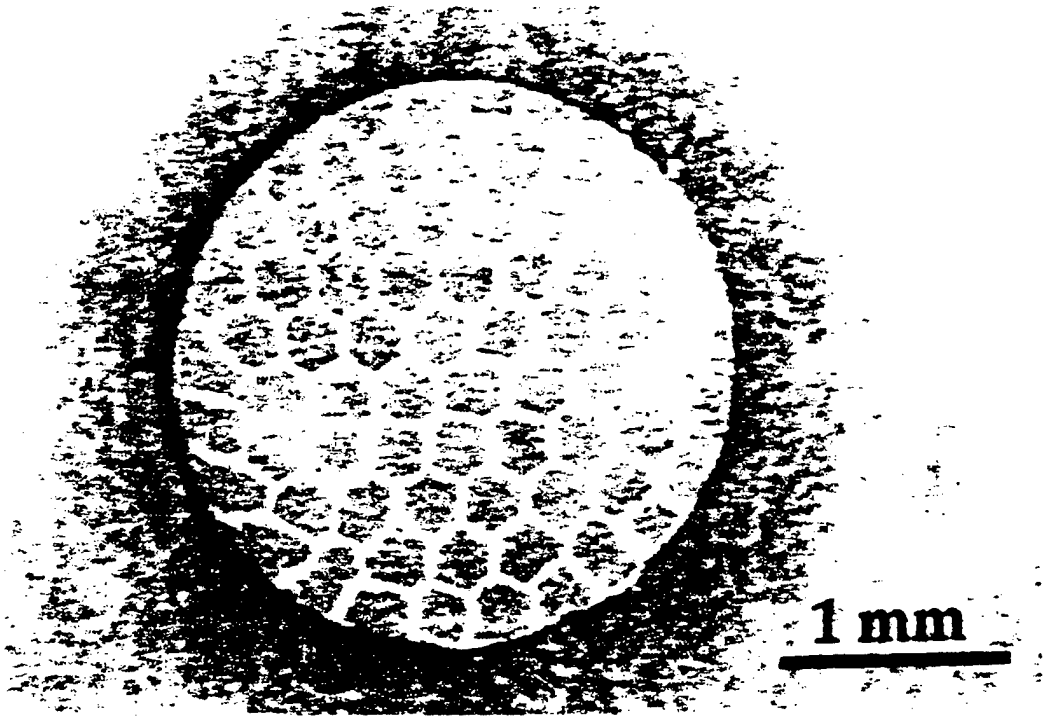

FIG. 7

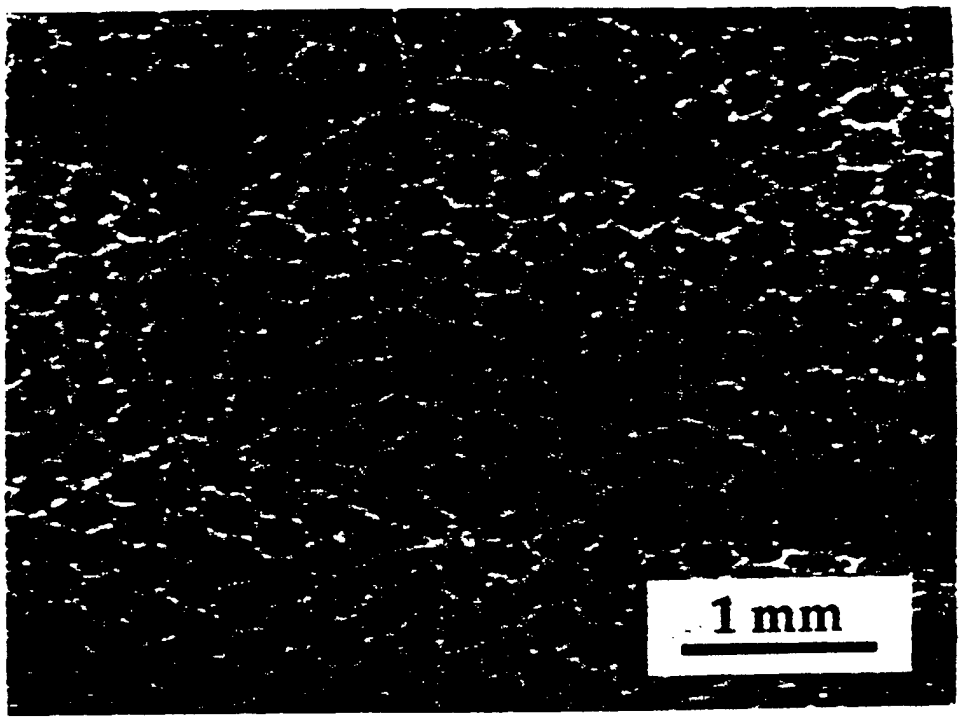

FIG. 8

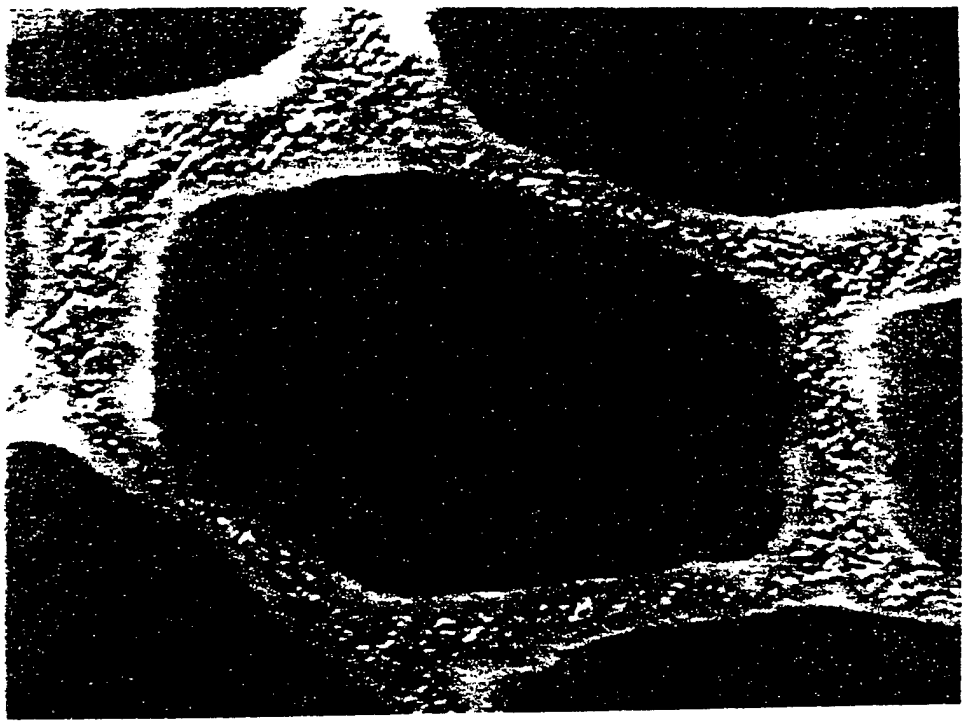

FIG. 9

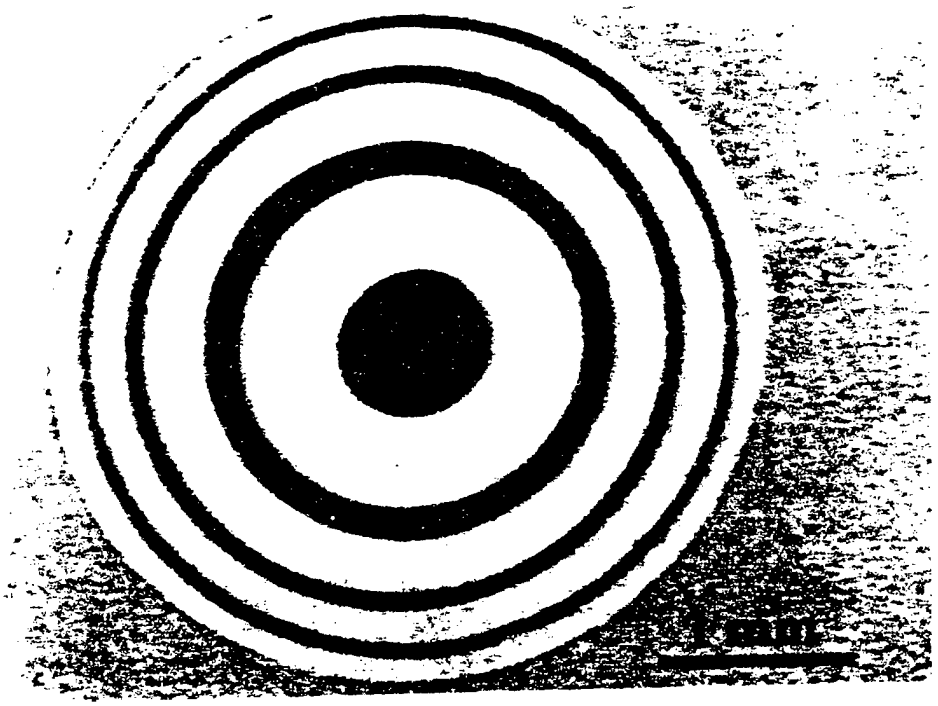

FIG. 10

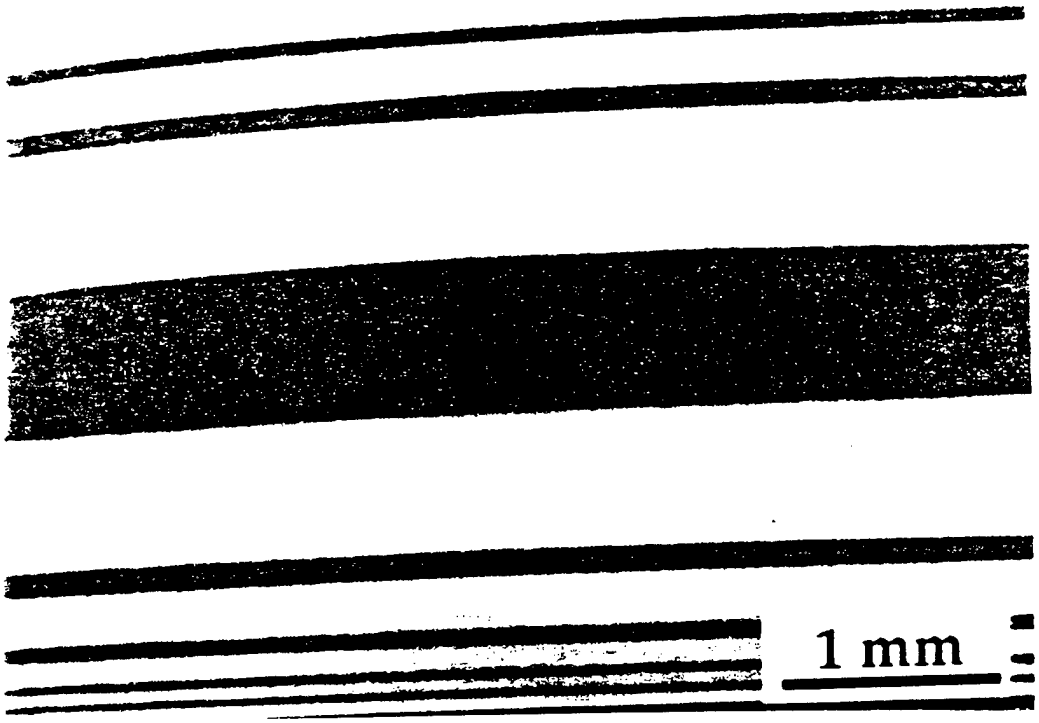

FIG. 11

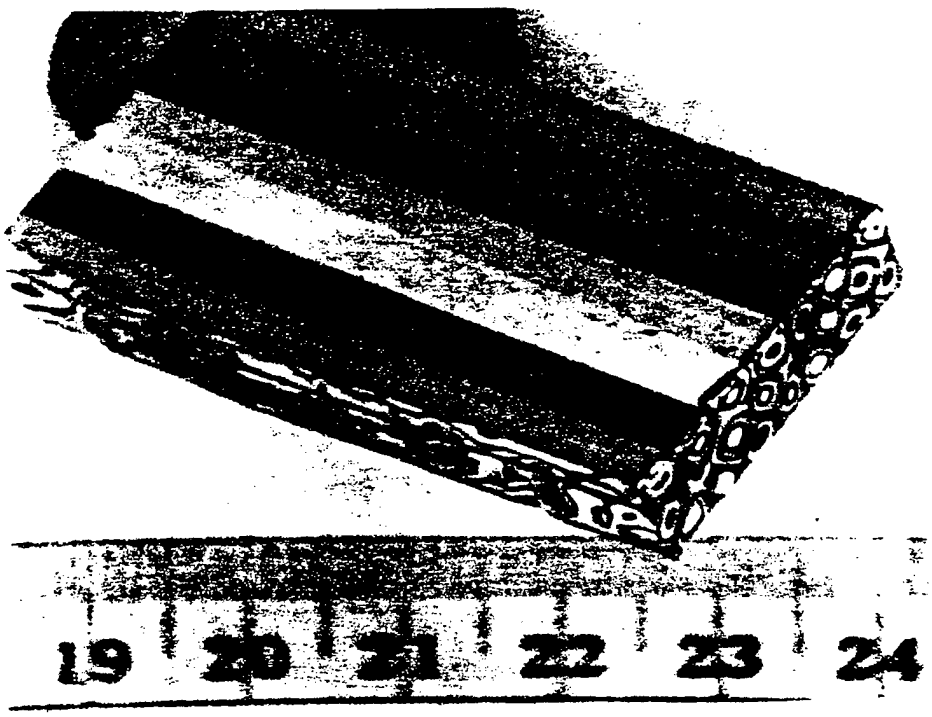

FIG. 12

PROCESS FOR PREPARING TEXTURED CERAMIC COMPOSITES

This patent was made with U.S. Government support under grant numbers N00014-93-1-0953 and N00014-93-1-0302 awarded by the Office of Naval Research. The Government has certain rights in the invention described herein.

TECHNICAL FIELD OF THE INVENTION

The present invention relates to methods for preparing textured ceramic composites, such as fibrous ceramic monoliths, using ceramic green fibers as well as to methods for the preparation of such ceramic green fibers having specific textures.

BACKGROUND OF THE PRESENT INVENTION

Attractive properties can be obtained from ceramic composites having a texture in which the distribution of two or more materials are well controlled. An example of such textured ceramic composites are fibrous monolithic ceramics. Unlike ordinary ceramics which abruptly and catastrophically suffer tensile fracture, fibrous monoliths have the unique property of non-brittle fracture—they gracefully split and delaminate, like, e.g., wood, thereby providing for non-catastrophic failure. This property is of great value in many applications, e.g., high temperature structural applications such as those encountered by engine components as well as a number of other automotive structural applications.

A more detailed description of the structure and properties of such fibrous monolithic ceramics is provided in U.S. Pat. No. 4,772,524. This patent discloses a fibrous monolithic ceramic body as comprising a plurality of compacted, coated, and sintered fibers. These fibers comprise a core of a first ceramic composition, and a coating on that core of a different ceramic composition. This coating is referred to as a "debond phase," and serves as a "plane of weakness." The particular debond phase described in the '524 patent is said to be comprised of three ceramics—aluminum titanate, zirconia, and halfnia—all of which possess a tendency to spontaneously microcrack. By providing a layer of these microcracked ceramics, it was found that the desired "plane of weakness" was formed in the fiber.

It is this plane of weakness which provides a fibrous monolith prepared using such a fiber, after sintering, with a non-brittle fracture characteristic. Specifically, the interface, which defines a plane of weakness, will function to deflect a crack in the coating, or "debond phase, from normal to the plane of weakness to a direction parallel to the plane of weakness. Thus, catastrophic failure of the fibrous monolith prepared using such fibers is avoided.

The '524 patent further discloses a process for preparing such fibrous monolithic ceramics. This process comprises coating a fugitive cotton thread by passing that thread first through a suspension of the core composition, and subsequently through the coating composition, to provide a ceramic fiber. These fibers are then arranged together to form the desired fibrous monolith.

Since the issuance of the '524 patent, new varieties of fibrous monolithic ceramics have been discovered. See, e.g., S. Baskaran et al., "SiC-Based Fibrous Monolithic Ceramics," *Ceramic Sci. & Eng. Proc.* 14 (9–10) pp. 813–823; S. Baskaran et al., "Fibrous Monolithic Ceramics, I: Fabrication, Microstructure, and Indentation Behavior," *J. Am. Cer. Soc'y* 76 (9), pp. 2209–16 (1993); S. Baskaran et al., "Fibrous Monolithic Ceramics, II: Flexural Strength and Fracture Behavior of the SiC/Graphite System," *J. Am. Cer. Soc'y* 76 (9) pp. 2217–24 (1993); S. Baskaran et al., "Fibrous Monolithic Ceramics, III: Mechanical Properties and Oxidation Behavior of the SiC/BN System," *J. Am. Cer. Soc'y* 77 (5) pp. 1249–55 (1994); S. Baskaran et al., "Fibrous Monolithic Ceramics, IV: Mechanical Properties and Oxidation Behavior of the Alumina/Ni System," *J. Am. Ceramic Soc'y*, 77, (5) pp. 1256–62 (1994); and D. Popovic' et al., "Silicon Nitride and Silicon Carbide Fibrous Monolithic Ceramics" 42 *Silicon Based Structural Ceramics* (B. W. Sheldon et al. eds., Am. Cer. Soc'y, Westerville, Ohio, 1994) pp. 173–86. In these newly discovered ceramic fibrous monoliths, the ceramic fibers from which they are prepared establish a plane of weakness therein by using a graphite layer or a boron nitride layer. The core composition, in contrast, was able to be prepared from a wide variety of ceramics including, e.g., silicon carbide, silicon nitride, and alumina.

In conjunction with or shortly after the discovery of the aforementioned new materials, new methods for preparing the ceramic fibers used to fabricate fibrous monoliths were also discovered. Specifically, it was taught that the core of a green ceramic fiber could be prepared either by dry spinning or melt spinning a composition comprising a polymer and ceramic powder. To complete the ceramic fiber, it was further taught that the coating layer was to be subsequently applied by dipping the core into a slurry of the debond phase composition.

Three U.S. patents have issued which involve the extrusion of a mixture of a ceramic powder and a polymer to form a fiber. The first patent, U.S. Pat. No. 4,908,340, discloses the extrusion of ceramic green fibers by melt spinning a mixture of thermoplastic polymers and ceramic powders. The second, U.S. Pat. No. 4,990,490, describes a process for the thermoplastic extrusion of green fibers from superconducting ceramics which are subsequently coated with metal powders. The third patent, U.S. Pat. No. 5,041,248 describes the extrusion of green fibers by melt spinning polyisobutylene with ceramic powders. This patent further discloses that its thermoplastic extrusion process may be used to make sintered ceramic bars, rods, tubing, or fibers from ceramic-polymer mixtures. The mixtures are described as those in which the polymer acts as a fugitive vehicle, it being later removed during the heat treatment required to obtain a sintered ceramic product.

In summary, fibrous monoliths have traditionally been fabricated using fibers that were prepared by the laborious process of dip-coating previously extruded solid ceramic cores in a coating composition comprising ceramics and polymers. While this provides a textured fiber, it is slow, inconvenient to set-up and use, difficult to control, and is unable to provide a uniformly-textured fiber.

Thus, there exists a need for a more efficient method for preparing fibrous monolithic ceramics which exhibit non-brittle fracture characteristics using green ceramic fibers. The exists a further need for a method by which the texture of fibers used to prepare such monoliths can be more readily controlled.

It is therefore an object of the present invention to provide a relatively efficient method for preparing fibrous monolithic ceramics which exhibit non-brittle fracture characteristics from green ceramic fibers.

Another object of the present invention is to provide a relatively efficient method for preparing such green ceramic fibers despite the presence of high levels of ceramic particulate loading in any composition from which the fibers are prepared.

A further object of the present invention is to provide a green ceramic fiber useful for preparing fibrous monolithic ceramics in which the texture of the fiber is precisely controllable within defined parameters.

Yet another object of the present invention to provide a method for increasing the strength of fibrous monolithic ceramics.

These and other objects and advantages of the present invention, as well as additional inventive features, will be apparent from the description of the invention provided herein.

BRIEF SUMMARY OF THE INVENTION

In one aspect, the present invention provides a method for the preparation of a fibrous monolithic ceramic which exhibits non-brittle fracture characteristics from green monofilament ceramic fibers having a controlled texture. This method comprises: (a) forming a first ceramic-laden composition comprising a thermoplastic polymer and at least about 40 vol. % of a ceramic particulate into a substantially cylindrical core, (b) applying a layer of a second ceramic-laden composition comprising a thermoplastic polymer and at least about 40 vol. % of a ceramic particulate which differs from the particulate contained in the first composition onto the core to form a substantially cylindrical feed rod having an average initial diameter, (c) extruding the feed rod to form a green ceramic monofilament fiber which has an average diameter that is less than the average diameter of the feed rod, and (e) arranging the green ceramic monofilament fibers into a desired configuration to provide a green fibrous monolith, wherein, during the extrusion step, each ceramic-laden composition has a rheology which is approximately equivalent to that of each other ceramic-laden composition, and, if the ceramics present in the extruded ceramic monofilament fiber are sintered, a plane of weakness defined by the interface of the core and the layer is provided, the interface being relatively weaker than the core. Of course, the green fibrous monolith may be sintered to provide a fibrous monolith.

Another aspect of the present invention provides a method for the preparation of a fibrous monolithic ceramic which also exhibits non-brittle fracture characteristics. This method is the same as that described in the preceding paragraph, but further comprises extruding at least two of the green monofilament ceramic fibers substantially simultaneously to form a multifilament green ceramic fiber, and then using those multifilament fibers to prepare a green fibrous monolith. It is believed that the use of such multifilament fibers will cause the fibrous monolith to possess a greater strength as compared to a fibrous monolith prepared using monofilament fibers.

Further aspects of the present invention provide methods for the preparation of the mono- and multi-filament fibers used in preparing the fibrous monolithic ceramics in which the texture of the fibers may be readily controlled.

The invention may best be understood with reference to the accompanying drawings wherein illustrative embodiments are shown and in the following detailed description of the preferred embodiments.

BRIEF DESCRIPTION OF THE DRAWINGS

FIG. 1 is a photograph of a molded core for a feed rod prepared in accordance with a method of the present invention.

FIG. 2 is a photograph of one-half of a cylindrical shell which, with its other half, is used to clad the molded core depicted in FIG. 1.

FIG. 3 is a photograph of the assembled feed rod which comprises the core depicted in FIG. 1 and two one-half cylindrical shells depicted in FIG. 2.

FIG. 4 is a photomicrograph of an axial cross-section of a monofilament green fiber prepared in accordance with a method of the present invention.

FIG. 5 is a photomicrograph of a longitudinal cross-section of a monofilament green fiber prepared by a method of the present invention.

FIG. 6 is a photomicrograph of an axial cross-section of a monofilament green fiber prepared by a method of the present invention which will serve as one filament for the preparation of a multifilament green fiber.

FIG. 7 is a photomicrograph of an axial cross-section of a multifilament green fiber prepared by a method of the present invention.

FIG. 8 is a photomicrograph of an axial cross-section of a textured green ceramic fibrous monolith prepared using a multifilament green fiber prepared in accordance with a method of the claimed invention.

FIG. 9 is a photomicrograph of an axial cross-section of a pressure sintered ceramic/metal monolith having zirconium oxide cells and metallic nickel cell boundaries which are separated by an aluminum oxide interphase, which monolith was prepared using a multifilament green fiber.

FIG. 10 is a photomicrograph of an axial cross-section of a filament which was axially extruded in a manner of the present invention which demonstrates its "tree ring" structure.

FIG. 11 is a photomicrograph of a longitudinal cross-section of a filament which was axially extruded in a manner of the present invention which demonstrates its "tree ring" structure.

FIG. 12 is a photograph of a green fibrous monolith prepared in a manner of the present invention by molding green ceramic filaments having a "tree ring" structure.

DESCRIPTION OF THE PREFERRED EMBODIMENTS

One aspect of the present invention provides a method for preparing fibrous monolithic ceramics having non-brittle fracture characteristics using a textured ceramic fiber which has been prepared by the simultaneous extrusion of a particular ceramic feed rod. The feed rod comprises a core prepared from a first ceramic composition and a shell which surrounds that core that is prepared from a second, and different, ceramic composition. Each of the compositions used to prepare the aforementioned fiber comprise a ceramic particulate component and a thermoplastic polymer component, the latter acting as a fugitive carrier for the ceramic particulates, i.e., the polymer is removed when the fiber, or a monolith prepared therefrom, is subjected to high temperatures, such as those required to sinter the ceramic particles present in the compositions.

Specifically, this aspect of the present invention comprises forming a first ceramic-laden composition comprising a thermoplastic polymer and at least about 40 vol. % of a ceramic particulate into a substantially cylindrical core. Subsequently, a layer of a second ceramic-laden composition comprising a thermoplastic polymer and at least about 40 vol. % of a ceramic particulate which differs from the ceramic particulate contained in the first composition is applied onto the core to form a substantially cylindrical feed rod.

Prior to the discovery of the present invention, it was appreciated by those skilled in the art that the introduction

of such relatively high levels of ceramic particulates, e.g., above about 40 vol. %, into thermoplastic polymers would make the extrusion of such loaded polymers very difficult. One of the reasons for this is the dramatic changes that occur in the rheology of the molten polymer mixture. Specifically, such mixes were known to possess, at least, significant yield stress and a much higher viscosity as compared to the unfilled polymer. Until the discovery of the present invention, then, such problems were thought to foreclose the ability of one to successfully extrude more than one such composition simultaneously, i.e., using two continuous extruders to feed two such molten polymer compositions through a complex coextrusion die, and still obtain a usable green ceramic fiber therefrom. One of the aspects of the present invention is the recognition that a desired geometry in the fiber product may be obtained by extruding a "controlled geometry" feed rod, i.e., the desired fiber geometry is created in the feed rod itself. This method allows a fiber of a particular desired texture to be prepared by simple piston extrusion through a simple extrusion die.

In order to provide a fibrous monolith having non-brittle fracture characteristics, the components which comprise the compositions from which the feed rod is prepared should be selected so that, if one sinters the extruded ceramic fiber, a plane of weakness defined by the interface of the core and the layer is provided, wherein the interface is relatively weaker than the core. Although specific examples of materials which will provide a fiber having such attributes will be provided herein, the selection of such materials is well within the means of one skilled in the art due to the availability of published materials on the subject of fibrous monolithic ceramics.

In preparing the ceramic-laden compounds used in the inventive methods, the fine ceramic powder will typically be blended with a fiber-forming polymer and, advantageously, one or more processing aids. Most fiber-forming thermoplastic polymers can be used in the compositions of the present invention, but preferred polymer systems are the highly flexible polymers and copolymers, advantageously ethylene polymers and copolymers, and preferably polyethylene, ethylene-ethyl acetate copolymers ("EEA") (e.g., DPDA-618NT, Union Carbide) and ethylene-vinyl acetate copolymers ("EVA") (e.g., ELVAX 470, E. I. DuPont Co.).

A wide variety of powder ceramics may also be used in the ceramic-laden compositions, affording a wide flexibility in the composition of the ultimate textured ceramic composite. Advantageously, powders which may be used in the first ceramic-laden composition to provide the core of the feed rod include ceramic oxides, ceramic carbides, ceramic nitrides, ceramic borides, and silicides. Preferred powders for use in that composition include aluminum oxide, barium oxide, beryllium oxide, calcium oxide, cobalt oxide, chromium oxide, dysprosium oxide and other rare earth oxides, lanthanum oxide, magnesium oxide, manganese oxide, niobium oxide, nickel oxide, aluminum phosphate, lead oxide, lead titanate, lead zirconate, silicon oxide and silicates, thorium oxide, titanium oxide and titanates, uranium oxide, yttrium oxide, yttrium aluminate, zirconium oxide and its alloys, boron carbide, iron carbide, halfnium carbide, molybdenum carbide, silicon carbide, tantalum carbide, titanium carbide, uranium carbide, tungsten carbide, zirconium carbide, ceramic nitrides including aluminum nitride, cubic boron nitride, silicon nitride, titanium nitride, uranium nitride, yttrium nitride, zirconium nitride, aluminum boride, halfnium boride, molybdenum boride, titanium boride, zirconium boride, and molybdenum disilicide.

In regard to the powders suitable for use in the second composition, the composition which provides the debond layer, there are advantageously included: agents known, from the available literature, to create weak interfaces such as fluoromica, tin oxide and lanthanum phosphate; agents known, from the available literature, to create porosity in a layer which function to create a weak interface; graphite powders and graphite-containing powder mixtures; and hexagonal boron nitride powder and boron nitride-containing powder mixtures. If a metallic debond phase is desired, reducible oxides of metals may be used, e.g., nickel and iron oxides, or powders of metals, e.g., nickel, iron, cobalt, or their alloys.

In regard to ceramic powder size, ultrafine powders have been successfully used, e.g., HSY-3.0 zirconia (a specific surface area of 7.0 m^2/g and an average particle size of 1 micrometer, available from Daichi Kigenso) and Cabot® Black Pearl 2000 carbon black (a specific surface area of 1500 m^2/g and an average particle size of 12 nanometers, available from Cabot Corporation). However, relatively coarse powders, e.g., those having average diameters above about 5 μm and up to about 10 μm, may also be used successfully in the ceramic-laden compositions, e.g., an 80% nickel/20% chromium alloy powder.

The level of powder loading in each composition should range from at least about 40 vol. %, and may advantageously range from about 40 vol. % to about 70 vol. %. Preferably, the loading may comprise about 50 vol. %. These levels are selected in order to provide good sintering behavior of the powder. Additional amounts of processing aids, as described further in the following paragraph, may be added to improve the dispersion of the powder within the composition, particularly when the powder loading exceeds about 60 vol. %.

As mentioned in the previous paragraph, a processing aid is advantageously included in the compositions in order to reduce the viscosity of the polymer compositions, aid in the dispersion of the powder in the compositions, and act as a lubricant for the compositions during extrusion. Many different oils, waxes, stearates, and fatty acids may be used, with preferred processing aids including methoxypolyethylene glycol having a MW of about 550 (e.g., MPEG 550 or Carbowax® 550, Union Carbide) and mineral oil, such as heavy mineral oil (Mineral Oil White, Heavy, Labguard®) or light mineral oil ((Mineral Oil White, Light, Labguard®) because they do not significantly degrade weaken or embrittle the green ceramic fiber.

It was determined that the compounding or mixing of the powders with the polymer and processing aids may be accomplished according to procedures known in the art of plastics compounding, despite the fact that the filler loading is higher than that experienced in typical plastic compositions. As will be appreciated by those skilled in the art, however, different powder/polymer/processing aid combinations require slightly different compounding techniques for providing the proper dispersion of those components in the ceramic-laden composition.

After the feed rod has been prepared from the appropriate ceramic/polymer compositions, it is extruded through an extrusion die to provide the desired green ceramic fiber. When the feed rod is the same shape as the orifice, as for example when both are round (the feed rod being substantially cylindrical), and certain other conditions are met, the flow field of the extrudate is such that there is little or no axial distortion. Thus, the present invention provides a method by which feed rods with a certain axially symmetric pattern or texture on a coarse scale can be extruded to form

a nearly identical version of that pattern, but on a smaller scale. One is able to obtain such small scale axial texture in a ceramic fiber by the coextrusion of an axially symmetric feed rod.

For example, consider the scenario wherein one desires to prepare a 300 μm diameter green fiber having a 250 μm diameter core of material A, with 50 μm thick cladding of material B. To produce this fiber, a 22 mm controlled geometry feed rod is prepared by molding material to provide a core rod (a solid cylinder) having a diameter of 18.3 mm, and combining this rod with a hollow cylindrical shell (e.g., provided by molding two half cylindrical shells that, when placed onto the core, will provide a complete cylindrical shell) that has been molded using material B. This hollow shell has a thickness of 3.7 mm, i.e., the shell has an inner diameter of 18.3 mm and an outer diameter of 22 mm. This feed rod is then suitably extruded through a 300 μm orifice at the appropriate temperature and pressure to provide the desired 300 μm green ceramic fiber.

In contrast to the axial symmetry, however, is the effect extrusion has upon the composition in the radial direction. Specifically, in the radial direction, the flow field present during extrusion causes distortions which result in the preparation of a non-axially symmetric fiber. For example, when one provides a feed rod having a sequence of layers of different compositions in the axial direction, such layers can be dramatically extended by the flow field to produce a pattern which is rather like tree rings. It has been recognized, however, that this effect can be used in a positive manner to create another distinct type of fine-scale texture in radially coextruded ceramic fibers.

Despite the foregoing, and as mentioned in a previous paragraph, preparing a ceramic fiber using a coextrusion method which possesses the same axial geometry as a two component feed rod is difficult. The extrusion will, if uncontrolled, cause distortion in the geometry of the feed rod as it passes through the extrusion die. In order to avoid such unwanted distortion, the rheology of the compositions being extruded should be substantially identical. Advantageously, and further, the temperature and rate at which the extrusion is conducted should also be selected so as to minimize the distortion in the geometry of the feed rod. One particular aspect of the rheology that should be controlled to retain this geometry is the viscosity of each composition. More specifically, each ceramic-laden composition should possess a viscosity which is approximately equivalent to that of each other ceramic-laden composition. Without such matching and careful control, flow instabilities between the two compounds will result, yielding a fiber which does not substantially replicate the original geometry of the feed rod.

As with any extrusion process, the reduction ratio is another important parameter. Although certain reduction ratios are provided in the Examples which follow, they should be considered to be merely illustrative, and not limiting. In the particular case of multifilament coextrusion, which will be discussed in a subsequent section, it should be recognized that a wide variety of spatial scales of the extrudate can be obtained by varying the reduction ratios of the first and second extrusion steps. It should further be noted that three or more extrusion steps could be completed in series to provide a fiber of a very fine diameter.

Moreover, while the Examples disclose the use of generally cylindrical feed rods, the claimed invention is not necessarily limited to that geometry. Other shapes could also be co-extruded in the manner of the present invention.

If desired, and after the feed rod has been extruded and a green ceramic fiber has been provided in the manner of the present invention, one may apply at least one further layer of a ceramic-laden composition comprising a thermoplastic polymer and at least about 40 vol. % of a ceramic particulate onto the fiber. When this scenario is undertaken, one essentially forms another feed rod, a second feed rod. This second feed rod may then be extruded to provide a green monofilament ceramic fiber having multiple layers of ceramic-laden compositions. This step may, if desired, be repeated any number of times. A second, and related, scenario provides for a further layer of ceramic-laden composition being layered onto an existing layer before the feed rod is extruded, i.e., the core material may be surrounded by one, two, or several layers of ceramic compositions. In either scenario, however, the ceramic particulate in each further layer should differ from that contained in the composition onto which the one further layer is applied.

After one ceramic fiber has been extruded, it may, if desired, be extruded with at least one other such fiber of the same or different composition and/or texture to provide a multifilament ceramic fiber. This may be achieved by molding a number of such fibers to form a new multifilament feed rod, and then extruding that newly formed feed rod. This process may be repeated any number of times to provide a multifilament fiber having very small, i.e., fine, filament diameters. Of course, the temperature and feed rate of the multifilament feed rod should be controlled to ensure that the geometry of the feed stock is not altered during extrusion. The multifilament green ceramic fibers provided by the foregoing process may be arranged to provide a green fibrous monolithic ceramic. It is believed that, because such fibers contain a great number of fine filaments, the monolith prepared from such fibers will possess greater strength that monoliths prepared using a monofilament fiber of an equivalent diameter.

After the coextruded product, either monofilament or multifilament, has been prepared, it can further be shaped by known means to produce green ceramic articles, such as green fibrous monoliths. Typically, the coextruded fiber or fibers will be molded by pressing in an appropriate mold at a temperature and pressure which will cause the fibers to form a solid, dense body from the individual mono- or multi-filament fibers. Any shape which can be compression molded or otherwise formed by plastic deformation can be obtained with the coextruded product. The molded article thus obtained is a ceramic "green body." The ceramic green body so molded has the desired texture created by the arrangement of the coextruded fibers. For example, a uniaxially aligned fibrous monolith can be obtained by the uniaxial lay-up of the coextruded fibers prior to molding, a random felt fibrous monolith can be obtained by molding randomly arraigned coextruded fiber, or a woven architecture can be obtained by molding a shape from previously woven coextruded green fiber. The coextruded product permits a wide variety of composite architectures to be fabricated in a molded green body.

Another important aspect of the coextruded product is that it serves as a ceramic green body, and hence can be treated to produce a ceramic article. This implies that the polymer and organic processing aids can be removed by one of the methods commonly employed in the field of ceramics, without damaging the molded article. One such example of polymer removal (or "binder burnout") is slow baking the green article to about 500° C., with a heating schedule determined by the characteristics of the polymer, the powder, and the geometry of the molded article, using

techniques known in the art of molded ceramics and powder metallurgy. The ceramic body formed thereby may then be densified, by sintering or pressure sintering, to produce a high quality ceramic article, e.g., a fibrous monolith.

The conditions for sintering or pressure sintering are peculiar to the particular material. For a given material system, the densification conditions for textured ceramic composite made from coextruded product are similar to the conditions for the same material made with ordinary powder processing. Thus, such densification conditions can be readily determined by one skilled in the ceramic art.

The following examples further illustrate the present invention but, of course, should not be construed as in any way limiting its scope.

EXAMPLE 1

This example illustrates the preparation of a silicon nitride/boron nitride monofilament fiber in accordance with one aspect of the present invention.

1. Silicon nitride compound:
   - A. Sinterable silicon nitride powder (E-10, UBE Chemical, Tokyo, Japan) mixed with sintering aids (9 wt % yttria powder and 3 wt % alumina powder): 37.23 g
   - B. Ethylene Vinyl Acetate copolymer: 7.65 g
   - C. Heavy Mineral oil: 3.21 g
2. Boron nitride compound:
   - A. Boron nitride powder (HCP, Advanced Ceramic Corporation, Cleveland, Ohio): 24.75 g
   - B. Ethylene Vinyl Acetate copolymer: 10.34 g
   - C. Methoxypolyethylene Glycol (MW 550): 0.75 g

The two ceramic compounds were prepared separately. The mixing was carried out in a Brabender Plastograph blender whose mixing bowl was preheated to about 120° C.–150° C. The ethylene copolymers and a portion of the processing aid were first added to the mixing bowl until they were melted and the torque reached a steady value. The dry powders were then added incrementally so that they blended thoroughly with the molten polymer. The balance of the processing aid was added incrementally with the powder. This compounding was continued until the apparent viscosity of the compound, as indicated by the torque rheometer function of the Brabender Plastograph, reached the desired level. For this example, the viscosity of the boron nitride compound was adjusted by the addition of processing aid in an amount such that its viscosity approximately matched the viscosity of the silicon nitride compound, i.e., about 18,000 poise at 170° C. The mixed compound was then removed from the blender and cooled.

A feed rod was molded from the silicon nitride compound using a 22 mm cylindrical mold. To accomplish this, granulated pieces of the compound were loaded into the mold and then molded at 150° C. and 23.2 MPa. After cooling, the molded feed rod was ejected. An example of a feed rod prepared by this process is illustrated in FIG. 1.

Cylindrical shells of the boron nitride compound were compression molded using a mold to create a shell of the desired dimensions. To accomplish this, granulated pieces of the compound were loaded into the mold and subsequently molded at 150° C. and 8.9 MPa. After cooling, the shell segments were removed from the mold. An example of shells prepared by this process is illustrated in FIG. 2.

A controlled geometry feed rod was then assembled by combining the silicon nitride core rod with the two boron nitride half-cylindrical shells. An example of a feed rod prepared in this manner is illustrated in FIG. 3. This feed rod was then loaded into the extrusion cylinder of a Bradford laboratory fiber extrusion machine (Bradford University Research, Bradford, UK). The cylinder was fitted with an extrusion die having a 285 μm diameter. Extrusion was commenced, and conducted at about 165° C. A monofilament coextruded silicon nitride/boron nitride fiber was obtained.

The extrudate was collected continuously on a spooler. FIG. 4 illustrates a cross-section of a representative monofilament coextruded fiber prepared by the foregoing method, and FIG. 5 shows a longitudinal cross-section of that fiber.

After arranging the fibers in a desired architecture and molding them to a desired shape, the green fibrous monolithic ceramic prepared thereby was baked to remove the binder. The resulting fibrous monolith was pressure sintered at 1750° C.

EXAMPLE 2

This example illustrates the preparation of a silicon carbide/boron nitride monofilament fiber in accordance with one aspect of the present invention.

1. Silicon carbide compound:
   - A. Sinterable silicon carbide powder (B-10, H. C. Starck, Newton, Mass.) mixed with sintering aids (11.1 wt % aluminum nitride powder and 8.9 wt % alumina powder): 39.41 g
   - B. Ethylene Vinyl Acetate copolymer: 8.35 g
   - C. Heavy Mineral Oil: 2.54 g
2. Boron nitride compound:
   - A. Boron nitride powder (HCP): 27.0 g
   - B. Ethylene Vinyl Acetate copolymer: 11.28 g
   - C. Methoxypolyethylene glycol [MW 500]: 0.87 g

The two ceramic compounds were prepared separately as in Example 1. For this example, both the silicon carbide compound and the boron nitride compound were adjusted to an apparent viscosity of about 13,000 poise at 170° C. The mixed compound was removed from the blender and cooled. As in Example 1, a feed rod was molded from the silicon carbide compound using a 22 mm cylindrical mold. Flat sheets of the boron nitride compound were compression molded by squeezing the granulated compound between flat steel sheets at a temperature of 80°–150° C. After cooling, the flat sheets were cut to the desired size and wrapped around the feedrod of the silicon carbide compound. The thickness of the sheets was adjusted to achieve the desired ratio of boron nitride to silicon carbide. A controlled geometry feedrod was then assembled from the boron nitride wrapped silicon carbide rod, and was extruded as in Example 1 to obtain monofilament coextruded silicon carbide/boron nitride fiber. The extrudate was collected continuously on a spooler.

After arranging the fibers in the desired architecture and molding them to the desired shape, the resulting green fibrous monolithic ceramic was baked to remove the binder and the fibrous monolith is pressure sintered to provide the finished fibrous monolith article.

EXAMPLE 3

This example illustrates the preparation of an aluminum oxide/80% nickel-20% chromium alloy monofilament fiber in accordance with one aspect of the present invention.

1. Aluminum oxide compound:
   - A. Sinterable aluminum oxide powder (A16SG, ALCOA, Bauxite, Ark.): 44.55 g

B. Ethylene Vinyl Acetate copolymer: 10.34 g

C. Heavy Mineral oil: 2.32 g

2. Nickel-Chromium compound:

A. Nickel-Chromium powder: 92.40 g

B. Ethylene Vinyl Acetate copolymer: 10.34 g

C. Methoxypolyethylene Glycol [MW 550]: 0.35 g

The two ceramic compounds were prepared separately as in the preceding examples with a Brabender Plastograph at about 150° C. The aluminum oxide compound was adjusted to an apparent viscosity of 15.000 poise at 150° C.. and the nickel-chromium compound to an apparent viscosity of about 13.000 poise at 150° C. A core rod was molded from the aluminum oxide compound in the manner set forth in the prior examples. and cylindrical shells of the nickel oxide compound were compression molded to create a shell of the desired dimensions. A controlled geometry feedrod was then assembled by combining the core rod with the two half-cylindrical shells. This feed rod was loaded into the extrusion cylinder of a Bradford laboratory fiber extrusion machine. The cylinder was fitted with an extrusion die having a 285 micrometer diameter. A monofilament coextruded aluminum oxide/nickel oxide fiber was obtained by extruding the feed rod at about 150° C. The extrudate was collected continuously on a spooler.

After arranging the fibers into a desired configuration and molding them to obtain the desired green fibrous monolithic ceramic. the monolith was baked to remove the binder and then pressure sintered at temperature of about 1350° C. to provide a fibrous monolith.

EXAMPLE 4

This example illustrates the preparation of a silicon carbide/boron nitride multifilament fiber in accordance with one aspect of the present invention.

1. Silicon carbide compound:

A. Sinterable silicon carbide powder mixed with sintering aids (11.1 wt % aluminum nitride powder and 8.9 wt % alumina powder): 36.13 g

B. Ethylene Vinyl Acetate copolymer: 7.57 g

C. Polyethylene Glycol [MW 550]: 0.75 g

2. Boron nitride compound:

A. Boron nitride powder: 24.75 g

B. Ethylene Vinyl Acetate copolymer: 10.23 g

C. Methoxypolyethylene Glycol [MW 550]: 0.75 g

The components of each compound were mixed in the manner set forth in Example 2. The apparent viscosity of both the silicon carbide compound and the boron nitride compound were then adjusted to an apparent viscosity of about 14.500 poise at 150° C. A controlled geometry feedrod was then prepared according to the method of Example 1. and 2.3 mm diameter monofilament fibers were provided by extrusion of the feed rods. An example of those extruded fibers is set forth in FIG. 6.

The 2.3 mm monofilament extruded fibers were then cut to a length appropriate for a feed rod and bundled together. About 65–70 of the 2.3 mm fibers were tightly packed together into a molding cylinder. wherein they were molded at 150° C. to form a multifilament feedrod. This multifilament feedrod was subsequently extruded at 110° C. through a 2.3 mm orifice to produce multifilament rod. as illustrated in FIG. 7.

After repeating the foregoing steps so that a number of multifilament fibers are prepared. a number of such fibers are arranged into a desired shape and molded to provide a green fibrous monolithic ceramic. An example of this ceramic is set forth in FIG. 8. The green ceramic monolith was then baked to remove the binder. and the resulting article pressure sintered to provide a fibrous monolith.

EXAMPLE 5

This example illustrates the preparation of a silicon nitride/boron nitride multifilament fiber in accordance with one aspect of the present invention.

1. Silicon nitride compound:

A. Sinterable silicon nitride powder mixed with sintering aids (9 wt % yttria powder and 3 wt % alumina powder): 37.23 g

B. Ethylene Vinyl Acetate copolymer: 7.65 g

C. Heavy Mineral oil: 2.16 g

D. Methoxypolyethylene Glycol [MW 550]: 1.0 g

2. Boron nitride compound:

A. Boron nitride powder: 24.75 g

B. Ethylene Vinyl Acetate copolymer: 10.34

C. Methoxypolyethylene Glycol [MW 550]: 0.75 g

The components of each composition were compounding in the manner set forth in Example 1. The apparent viscosity of both the silicon nitride compound and the boron nitride compound were then adjusted to an apparent viscosity of about 18.000 poise at 170° C. A controlled geometry feedrod was then prepared by the method of Example 1. and 3 mm monofilament fibers were prepared by extrusion of the feed rod. About 30–50 of these 3 mm monofilament fibers were then cut to an appropriate length for a feed rod. and bundled together and molded. in the manner of Example 4. to form a multifilament feedrod. The multifilament feedrod was subsequently extruded at 110° C. through a 3 mm orifice to produce multifilament fiber. After preparing a number of such multifilament fibers and arranging them into a desired configuration. the configured fibers were molded to provide a green fibrous monolithic ceramic. This monolith was then baked to remove the binder. and the resulting article pressure sintered to provide a fibrous monolith.

EXAMPLE 6

This example illustrates the preparation of an alumina/graphite multifilament fiber in accordance with one aspect of the present invention.

1. Alumina compound:

A. Sinterable alumina powder: 44.55 g

B. Ethylene Vinyl Acetate copolymer: 10.23 g

C. Polyethylene Glycol [MW 550]: 0.5 g

2. Graphite compound:

A. Graphite powder: 24.75 g

B. Ethylene Vinyl Acetate copolymer: 11.26 g

C. Polyethylene Glycol [MW 550]: 0.5 g

Each of the compounds were compounded in the manner set forth in Example 1. The apparent viscosity of both the alumina compound and the graphite compound were adjusted to an apparent viscosity of about 19.000 poise at 170° C. A controlled geometry feedrod was then prepared in accordance with the method of Example 4. and 2.3 mm diameter monofilament fibers were then prepared by extruding the feedrod. These 3 mm monofilament coextruded fibers were then cut to a length appropriate for a feedrod. and bundled together and molded as in Example 4 to provide a feed rod. This multifilament feed rod was subsequently extruded through a 2.3 mm orifice to produce a multifilament ceramic fiber.

After preparing a number of such fibers. arranging the fibers into a desired shape. and molding the shaped article.

a green fibrous monolithic ceramic was obtained. This monolith was then baked to remove the binder, and subsequently sintered to provide a fibrous monolith.

EXAMPLE 7

This example illustrates the preparation of a zirconia oxide/aluminum oxide/nickel oxide multifilament fiber in accordance with one aspect of the present invention. This example will further illustrate the preparation of a zirconia/nickel fibrous monolith, wherein an alumina interphase exists between the zirconia and the nickel.

1. Zirconia oxide compound:
   - A. Sinterable zirconia—3 mole percent yttria powder: 66.99 g
   - B. Ethylene Vinyl Acetate copolymer: 10.34 g
   - C. Methoxypolyethylene Glycol [MW 550]: 1.38 g
2. Aluminum oxide compound:
   - A. Sinterable aluminum oxide powder: 44.55 g
   - B. Ethylene Vinyl Acetate copolymer: 10.34 g
   - C. Methoxypolyethylene Glycol [MW 550]: 1.0 g
3. Nickel oxide compound:
   - A. Nickel oxide alloy powder: 73.37 g
   - B. Ethylene Vinyl Acetate copolymer: 10.34 g
   - C. Methoxypolyethylene Glycol [MW 550]: 1.38 g

Each of the compounds were compounding in the manner set forth in prior Examples. The apparent viscosity of both the zirconia compound and the nickel oxide compound were adjusted so that they were similar. The aluminum oxide compound was prepared according to the method set forth in Example 6. A feedrod was then molded from the zirconia in the manner as described in previous examples. Flat sheets of the alumina compound and the nickel oxide compound were compression molded in accordance with the method of Example 2. The thickness of the sheets were controlled to achieve the desired ratio of nickel to zirconia and alumina to zirconia in the feed rod. The alumina sheet was then wrapped around the zirconia rod, and the nickel oxide sheet was wrapped around the alumina sheet to fabricate the controlled geometry feedrod. The three-component feedrod was then extruded to provide a 2.3 mm monofilament fiber. As in Example 4, a number of these fibers were then bundled to create a multifilament feed rod, which feed rod was then extruded as before to form multifilament fiber.

After preparing a number of such multifilament fibers, arranging the fibers into a desired shape, and molding the shaped article, a green fibrous monolithic ceramic was obtained. This monolith was then baked to remove the binder, the nickel oxide was reduced to metallic nickel, and subsequently sintered to provide a fibrous monolith. The three-layer textured zirconium oxide/aluminum oxide/nickel green fiber is illustrated in FIG. **9**.

EXAMPLE 8

This example illustrates the preparation of a "tree ring" texture in aluminum oxide/iron oxide fibers, using axial coextrusion, in accordance with one aspect of the present invention.

1. Alumina compound:
   - A. Sinterable alumina powder: 44.43 g
   - B. Ethylene Vinyl Acetate copolymer: 7.57 g
   - C. Methoxypolyethylene Glycol [MW 550]: 0.42 g
2. Iron oxide compound:
   - A. Iron oxide (hematite) powder: 57.64 g
   - B. Ethylene Vinyl Acetate copolymer: 10.23 g
   - C. Methoxypolyethylene Glycol [MW 550]: 0.5 g

The aluminum oxide compound and the iron oxide compound were compounded as in previous examples. Using the method of Example 6, flat sheets, 0.5 mm thick, were pressed from the alumina and iron compounds. Using a punch, 22 mm diameter discs were cut from these sheets. A feedrod was prepared by stacking these discs in a particular sequence, which was for this example, three white aluminum oxide discs, one red iron oxide disc, etc. After compression molding that stack at a temperature of 160° C. and a load of 10,000N, solid feed rod with axial compositional variations was obtained. This feed rod was extruded at 180° C. through a 2.3 mm orifice to obtain a green fiber with a texture similar to tree rings. An example of this fiber is shown in FIG. **10** (axial section) and FIG. **11** (radial section). A uniaxial layup of these fibers was molded to produce a textured green ceramic article having a wood-like appearance, as illustrated in FIG. **12**.

EXAMPLE 9

This example illustrates the preparation of silicon nitride/boron nitride fibers using "chip and washer" axial extrusion, in accordance with one aspect of the present invention.

1. Silicon nitride compound:
   - A. Sinterable silicon nitride powder mixed with sintering aids (9 wt % yttria powder and 3 wt % alumina powder): 36.50 g
   - B. Ethylene Vinyl Acetate copolymer: 9.30 g
   - C. Heavy Mineral oil: 2.16 g
   - D. Methoxypolyethylene Glycol [MW 550]: 1.0 g
2. Boron nitride compound:
   - A. Boron nitride powder: 24.75 g
   - B. Ethylene Vinyl Acetate copolymer: 10.34 g
   - C. Methoxypolyethylene Glycol [MW 550]: 0.75 g

The silicon nitride compound and the boron nitride compound were compounded as in previous examples. Using the method of Example 2, the silicon nitride compound and boron nitride compound were compression molded at 150° C. between flat steel sheets to provide flat sheets of each material of 0.3 mm in thickness. Using a punch, 22 mm diameter discs were cut from the silicon nitride sheets. "Washers" were cut from the boron nitride sheets, the washers having a 22 mm outer diameter and a 6 mm inner diameter. A 6 mm silicon nitride disc was then placed into the central hole of the boron nitride disc. A feedrod was prepared by stacking those multi-component discs in a particular sequence, which was for this example four grey silicon nitride discs, one white boron nitride disc, etc.

After compression molding at 150° C. and a load of 23.2N, a solid feed rod with axial compositional variations was obtained. This feed rod was extruded at 110° C. through a 3 mm orifice to obtain a green fiber having a texture similar to tree rings. A uniaxial layup of these fibers was molded to produce a textured green ceramic. After molding a number of such fibers into a desired shape to provide a green fibrous monolithic ceramic, the monolith was baked to remove the binder. The resulting article was then pressure sintered to provide a fibrous monolith having a wood-like appearance.

While the examples included herein utilize piston extrusion, it is believed that other extrusion methods known in the art could also be used. As one example, continuous bicomponent extrusion of highly loaded ceramic systems could be accomplished if properly designed bicomponent spinning dies were utilized.

All of the references cited herein are hereby incorporated in their entireties by reference.

While this invention has been described with an emphasis upon preferred embodiments, it will be obvious to those of ordinary skill in the art that variations of the preferred embodiments may be used and that it is intended that the invention may be practiced otherwise than as specifically described herein. Accordingly, this invention includes all modifications encompassed within the spirit and scope of the invention as defined by the following claims.

We claim as our invention:

1. A method for preparing a green fibrous monolith comprising

extruding at least a first feed rod to provide a green ceramic fiber, the first feed rod being prepared by forming a first ceramic-laden composition comprising a thermoplastic polymer and at least about 40 vol. % of a ceramic particulate into a substantially cylindrical core and applying a second ceramic-laden composition comprising a thermoplastic polymer and at least about 40 vol. % of a ceramic particulate which differs from the first ceramic-laden composition onto the core, and

forming a green ceramic monolith by shaping at least the green ceramic fiber.

wherein during the extrusion step, each ceramic-laden composition has a viscosity that is approximately equivalent to that of each other ceramic-laden composition.

2. The method according to claim 1, wherein the green ceramic fiber is provided by substantially simultaneously extruding the first feed rod and a second feed rod,

wherein the second feed rod is prepared by forming a third ceramic-laden composition comprising a thermoplastic polymer and at least about 40 vol. % of a ceramic particulate into a substantially cylindrical core and applying a layer of a fourth ceramic-laden composition comprising a thermoplastic polymer and at least about 40 vol. % of a ceramic particulate which differs from the particulate contained in the third composition onto the core, and

wherein the third ceramic-laden composition is different from the first ceramic-laden composition.

3. The method according to claim 2, wherein the third ceramic-laden composition is different from the first and second ceramic-laden compositions.

4. The method according to claim 3, wherein the fourth ceramic-laden composition is different from the first and second ceramic-laden compositions.

5. The method according to claim 1, further comprising preparing the first feed rod by applying a layer of a third ceramic-laden composition comprising a thermoplastic polymer and at least about 40 vol. % of a ceramic particulate onto the second ceramic-laden composition, wherein the composition of the third ceramic-laden composition differs from the composition of the second ceramic-laden composition.

6. A method for preparing a green fibrous monolith from at least one green ceramic fiber having a controlled texture comprising

(a) forming a first ceramic-laden composition comprising a thermoplastic polymer and at least about 40 vol. % of a ceramic particulate into a substantially cylindrical core.

(b) applying a layer of a second ceramic-laden composition comprising a thermoplastic polymer and at least about 40 vol. % of a ceramic particulate which differs from the particulate contained in the first composition onto the core to form a substantially cylindrical feed rod having an average diameter,

(c) extruding the feed rod to provide at least one green ceramic fiber which has an average diameter that is less than the average diameter of the feed rod, and

(d) shaping the at least one green ceramic fiber to provide the green fibrous monolith,

wherein, during the extrusion step, each ceramic-laden composition has a viscosity which is approximately equivalent to that of each other ceramic-laden composition, and, when the ceramics present in the extruded at least one green ceramic fiber are sintered, a plane of weakness defined by the interface of the core and the layer is provided, the interface being relatively weaker than the core.

7. The method according to claim 6, wherein when at least two green ceramic fibers are used to provide the green fibrous monolith, one of the fibers having a composition that is different from at least one of the other fibers.

8. The method according to claim 6, the method further comprising heating the green fibrous monolith to sinter the ceramic particles therein, thereby providing a fibrous monolith.

9. The method according to claim 6, further comprising

forming a third ceramic-laden composition comprising a thermoplastic polymer and at least about 40 vol. % of a ceramic particulate into a substantially cylindrical core,

applying a layer of a fourth ceramic-laden composition comprising a thermoplastic polymer and at least about 40 vol. % of a ceramic particulate which differs from the particulate contained in the third composition onto the core to form a second substantially cylindrical feed rod having an average diameter,

extruding the second feed rod to form a second green ceramic fiber which has an average diameter that is less than the average diameter of the second feed rod, and

shaping at least the second green ceramic fiber and the first green ceramic fiber to provide the green ceramic monolith,

wherein the third ceramic-laden composition is different from the first ceramic-laden composition.

10. The method according to claim 9, wherein the third ceramic-laden composition is different from the first and second ceramic-laden compositions.

11. The method according to claim 10, wherein the fourth ceramic-laden composition is different from the first and second ceramic-laden compositions.

12. The method according to claim 6, wherein before the first green fiber is used in step (d) to provide the green fibrous monolith, the average diameter possessed by the first green ceramic fiber after step (c) is further reduced by extruding the green ceramic fiber.

13. A method for preparing a green fibrous monolith from at least one green multifilament ceramic fiber having a controlled texture comprising

(a) forming a first ceramic-laden composition comprising a thermoplastic polymer and at least about 40 vol. % of a ceramic particulate into a substantially cylindrical core.

(b) applying a layer of a second ceramic-laden composition comprising a thermoplastic polymer and at least about 40 vol. % of a ceramic particulate which differs from the particulate contained in the first composition onto the core to form a substantially cylindrical feed rod having an average diameter,

(c) extruding the feed rod to provide at least two green ceramic fibers, each fiber having an average diameter that is less than the average diameter of the feed rod,

(d) extruding the at least two green ceramic fibers substantially simultaneously to form at least one multifilament green ceramic fiber, and

(e) shaping the at least one multifilament green ceramic fiber to provide the green fibrous monolith.

wherein, during each extrusion step, each ceramic-laden composition has a viscosity which is approximately equivalent to that of each other ceramic-laden composition, and, when the ceramics present in the at least one green ceramic fiber are sintered, a plane of weakness defined by the interface of the core and the layer is provided, the interface being relatively weaker than the cores.

14. The method according to claim 13, the method further comprising heating the green fibrous monolith to sinter the ceramic particles therein, thereby providing a fibrous monolith.

* * * * *

REPORT DOCUMENTATION PAGE

Form Approved
OMB No. 0704-0188

1. AGENCY USE ONLY (Leave blank)	2. REPORT DATE	3. REPORT TYPE AND DATES COVERED
	August 25, 1997	Final Report 4/1/91 - 3/30/93

4. TITLE AND SUBTITLE

Tough Ceramics from Fibrous Monoliths

5. FUNDING NUMBERS

N00014-91-J-1999

6. AUTHOR(S)

John W. Halloran

7. PERFORMING ORGANIZATION NAME(S) AND ADDRESS(ES)

University of Michigan
Division of Research Development Administration
1058 Wolverine Tower
3003 South State St.
Ann Arbor, MI 48109-1274

8. PERFORMING ORGANIZATION REPORT NUMBER

9. SPONSORING / MONITORING AGENCY NAME(S) AND ADDRESS(ES)

Steven G. Fishman
Office of Naval Research
800 North Quincy St.
Arlington, VA 22217-5660

10. SPONSORING / MONITORING AGENCY REPORT NUMBER

11. SUPPLEMENTARY NOTES

12a. DISTRIBUTION / AVAILABILITY STATEMENT

Unlimited public availability

12b. DISTRIBUTION CODE

13. ABSTRACT *(Maximum 200 words)*

During this 1991-1993 grant, the University of Michigan developed "fibrous monolithic ceramics", a new class of monolithic ceramics with properties comparable to ceramic fiber reinforced ceramic matrix composites (CMC's). They consist of a 250-micron "cells" of a strong polycrystalline ceramic, such as silicon carbide or silicon nitride, separated by "cell boundaries" from materials, such as boron nitride, which promote crack deflection and delamination. These materials show graceful failure in flexure, with strengths around 350 MPa and work of fracture around 2000 J/m^2. Fibrous monolithic ceramics are made from conventional low-cost ceramic powder, using extrusion methods common in conventional ceramic manufacture. We have demonstrated successful fibrous monoliths with silicon carbide, silicon nitride, and alumina, using weak interfaces of graphite or boron nitride. The boron nitride systems are resistant to oxidation. Their room temperature properties are unaffected by exposure at 1400°C.

14. SUBJECT TERMS

ceramic composites, fibers, structural ceramics, silicon nitride

15. NUMBER OF PAGES

12

16. PRICE CODE

17. SECURITY CLASSIFICATION OF REPORT	18. SECURITY CLASSIFICATION OF THIS PAGE	19. SECURITY CLASSIFICATION OF ABSTRACT	20. LIMITATION OF ABSTRACT
unclassified	unclassified	unclassified	unlimited

GENERAL INSTRUCTIONS FOR COMPLETING SF 298

The Report Documentation Page (RDP) is used in announcing and cataloging reports. It is important that this information be consistent with the rest of the report, particularly the cover and title page. Instructions for filling in each block of the form follow. It is important to ***stay within the lines*** to meet ***optical scanning requirements***.

Block 1. Agency Use Only *(Leave blank)*.

Block 2. Report Date. Full publication date including day, month, and year, if available (e.g. 1 Jan 88). Must cite at least the year.

Block 3. Type of Report and Dates Covered. State whether report is interim, final, etc. If applicable, enter inclusive report dates (e.g. 10 Jun 87 - 30 Jun 88).

Block 4. Title and Subtitle. A title is taken from the part of the report that provides the most meaningful and complete information. When a report is prepared in more than one volume, repeat the primary title, add volume number, and include subtitle for the specific volume. On classified documents enter the title classification in parentheses.

Block 5. Funding Numbers. To include contract and grant numbers; may include program element number(s), project number(s), task number(s), and work unit number(s). Use the following labels:

C	- Contract	**PR**	- Project
G	- Grant	**TA**	- Task
PE	- Program Element	**WU**	- Work Unit Accession No.

Block 6. Author(s). Name(s) of person(s) responsible for writing the report, performing the research, or credited with the content of the report. If editor or compiler, this should follow the name(s).

Block 7. Performing Organization Name(s) and Address(es). Self-explanatory.

Block 8. Performing Organization Report Number. Enter the unique alphanumeric report number(s) assigned by the organization performing the report.

Block 9. Sponsoring/Monitoring Agency Name(s) and Address(es). Self-explanatory.

Block 10. Sponsoring/Monitoring Agency Report Number. *(If known)*

Block 11. Supplementary Notes. Enter information not included elsewhere such as: Prepared in cooperation with...; Trans. of...; To be published in.... When a report is revised, include a statement whether the new report supersedes or supplements the older report.

Block 12a. Distribution/Availability Statement. Denotes public availability or limitations. Cite any availability to the public. Enter additional limitations or special markings in all capitals (e.g. NOFORN, REL, ITAR).

- **DOD** - See DoDD 5230.24, "Distribution Statements on Technical Documents."
- **DOE** - See authorities.
- **NASA** - See Handbook NHB 2200.2.
- **NTIS** - Leave blank.

Block 12b. Distribution Code.

- **DOD** - Leave blank.
- **DOE** - Enter DOE distribution categories from the Standard Distribution for Unclassified Scientific and Technical Reports.
- **NASA** - Leave blank.
- **NTIS** - Leave blank.

Block 13. Abstract. Include a brief ***(Maximum 200 words)*** factual summary of the most significant information contained in the report.

Block 14. Subject Terms. Keywords or phrases identifying major subjects in the report.

Block 15. Number of Pages. Enter the total number of pages.

Block 16. Price Code. Enter appropriate price code *(NTIS only)*.

Blocks 17. - 19. Security Classifications. Self-explanatory. Enter U.S. Security Classification in accordance with U.S. Security Regulations (i.e., UNCLASSIFIED). If form contains classified information, stamp classification on the top and bottom of the page.

Block 20. Limitation of Abstract. This block must be completed to assign a limitation to the abstract. Enter either UL (unlimited) or SAR (same as report). An entry in this block is necessary if the abstract is to be limited. If blank, the abstract is assumed to be unlimited.